UiT The Arctic University of Norway

Department of Arctic and Marine Biology

# Coping with change: The role of environmental parameters for *Calanus* lipid storage in Northeast Greenland fjords

Anita Holmgren

Master's thesis in Biology (BIO-3950), August 2023

# Abstract

The importance of *Calanus* in the Arctic pelagic ecosystem is well established in the Norwegian-Arctic region. However, research on *Calanus* in Northeast Greenland remains limited. *Calanus* condition and role in the Arctic pelagic ecosystem might be different on the western side of the Fram strait because of influence from the East Greenland current that brings cold and less saline water in from the oligotrophic Arctic Basin. As the Arctic is entering a time of climate change, it is important to establish baseline knowledge about all regions of the Arctic. This study investigated the lipid content of *Calanus* in three distinct fjord systems in post-bloom conditions, along with several environmental parameters. *Calanus* had started seasonal migration. The individuals that already had migrated had a higher lipid content relative to size than individuals still residing in the surface. It was found that individual lipid content scaled exponentially with prosome length, with a significant species-specific difference between *C. glacialis* and *C.hyperboreus*. Differences in abundance, species and size composition induced differences in the total amount of lipid stored in *Calanus* spp overwintering stages. This was in part related to parameters in the environment. The northernmost fjord, Besselfjord, was filled with Polar water, and it was estimated that most of the nutrients had been incorporated in diatoms.Here we found the second highest amount of lipid in *Calanus*. Another sill fjord, Breddefjorden, had inflow of Atlantic water and a weaker nutrient-diatom link, as well as little total lipid in *Calanus*. Eskimones, a station located in the more open Godthaabs Golf, had the highest amount of lipid stored in *Calanus* overwintering stages, but a very weak estimated nutrient-diatom link. This might suggest other important sources of carbon. As *Calanus*' ability to generate and store lipids is important for individual survival and the energy flow from primary producers to higher trophic levels, changes in the environment that influence lipid accumulation could cause cascading effects. It is therefore important to identify significant environmental variables. This study contributes to a knowledge base, which will be important in the future when assessing how well these copepods are coping with a changing Arctic.

## Acknowledgement

First of all I want to thank my superviser Fredrika Norrbin. This year I have learned so much about Arctic zooplankton ecology through our many discussions about themes included, and not included, in this thesis. I also want to thank you for your attention, kindness, patience and openness towards my many ideas. It has been a pleasure diving into the fjords of Northeast Greenland with you, even though there have been times of turbulent water.

At times I felt completely lost in the dark ocean of statistics. I don't know where this thesis had sailed without Einar Magnus Nilssen. Thank you for taking the time to help me towards the analysis presented in this thesis. I have learned so much of you about using, and when to not use, statistics in biology. Your patience, knowledge and enthusiasm is truly remarkable. I would also like to thank Svein Kristiansen. It would not have been possible to collect data on all the environmental parameters presented in this thesis without you.

As the TUNU-VIII expedition was my first research expedition, I was very nervous when boarding Kronprins Haakon last year. The TUNU-family took me in with open arms and I had the most amazing time in Northeast Greenland. I especially want to thank Arve Lynghammar for being such a fun, organized and kind expedition leader. I also want to thank Jan Sverre Laberg for spending the time to talk with me about bottom bathymetry and sharing geological data. Also the crew of Kronprins Haakon were amazing, helping with everything from calibrating the VPR to securing knots on the plankton net.

I want to thank Derrick Kwame Odei, Johanna Hovinen, Paul Dubourg, Christien Laber and Lucie Goraguer for analysing samples. This thesis would not have been possible without you. I also want to thank Malin Daase and Elisabeth Halvorsen for advising me on zooplankton identification and giving advises about this thesis.

This thesis marks the end of my five years of education. It has truly been an adventure. A very fun one. First, I want to thank NTNU for my time in Trondheim, and Studentersamfundet for being the place I spent most of that time. My life changed when I was introduced to Arctic biology at UNIS. I especially want to thank Janne Søreide, that open my eyes to Arctic marine ecology and showed me my first *Calanus*. As I fell in love with the Arctic systems, a master at UiT was the obvious choice - a decision I have not regretted for a second. It has been amazing to study at UiT, close to the research community, nature, and my home in Honningsvåg.

Last, but not least, I want to thank my friends and family. Thanks to my mum and dad for always encouraging my curiosity around nature. Thank you to my sister for helping me handle my inner control-freak, accepting that I will never understand all the chaos. I feel so blessed to have had the network of people during my time in Trondheim, Svalbard and Tromsø. None of you are forgotten. I especially want to thank my fellow masterstudents Julie, Villads, Kristin and Emilie for sharing all the ups and downs. My badass Svalbard babes also deserves a mention. An exstra shoutout goes to Michel, Hugh, Tora, Simon and Villads for helping me with language, front page and verifying the statistics.

# Contents

# List of Figures

# List of Tables

# 1 Introduction

## 1.1 The role of *Calanus* in the food chain

The Arctic pelagic ecosystem is a highly pulsed system, with a long, dark winter followed by a short and intense spring bloom (Sakshaug et al., 2009). During the spring bloom, solar energy is converted into carbohydrates through primary production in ice algae and phytoplankton. Secondary producers, especially *Calanus* spp., transform carbohydrates into high energy lipids (Falk-Petersen et al., 2007). These lipids are stored inside the copepod's body, both preparing the animal for overwintering and serving as a link in the energy flow between primary producers and higher tropic levels. The accessible energy is converted from large quantities of phytoplankton, with 10-20% of the dry mass as lipids, into high quality zooplankton, with 50-70% of the dry mass consisting of lipid (Falk-Petersen et al., 1990). Fish, seabirds and marine mammals come from near and far to partake in this feast of fat. *Calanus* spp. is an important prey for local predators like the polar cod, which again are consumed by seals, whales, and seabirds (Daase et al., 2021; Hop and Gjøsæter, 2013). The high concentration of lipid rich prey in the surface also attracts migrating animals, which carry energy from the Arctic spring to southern latitudes. When the polar day sets, the energy preserved in the *Calanus* lipid sacs will prevail, sustaining predators during the polar night (Kunisch et al., 2023).

Zooplankton, then especially *Calanus*, have received much attention in the Norwegian Arctic region east of the Fram Strait. Areas west of the Fram Strait, in Northeast Greenland, are less explored, except for extensive, long-term Danish projects in Young Sound (Middelbo et al., 2018; Sejr et al., 2022). The Arctic is now entering an era of rapid change due to global warming. To assess changes in the environment, there is a need for baseline knowledge. As there are large regional differences in the Arctic, it is important to investigate all areas. This thesis describes the lipid content in three *Calanus* species during an autumn-situation in three Northeast Greenland fjord systems, together with environmental variables in their fjord habitats.

## 1.2 Arctic fjords: Seasonality and the Arctic spring bloom

The coastline of Greenland mainly consists of deep fjords carved out by glaciers (Cottier et al., 2010). The physical processes inside the fjords set the framework for the marine environment, through exchange of water masses, water mass transformation and estuarine circulation. Some fjords have one or more sills that limit exchange of water and organisms between the fjord and shelf or different basins within the fjord. The classical three-layer model of a sill fjord consists of a deep, an intermediate and a surface layer (Farmer and Freeland, 1983). The surface layer contains fresh, local water, the intermediate water layer is advected into the fjord at the depth of the sill and the deep layer typically consists of more saline and cold water.

The strong seasonality of the Arctic is a driving force in the dynamical processes inside arctic fjords (Cottier et al., 2010). During the autumn, decreasing air temperature and wind chills the water

temperature and deepens the surface mixed layer. The winter arrives with cold temperatures, causing sea ice formation with brine release (very dense, salty water). Brine expulsion leads to deep convection in the water column. When the sun returns in spring, the ice starts to heat up. Ice melting and run-off from land lower the salinity in the surface, stratifying the water column (creating a pycnocline). As summer arrives, more heat in the surface increases the surface temperature and the classical three-layer structure is restored.

Inorganic nitrogen and phosphorus, as well as silicate for diatoms, is crucial for phytoplankton growth. Because of the vertical mixing during winter, sea ice covered fjords generally have a homogeneous water column with a high concentration of nutrients in the upper water column before the ice breaks up (Cottier et al., 2010). Light is then the limiting factor for photosynthesis (Mundy et al., 2005). Even when the light has returned to the surface, the underside of the ice cover can remain dark for quite some time. The thickness of the ice, and especially the snow covering the ice surface, plays a significant role in how much solar radiation penetrates the ice. The first organisms to utilize the little solar irradiance in spring are sea ice algae that reside in the network of brine channels in the bottom part of the sea ice. The sea ice algae bloom is rapid and often dominated by big, pennate diatoms, which provide an important early food source for grazers like *Calanus* spp. (Søreide et al., 2010).

As the sea ice melts, the algae are released into the surface waters, where they either sink to the bottom or get consumed. When direct sunlight reaches open water, the pelagic spring bloom is initiated. High nutrient concentrations in the surface facilitate growth of big phytoplankton, like diatoms. Although diatom cells are heavy, the pycnocline (the density discontinuity created by temperature and salinity differences in the water column) prevents them from sinking out of the euphotic zone. The pycnocline also prevents flux of nutrients from the lower, denser water masses. As the surface waters are depleted of nutrients, smaller phytoplankton, autotrophic flagellates and bacteria start competing with the larger and more nutrient-demanding diatoms (Thingstad et al., 2008).

## 1.3 The *Calanus* complex

On the Atlantic side of the Arctic, there are three main species of the genus *Calanus*; *C. hyperboreus*, *C. glacialis* and *C. finmarchicus*. The copepods develop from an egg to adult male or female through six nauplii stages and five copepodite stages. They are effective filter feeders who accumulate energy rapidly. In addition to accumulating lipids synthesized by algae, they also have the capacity to transform the carbohydrates into high energy storage lipids, wax-esters, which are stored in an oil sac in their bodies (Lee et al., 2006). Wax esters consist of long-chain primary alcohol and long-chain fatty acids. In addition to being very high in energy, the wax esters allow *Calanus* to be neutrally buoyant in deep and cold waters, facilitating seasonal vertical migration. These properties of quick accumulation of energy and energy storage capacity makes *Calanus* spp. highly adapted to the conditions in the Arctic.

The three *Calanus* species are believed to differ in their geographical distribution (Falk-Petersen et al., 2007). *C. hyperboreus* is centred in the deep arctic basins, *C. glacialis* resides on the shallower

arctic shelf areas, while *C. finmarchicus* is an Atlantic deep-water species advected with ocean currents to the Arctic. The three species also differ in size, life span and reproduction. The *Calanus* complex spans from income to capital breeders (Varpe and Ejsmond, 2018). Income breeding is when the organism depends on external energy sources (food intake) to reproduce, while capital breeders utilize the organism's internal energy reserves.

Higher latitudes, with more extreme light conditions and thicker multi-year sea ice, narrows the time window in which primary production is possible. *C. hyperboreus* has adapted to this uncertainty with larger lipid reserves and a flexible life cycle (Falk-Petersen et al., 2007). Depending on the amount of primary production, this copepod can complete its life cycle in $2-5$ years. *C. hyperboreus* are capital breeders, an adaptation that make it possible to use the whole spring bloom period. The eggs contain droplets of wax-esters which allows the nauplii to develop through the first few stages (Lee et al., 2006) until the sea ice algae bloom arrives. In this way, the nauplii can immediately take advantage of the first high quality algae, and quickly grow into copepodite stage III (Daase et al., 2021). They can overwinter at this stage and then use the following years to develop and build up the energy reserves needed to become adult, reproduce and complete their life cycle.

*C. glacialis* is generally found in the shelf areas with seasonal sea ice cover. They have adapted a mixed strategy where a copepod starts the season as a capital breeder and then transitions to income breeding with the onset of the spring bloom (Varpe and Ejsmond, 2018). A study from the Arctic shelf seas showed that females used the sea ice algae bloom for maturation and reproduction, and then the offspring fed upon the subsequent phytoplankton bloom (Søreide et al., 2010). However, since *C. glacialis* are partly capital breeders, they can reproduce in time for the phytoplankton bloom in the case of an unsuccessful sea ice algae bloom Daase et al. (2021). During the first spring and summer, the offspring develop to stage CIV or CV, depending on how good the conditions are, before overwintering. *C. glacialis* can use one or two years to complete its life cycle.

*C. finmarchicus* are adapted to open, ice-free waters. They are income breeders and utilize the phytoplankton bloom in spring for reproduction (Falk-Petersen et al. (2007), Varpe and Ejsmond (2018)). This species has a one-year life cycle, where the egg develop to copepodite stage CV the first spring and summer before they descend to deeper waters in autumn and then ascend to reproduce the following spring.

Differences in life history traits may have caused differences in morphological traits, where the arctic *C. hyperboreus* and *C. glacialis* are able to store 25 and 10 times more lipid than the Atlantic *C. finmarchicus* because of differences in size (Falk-Petersen et al., 2007). However, due to individual plasticity and regional differences, *C. finmarchicus* and *C. glacialis* have substantial overlap in their size ranges, and molecular methods are needed to separate the two species (Choquet et al., 2018).

## 1.4 West of the Fram Strait

### 1.4.1 Ocean currents on the Northeast Greenland shelf

There are two main currents influencing Northeast Greenland; the cold, fresh East Greenland current (EGC) and the warm, saline Recirculating Atlantic current (RAC) (Gjelstrup et al., 2022). Cold and fresh polar water (PW), which is formed in the central Arctic Ocean, is transported out of the Arctic Mediterranean with the upper 150-200 m of the EGC along the East Greenland shelf. The RAC has its origin in the Gulf of Mexico, continuing via the Norwegian Atlantic current, which merges with the West Spitsbergen current at the west coast of Svalbard. About half of this current enters the Arctic basin as the Atlantic Circumpolar boundary current (ACBC) and the other half travels eastwards across the Fram Strait as the Recirculating Atlantic current (RAC). The Atlantic water from the south hold much more nutrients than the polar water from the oligotrophic Arctic Ocean (Bluhm et al., 2015).

### 1.4.2 Plankton communities in Northeast Greenland

As plankton are defined by their inability to move horizontally against currents, the ocean currents strongly influence the plankton community. A plankton can be advected great distances through its life span, or even within a season. It can therefore be difficult to link environmental variables to the plankton community and conditions, as the organisms might have evolved in a different environment than in which they were sampled. This challenge can be partly overcome by studying plankton in sill fjords, where limiting exchange of water and organisms is limited.

As mentioned, the fjords of Northeast Greenland, except Young Sound, are little explored in terms of plankton communities. In September 2017 there was a survey of spatial occurrence and abundance of marine zooplankton in Besselfjord, Dovebugt and the shelf outside with the TUNU- project. *Pseudocalanus* spp. and *Oithona* sp. dominated in abundance, followed by *Calanus* spp., *Metridia* sp., *Microcalanus* sp., bivalve veliger, *Triconia* sp. and *Acartia* sp. (Beroujon, 2019; Beroujon et al., 2022). Radiolaria were more abundant in the innermost part of the fjord, while predators like *Aglantha digitale* and *Parasitta elegans* were only present in the middle part. *Calanus* spp. was found at all locations. In the middle basin of Besselfjord individuals from copepodite stage CII to adult females were found, while only CII-CV were found in the inner fjord.

In Young Sound, *Calanus* spp. is dominating the biomass inside the fjord (Middelbo et al., 2018). Other copepods were *Metridia longa*, *Pseudocalanus* spp., *Oithona similis* and *Triconia borealia* (earlier *Oncaea borealis*, (WoRMS Editorial Board, WoRMS Editorial Board)). Chaetognata, *Aglantha digitale*, *Limacina helicina* and Gastropoda were also more abundant in biomass. The biomass of *Calanus* was lower in the innermost part of the fjord, where there is located a land terminating glacier.

## 1.5 In the time of Climate Change

The Earth is currently facing climate change because of human influence. The human emissions of greenhouse gasses will force the Arctic into a warmer future with more participation (IPCC, 2023). The full consequences of this global warming and changes in weather and current patterns are still unclear. There have been identified two key areas where climate change will have an effect on the Arctic pelagic ecosystem; mismatch in timing of key life history events with the environment and atlantification where boreal species extend their geographical range northwards (Daase et al., 2021). For coastal ecosystems, a key driver of change will be increased terrestrial run-off from rivers, precipitation and glacier melt, consisting of freshwater with organic and inorganic matter (Sejr et al., 2022).

### 1.5.1 Mismatch in timing of key life-history events with the environment

Climate change will change the seasonal variations in environmental conditions, as it changes in the duration and extent of sea ice cover and increased temperature. The arctic species have naturally adapted the timing of life-history events to seasonal changes in their environment. Depending on the triggers of the life-history events, changing environments can lead to mismatch in timing between the organism and the seasonal cycle ((Cushing, 1973) in (Daase et al., 2021)). In *Calanus*, earlier ice break-up and phytoplankton spring blooms have caused a mismatch in the timing in the occurrence of the algae with the highest nutritional value and *Calanus* glacialis recruitment (Søreide et al., 2010).

### 1.5.2 Atlantification

Increased flow of Atlantic water to the Arctic has been registered on the east side of the Fram Strait for a long time. Recently, it has also reached the west side of the Fram Strait, Northeast Greenland (Gjelstrup et al., 2022). The Atlantic water brings heat, nutrients and Atlantic species. For the *Calanus* complex, this will likely cause changes in the species composition and may affect the life history strategy of the species already present (Weydmann-Zwolicka et al., 2022). A more Atlantic environment is favourable for the Atlantic *C. finmarchicus* (Aarflot et al., 2018), and a reproducing population has been identified east of the Fram strait (Tarling et al., 2022). It is not given that increased inflow of *C. finmarchicus* will outcompete *C. glacialis* . In Svalbard fjords, which have increasing Atlantic influence, it has been found that despite their similarities in appearance and niches they utilize different resources during recruitment (Hatlebakk et al., 2022). *C. glacialis* is adapted to the early arctic spring bloom, while *C. finmarchicus* utilizes the late autumn blooms. However, warmer water and a longer primary productivity season might shift the present *Calanus* populations towards an annual life cycle and income breeding (Renaud et al., 2018). As the life histories become more similar, the lipid content and size ranges will also overlap. In Svalbard fjords there were found no species-specific difference in lipid-storage capacity between *C. finmarchicus* , *C. glacialis* and *C. hyperboreus* (Renaud et al., 2018).

A shift from a multi-year life cycle to an annual life cycle would increase the turnover in the *Calanus* populations, increasing the amount of energy available for higher trophic levels (Renaud et al., 2018).

The smaller size would also imply less energy per individual. This can have big consequences for size selective predators like the little auk (Karnovsky et al., 2010) and polar cod (Hop and Gjøsæter, 2013). As the ice is thinning, increasing light intensity changes the conditions for visual predators. More Atlantic predators might move northwards and target the larger individuals of *Calanus* (Varpe et al., 2015).

### 1.5.3 Increased terrestrial run-off

The Greenland ice sheet is melting, especially on the eastern side, and the meltwater drains into the fjords of Northeast Greenland (Mattingly et al., 2023). This increases in terrestrial run-off that brings organic carbon and inorganic particles from land. In addition to altering the light availability through increased turbidity, the run-off is fresh and will decrease the salinity. In Northeast Greenland it can be assumed a lot of this run-off will come from melting glaciers. The effect of this on nutrient concentrations is very dependent on where the freshwater is introduced in the water column.

The sparkling blue marine terminating glaciers have sub-glacial run-off where fresh water enters the fjord from beneath the glacier. This has been recorded to cause upwelling of nutrients from the sea floor and increases primary production (Meire et al., 2017). On the other hand, run-off from land terminating glaciers trickles down over the ground, collecting dissolved and particular organic carbon, as well as other particles before it gathers as a fresh lid of murky water at the surface of the fjord.

As the surface becomes more fresh and warm, a more stable pycnocline will establish, which again permits mixing processes from renewing nutrient concentrations in the euphoric zone. Lower nutrient concentrations are favorable by smaller celled picoplankton, at the expense of the larger celled algae like diatoms (Li et al., 2009). Bacterial degradation of organic carbon may also compete for nutrients, especially in the case of light limitation, shifting the food web from autotrophic to heterotrophic pathways (Thingstad et al., 2008). In Young Sound, a fjord in Northeast Greenland, a gradient in the balance between heterotrophy and autotrophy was found between inner to outer fjord, because of higher turbidity and stratification in the inner part (Sejr et al., 2022). The phytoplankton community composition displayed a clear trend, where the inner parts of the fjord were dominated by ciliates and other heliozoans, while diatoms were the dominating taxa towards the fjord mouth.

*Calanus* can also feed on protists such as ciliates, but this microbial pathway is much less direct than the classical diatom-copepod link (Thingstad et al., 2008). This can have bottom-up effects, as energy is lost though respiration at each trophic level. *Calanus* also feed more efficiently on larger cells. A transition to more cells below 10 $\mu\ m$ have been shown to decrease the *Calanus* community grazing and lower *Calanus* biomass (Middelbo et al., 2018).

A reduction in *Calanus* biomass would also affect other ecosystem functions held by *Calanus*, in addition to being an important trophic link. The efficient filter feeding of *Calanus* is very sloppy, and it has been estimated that just about half of the carbon from *Calanus* prey is actually ingested, the

other half is transformed to dissolved organic carbon which supports the microbial foodweb (Møller et al., 2003). Because of the large size of *Calanus*, compared to other copepods, their faecal pellets are also larger, making them sink faster to the seafloor than phytoplankton aggregates. In this manner, the ability of *Calanus* to condense carbon supports the biological carbon pump.

## 1.6 This study

*Calanus* ability to accumulate lipids is crucial for individual survival through diapause through the polar night and as a trophic link in the arctic pelagic ecosystem, and therefore an interesting subject to investigate. The total lipid content can be estimated visually by measuring the *Calanus* lipid sac (**?**). Individuals of *Calanus* were photographed *in situ* with the Video Plankton recorder (VPR) and with a camera connected to a stereo microscope after being collected with a WP-2 net. Both methods have its advantages. Individuals recorded with the VPR can be directly linked to depth. Collecting the individuals with the WP-2 net makes it possible to record copepepodite stage and determine the species from DNA analyses.

Lipid content in *Calanus* spp. overwintering stages was investigated in three different fjords, as well as two shelf stations, during the autumn (August/September) in Northeast Greenland. The study is done within a limited time frame, and the state of *Calanus* lipids and fjord variables before and after this seasonal snapshot is unknown. The variables recorded in the fjord were bottom topography, presence of a marine/land terminating glacier, water masses, nutrient and chlorophyll *a* concentrations, protist and zooplankton community composition, the vertical distribution of *Calanus* as well as stage and species composition of the *Calanus* complex.

Studies in Svalbard waters have found a uniform accumulation of lipid with size for all *Calanus* within similar size-ranges Renaud et al. (2018). It is expected that the *Calanus* in Northeast Greenland follow the same pattern.

**Hypothesis 1: Lipid content relative to size (lipid fullness) is independent of species.**

Seasonal development in the Arctic pelagic ecosystem is characterized by peaks in ice algae and phytoplankton biomass in spring, followed by a peak in zooplankton biomass towards autumn (Daase et al., 2021). It has been found that the most lipid rich individuals are the first to seasonal migrate (Bailey, 2010).

**Hypothesis 2: Deep-dwelling individuals will have a higher lipid fullness than individuals residing in the surface.**

Different stations have different environmental factors and could be at a different stage of the seasonal development. This is expected to cause differences in *Calanus* lipid content between different locations.

Earlier ice break up and prolonged ice free seasons will lengthen the open water period and therefore increase primary production (Slagstad et al., 2015). As this study looks at several fjords, where the time of ice break up can be obtained through satelite images, there is expected to be a difference between the fjords in the period between ice break up and sampling.

**Hypothesis 3A: Earlier ice break up increases lipid content in *Calanus*.**

There will be more energy preserved as lipid in a system of bigger sized *Calanus* . As lipid content in *Calanus* spp. has been modelled to have an exponential relation to size (Renaud et al., 2018), more lipids will be stored in a *Calanus* community consisting of fewer large individuals rather than multiple small. Atlantic water bring smaller *C. finmarchicus* (Aarflot et al., 2018) which will shift the *Calanus* complex towards less total lipid stored in *Calanus* lipid sacs.

**Hypothesis 3B: Inflow of Atlantic water decreases the total lipid stored in *Calanus* spp.**

Terrestrial run-off has been causing more particles in the water, which causes higher turbidity. This has been observed to cause a shift from autotrophic to heterotrophic production in Young Sound (Sejr et al., 2022). Bacteria, which utilizes nutrients and organic carbon for growth, are very small. They are eaten by flagellates, which are again eaten by larger protists, such as ciliates, before they can get consumed by *Calanus*, which have a lower size-limit for prey at 10 $\mu m$ (Levinsen et al., 2000). When the nutrients are incorporated in this microbial food chain instead of the classical nutrient-diatom-copepod chain, less energy will reach *Calanus*, since energy is lost at each trophic level.

**Hypothesis 3C: Higher turbidity will decrease total lipid stored in *Calanus* spp.**

Large celled diatoms are thought to be abundant during the Arctic spring bloom as it is characterized by a high concentration of nutrients in the euphotic zone (Daase et al., 2021). *Calanus* feed efficiently on these large phytoplanktons, and the direct link in carbon flow looses little energy to respiration. As diatoms have a lower surface to volume ratio than smaller cells, like picoplankton, they might lose the competition for resources when nutrients are limited.

**Hypothesis 3D: High initial nutrient concentrations would have made conditions favourable for large celled diatoms, which would increase the amount of nutrient taken up in diatoms (strengthen the nutrient-diatom link) and increase total lipid stored in *Calanus* spp.**

# 2 Material and methods

## 2.1 The TUNU program

This master thesis is a part of the TUNU program at UiT. The aim of this long term research program is to broaden the knowledge for Northeast Greenland fisheries. Previously, the main focus was fish diversity and adaptations. In the later years benthos invertebrates, geology and zooplankton have become an integrated part. The expedition leader for the TUNU-VIII expedition was Arve Lynghammer, but the program has previously been led by Prof. Jørgen Schou Christiansen. The expedition team at the TUNU-VIII expedition is pictured in Fig. 1.

Figure 1: The team of the TUNU-VIII expedition to Northeast Greenland onboard RV Kronprins Haakon.

## 2.2 Study site

The data were collected during the TUNU-III expedition to Northeast Greenland 25.Aug - 9.Sept 2022 with RV Kronprins Haakon. Data used in this master thesis was mainly collected at eight locations along the coast of Northeast Greenland (Table.1 and Fig.2). These stations can be divided into four subareas. The three first subareas are fjords systems, while subarea 4 consists of two stations on the shelf.

Table 1: The name, subarea, date, time [UTC] (of CTD, WP-2 plankton and video plankton recorder), position and depth of the sampling locations used in this thesis.

| Station name | Date | Time CTD | Time WP-2 | Time VPR | Latitude | Longitude | Bottom depth[m] | Subarea |
|---|---|---|---|---|---|---|---|---|
| Dove Bugt | 29.08.22 | 09:09 | 13:37 | 12:18 | 76,733 | -19,296 | 226 | 1 |
| Besselfjord C | 30.08.22 | 06:04 | 10:09 | 11:50 | 75,977 | -20,313 | 447 | 1 |
| Besselfjord A | 31.08.22 | 06:10 | 08:40 | 10:33 | 75,970 | -21,696 | 231 | 1 |
| Breddefjord | 02.09.22 | 19:16 | 00:46 | 22:28 | 75,557 | -21,663 | 564 | 2 |
| Ardencaple | 03.09.22 | 11:36 | 13:15 | 09:10 | 75,099 | -19,867 | 343 | 2 |
| Eskimones | 04.09.22 | 06:22 | 10:47 | 08:25 | 74,068 | -21,468 | 416 | 3 |
| 76°North Bank | 28.08.22 | 19:43 | 14:17 | 14:53 | 75,971 | -16,455 | 70 | 4 |
| Davy Sund | 05.09.22 | 06.02 | 09:16 | 08:00 | 72,0812 | -20,758 | 210 | 4 |

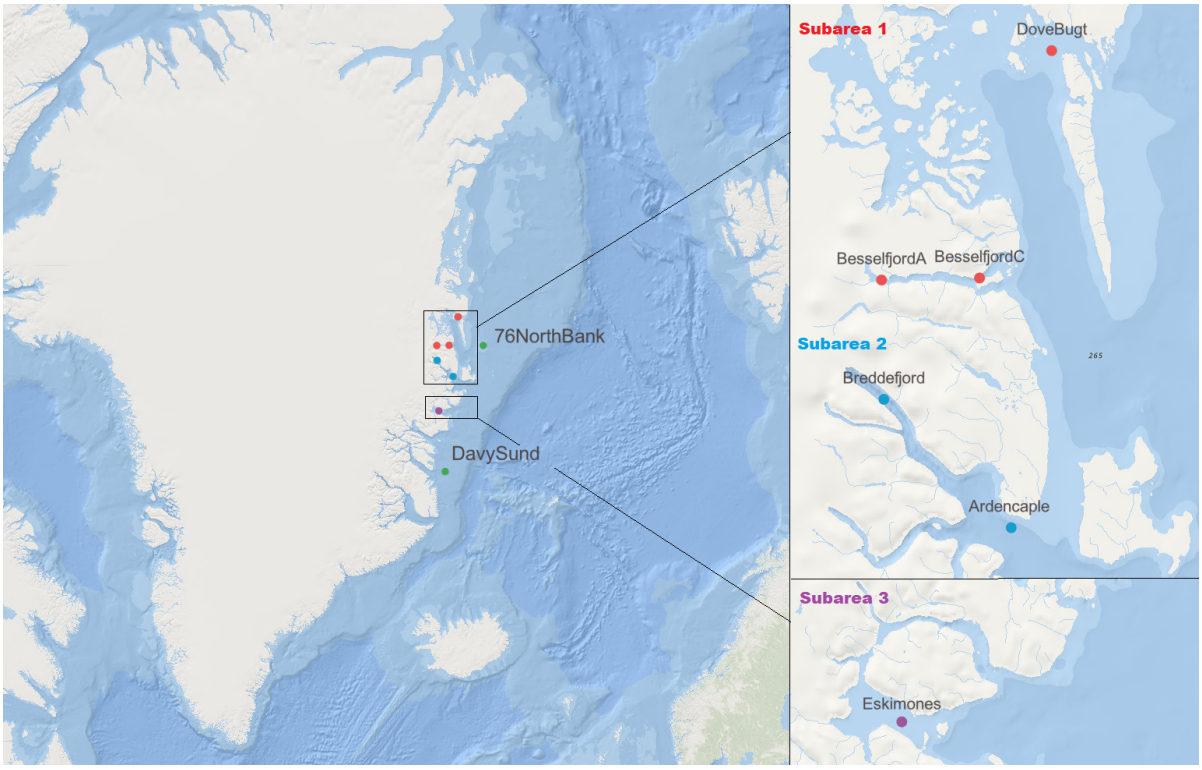


Figure 2: Map over the study area and the 8 stations (Table 1). The stations are divided into four subareas. Subarea 1 (red), 2 (blue) and 3 (purple) are fjord systems, while subarea 4 (green) consists of two stations on the shelf. The map is created using online ArcGIS® software by Esri.

Figure 3: Glacier in the bottom of Besselfjord. Photo is taken by Birgitte Rubæk.

### 2.2.1 Subarea 1: Dove Bugt and Besselfjord

The northernmost subarea is the large embayment Dove Bugt. Dove Bugt is confined from the north by the island Store Koldewey. Outside of Store Koldewey there was close drift ice. In Dove Bugt there was very open drift ice which became close drift ice towards the east and the mainland. The islands on the left side of the bay, Fig 2, were covered with ice. Dove Bugt is an outflow-pathway for the glacier Storstrømmen which is connected to the Greenland ice sheet (Arndt et al., 2015).

The bay is connected to the shelf by the deep cross-shelf Dove Bugt Through (Arndt et al., 2015). Water of Atlantic origin is flowing into the bought below 250 m depth (Rignot et al., 2022). In southern Dove Bugt the W-E orientated Besselfjord is positioned. Besselfjord has several basins separated by shallow sills (Zoller, 2020). There is still a glacier in the bottom of Besselfjord, see Fig. 3. It is a bit unclear whether this glacier is land or marine terminating, but it at least partly land terminating. In addition to the glacier at the head of the fjord, there are outlets from the Greenland ice cap, depicted in (Zoller, 2020).

Figure 4: Marine-terminating glacier in the bottom of Breddefjorden. Photo is taken by Birgitte Rubæk.

### 2.2.2 Subarea 2: Breddefjord and Ardencaple

Breddefjord is a deep fjord with more than 550 m depth which is separated from the coast by shallow sills (Arndt et al., 2015). The fjord is surrounded by steep mountains and has a marine terminating glacier (Fig. 3). Hochstettebugten Trough is connected to the fjord. Hochstetterbugten Trough has a reverse slope with a depth of about 300 m at the shelf and have a downward slope that go to 450 m depth before the sill at the entrance of Breddefjord. It merges with Dove Bugt Trough at the continental shelf.


Figure 5: Map over the area around Eskimones. The station sampled was in "Godthaabs Golf". The map is a section from the lager map called "Eskimoæs" by Army Map Service (AMSC), Corps of Engineers, U.S. Army (1952).

### 2.2.3 Subarea 3: Eskimones (Eskimonæs)

Eskimonæs has a long history in the European exploration of Northeast Greenland (Wordie et al., 1930). The actual place "Eskimonæs" is situated south on the island Clavering Ø (Army Map Service (AMSC), Corps of Engineers, U.S. Army (1952)). The sample location was in Godthaabs Golf, near Eskimonæs. Godhaabs Golf is connected to Copelands fjord (Fig. 5). In the entrance to the sampling location there were islands, Finch Øer. There was open water at the sampling location, with several icebergs floating around. The huge glacier Wordies Gletscher terminates into Wordies Bugt, which is connected to Godthaabs Golf. The fjord "Young Sound" is located north of Clavering Ø. The settlement Daneborg is located in the mouth of this fjord. Daneberg is the headquarters of the Danish Arctic special force "Siriuspatruljen". The University of Aarhus in Denmark have a long term marine research station in Young Sund, as a part of the Zackenberg Station.

### 2.2.4 Subarea 4: On the shelf - 76°North Bank and Davy Sund

76°North Bank and Davy Sund have a large geographical distance, but both locations are expected to be strongly affected by the ocean currents at the shelf. 76°North Bank is only 70 m deep, and is

a shallow bank north of the deep cross-shelf Dove Bugt Through. Davy Sound has a depth of 210 m (Table 1) and is located much further south (Fig. 2). It is located right outside the mouth of the fjord "Davy Sund" (Wordie et al., 1930). There was lot of sea ice was present when sampling at 76°North Bank and open water at Davy Sund.

#### 2.2.5 Past Sea ice conditions in Subarea 1-3

The TUNU-VIII expedition was set to late August/September, within the period of minimum ice coverage. However, the previous ice conditions during the spring would probably have had a large influence on the fjord biology. Ice maps made by Danish Meteorological Institute (2022) were used to roughly backtrack the timing of ice break up in the different fjords.

There was land fast ice at all fjord stations until $6^{th}$ of July. The southernmost station, Eskimones, was the first station to break up to very close dift ice $10^{th}$ of July, which later broke up to very open drift ice $17^{th}$ of July. Breddefjord followed with a change from land fast to close drift ice $17^{th}$ of July, and there was registered open water $10^{th}$ of August. In the northernmost fjord, Besselfjord, the land fast ice was present to $3^{th}$ of August, before it transitioned to open water $14^{th}$ of August. There was open drift ice present in Dove Bugt until $21^{th}$ of August, only one week before our arrival.

### 2.3 Hydrography and Swath bathymetry

Salinity and temperature were measured by the ship CTD (Seabird911plus, Seabird Electronics Inc., USA) and vertical profiles of theese parameters were made with Matlab (custom script by Norrbin, calling the function floataxis.m by Blair Greenan, Bedford Institute of Oceanography). Swath bathymetry in Besselfjorden and Breddefjorden was mapped by a Kongsberg Maritime Simrad EM 302 multibeam echo sounder. Petrel software was used to grid the data and transects were made using Global Mapper 18. Data were collected both during this TUNU-VIII expedition, and on the previous TUNU expedition on RV Helmer Hansen in 2017, described in Zoller et al. (2023).

Transects with bathymetry displaying salinity and temperature were made using R-studio (R Core Team, 2022). Spatial interpolation between the CTD data points was done using Multilevel B-spines through the MBA package (Finley et al., 2022) which relies on the underlying code developed by Hjelle (2001) from Lee et al. (1997). The transects were visualised using the ggplot2 package (Wickham, 2016). Other packages used were tidyverse (Wickham et al., 2019), lubridate (Grolemund and Wickham, 2011), mgcv (Wood (2011), Wood et al. (2016), Wood (2004), Wood (2017), Wood (2003)) and "reshape2" (Wickham, 2007).

### 2.4 Chlorophyll *a* and nutrient concentrations

Seawater was collected from the Niskin bottes on the CTD rosette at several depth intervals, as well as Chl *a* max (Table 2). Chl *a* max was determined on the downcast of the CTD by an attached

fluorescence sensor (WET Labs Fluometer).

Table 2: Depth at which water samples were taken.

| **Station** | **Nultrients and Chl*a* sample depths [m]** | **Chl *a* max [m]** |
|---|---|---|
| Besselfjord A | 1, 5, 10, 20, 40, 69, 100, 200, 226 | 33 |
| Besselfjord C | 1, 5, 10, 20, 40, 60, 100, 200, 440 | 34 |
| Dove bugt | 1, 5, 10, 20, 40, 60, 100, 200, 224 | 21 |
| Breddefjord | 1, 5, 10, 20, 40, 60, 100, 200, 300, 569 | 38 |
| Ardencaple | 1, 5, 10, 20, 40, 60, 100, 200, 335 | 40 |
| Eskimonæs | 1, 5, 10, 20, 40, 60, 100, 200, 409 | 28 |
| 76°North Bank | 1, 5, 10, 20, 40, 60, 63 | 32 |
| Davy Sund | 1, 5, 10, 20, 40, 60, 100, 200 | 45 |

To sample nutrients from the Niskin bottle, plastic test tubes were rinsed with seawater, filled and immediately frozen at -20°C. The concentrations of nitrate+nitrite, phosphate and silicate were later analysed on the lab. All the nutrients were measured in triplicates using the QuAAtro 39 (SEAL Analytical, Germany) which employs standard colorimetric methods. Calibration of the instrument was verified using reference nutrient seawater standards (Ocean Scientific International, Ltd., United Kingdom). The protocols used to measure nutrient concentrations were: no. Q-068-05 rev. 12 for nitrate (detection limit = $0,02\ \mu\ mol\ L^{-1}$), no. Q-068-05 rev. 12 for nitrite (detection limit = $0,02\ \mu\ mol\ L^{-1}$), no. Q-066-05 rev. 5 for silicate (detection limit = $0,02\ \mu\ mol\ L^{-1}$), and no. Q-064-05 rev. 8 for phosphate (detection limit = $0,02\ \mu\ mol\ L^{-1}$). Data analysis was done using the software AACE (SEAL Analytical, Germany).

Water for Chl *a* was collected with a 2 l plastic bottle, rinsed two times with the seawater. Three replicates of 650 ml were filtered onto GF/F filters with 0,7 $\mu\ m$ pore size (GE Healthcare, Dassel, Germany). The filters were folded, placed in plastic tubes and the tubes were wrapped in aluminum-foil and stored at -80°C until analysis. Back at UiT the samples were taken out of the freezer and 5 ml metanol was added to each tube. The aluminium-foil wrapped tubes were stored in the fridge for 12–24 hours. To assure room temperature when measured, the samples were taken out of the fridge about one hour before analysis. The filter was removed with tweezers and the metanol-mixture were mixed with a vortex mixer. 1 ml of the mixture was added into a cuvette. The cuvette surface was cleaned with a tissue and placed in a Turner 10-AU Fluorometer (Turner Designs, Cal., USA). The result was given in RFU (raw fluorescence unit). Two drops of 5% HCI were added to the cuvette before it was covered with parafilm, to prevent leakage, and mixed by turning the tube upside down. The acid broke Chl *a* into phaeophytin (which is a degraded form of Chl *a*). The fluorescence was measured again. The method described in Parsons (2013) were used to calculate the concentration of Chl *a*.

## 2.5 Plankton community

### 2.5.1 Protist community

Samples for phytoplankton species identification were collected from 5 m and chlorophyll max (Table 2). Seawater was collected in 100 ml dark glass bottles fixated with acidic Lugol's solution before being stored in a dark and cold place. The Utermöhl method (Karlson et al., 2010) was used when counting protist cells. 25 ml sample were sedimented onto a sedimentation plate holding 3 ml. A Nikon Eclipse Ti inverted microscope was used to identify and count the protist cells and determine the main taxa.

### 2.5.2 Zooplankton community

Zooplankton community samples were taken with a modified WP-2 net with an inner diameter of 0,56 m and 85 $\mu$m mesh size (Norrbin, 1996). The net was lowered down to about 5–10 m above the bottom with a speed of 0,5 $m \cdot s^{-1}$ and pulled up with a speed of 0,25 $m \cdot s^{-1}$. Seawater was used to rinse the net gently to concentrate the organisms in the cod end. There was no apparent clogging from algae or detritus, so the filtered water volume is given by Equation 1. The cod end was transferred to a bucket where individuals of *Calanus* spp. for the estimation of lipid content were picked out with pipettes and spoons. The rest of the sample was concentrated and fixated with a mixture of 4 % formaldehyde and 10% 1,2-propandadiol buffered with sodium tetraborate.

$$\text{Water volume}[m^3] = \text{Wire length}[m] \cdot (\frac{\text{Net diameter}[m]}{2})^2 \cdot \pi \tag{1}$$

Zooplankton was identified and counted using a Leica M205C stereo microscope (Leica Microsystems GmbH, Wetzlar, Germany) with species identification according to WoRMS (WoRMS Editorial Board, 2023). Most individuals were identified to genus, except some individuals where species-level identification was possible. The sample was diluted to 1-2 l and stirred in a figure-8 pattern before subsamples were taken out with a small beaker. At least 500 individuals were counted for each sample, more if certain taxa strongly dominated.

The total abundance in the sample is calculated by Equation 2 where X is the total individuals in the sample, n is the individuals counted and "subsample fraction" is the fraction of the total sample that is counted.

$$X = \frac{n}{\text{Subsample fraction}} \tag{2}$$

Abundance per square meter ($m^2$) was calculated by Equation 3 by multiplying the abundance per $m^3$ with the depth of sampling. As it is assumed the net was pulled vertically from the bottom, the depth of sampling equals the wire length.

$$\text{Abundance } [ind \cdot m^{-2}] = \frac{X[ind]}{\text{Water volume}[m^3]} \cdot \text{Wire length}[m] \tag{3}$$

## 2.6 Species and stage composition of *Calanus* spp.

The stage, morphological characteristics, prosome and urosome length were recorded in 100–150 individuals per sample. Individuals were determined to copepodite stage or adult females from number of urosome segments (Table 3). Absolute abundances were estimated similarly to other taxa, described in section 2.5.2. Individuals removed for live photography were added to the estimation of absolute abundances. Due to the controversies around distinguishing *C. finmarchicus* and *C. glacialis* based on size, the two species were not initially separated. The possibility to separate the two species based on prosome length is explored in section 2.6.4. Individuals selected for lipid estimation were determined to *C. finmarchicus* or *C. glacialis* by DNA analysis, described in section 2.6.2. *C. hyperboreus* was identified morphologically since it could not be identified using the applied DNA analysis method, see more in section 2.6.3.

Table 3: Stage descriptions to distinguish different copepodite stages and prosome length range ($\mu$m) of the three species *C.finnmarchicus*, *C. glacialis* and *C. hyperboreus*.
(Modified from (Daase and Eiane, 2007).)

| Stage | #swimming legs | #urosome segments | #prosome segments | C.finnmarchicus | C.glacialis | C.hyperboreus |
|---|---|---|---|---|---|---|
| **CI** | 2 | 2 | 3 | <810 | 810-900 | >900 |
| **CII** | 3 | 2 | 4 | <1170 | 1170-1350 | >1350 |
| **CIII** | 4 | 2 | 5 | <1470 | 1470-1950 | >1950 |
| **CIV** | 5 | 3 | 5 | <2010 | 2010-2910 | *(>2910) |
| **CV** | 5 | 4 | 5 | <2937 | >2937 | *(>4000) |
| **Adult female** | 5 | 4 (5 for males) | 5 | <3240 | >3240 | *(>4500) |
| * identified by characteristic spike on $5^{th}$ thoracic segment. | | | | | | |

### 2.6.1 Prosome length of *Calanus* spp. at different stations

Prosome length was measured for both live individuals and individuals fixated in formalin:1,2-propanediol. It is assumed that the fixation caused negligible changes in the prosome length. The total number of measured individuals per station, species and stage was recorded for each station (Table 4).

Notably, individuals were not randomly selected for the live photography, but rather picked from the entire sample. This approach might have resulted in larger individuals being measured more frequently, possibly skewing the data towards higher abundances of larger individuals. The selection of larger individuals for live photography was intentional, as the goal was to measure lipid content of overwintering stages, CIII, CIV and CV. This potential bias could have been avoided by removing all *Calanus* spp. individuals in a subsample, or selecting individuals for live photography from a different net sample.

### 2.6.2 Species identification of *C. finmarchicus* and *C. glacialis* based on DNA analysis

Sequencing of the individual's DNA is the most certain way to separate *C. glacialis* and *C. finmarchicus* (Choquet et al., 2018). Individuals of *Calanus* spp. selected from the WP-2 net sample for photographing

Table 4: Number of *Calanus* spp. individuals for which prosome length was measured, categorized by station, species and stage.

| **Stations** | **Species** | | | | | | | | | | | **Sum** |
|---|---|---|---|---|---|---|---|---|---|---|---|---|
| | ***C.finmarchicus/C.glacialis*** | | | | | | ***C.hyperboreus*** | | | | | |
| | **CI** | **CII** | **CIII** | **CIV** | **CV** | **AF** | **CII** | **CIII** | **CIV** | **CV** | **AF** | |
| BesselfjordA | - | - | 3 | 3 | 49 | 16 | - | 4 | 33 | 35 | 13 | 156 |
| BesselfjordC | 1 | 2 | 6 | 10 | 26 | 14 | - | 35 | 49 | 44 | 18 | 205 |
| Dovebugt | - | - | 7 | 11 | 44 | 6 | - | 68 | 26 | 17 | 1 | 180 |
| Breddefjord | - | - | 5 | 23 | 31 | 9 | 2 | 49 | 34 | 21 | 7 | 181 |
| Ardencaple | - | - | 4 | 15 | 57 | 10 | - | 19 | 42 | 12 | 7 | 166 |
| Eskimones | - | 1 | 25 | 43 | 35 | 5 | - | 18 | 43 | 17 | 3 | 190 |
| 76NorthBank | - | 1 | 11 | 21 | 49 | 16 | - | 55 | 33 | 28 | 9 | 223 |
| DavySund | - | 10 | 33 | 53 | 32 | 17 | - | 13 | 14 | 1 | - | 173 |
| Sum | 1 | 14 | 94 | 179 | 323 | 93 | 2 | 261 | 274 | 175 | 58 | **1474** |

and lipid estimation were frozen individually for subsequent DNA analysis.

The HotSHOT method described by Montero-Pau et al. (2008) was used to extract DNA. The *Calanus* spp. individuals were transferred to separate, labelled wells filled with 50 $\mu$l Alkaline lysis buffer, which was put on ice to keep a cold temperature. The wells were covered with strip caps, quickly centrifuged and heated for 30 min at 95°C. After the solution had cooled down there was added 50 $\mu$l of naturalizing solution.

To separate between the two species, the method developed by Smolina et al. (2014), and validated by Choquet et al. (2017), with the marker G-150 was used. The PCR master mix was made with 54$\mu$l Tough mix, 0,5$\mu$l G-150F, 0,5$\mu$l G150R and 3.3$\mu$l distilled water. 9,3 $\mu$l of the master mix solution was distributed into new strip tubes and 2,5 $\mu$l extracted DNA was added to each tube. The samples were briefly centrifuged before undergoing a sequence of 2 min at 94°C. This was followed by 35 cycles of 10 s at 94°C, 10 s at 55°C and 10 s at 72°C. After that, they were finishing with 5 min at 72 °C. 3 $\mu$l DNA gel loading dye was added to each sample before electrophoresis.

2% agarose gel was prepared. DNA from reference individuals of *C. finmarchicus* and *C. glacialis* were added in the two first wells. Samples were added in the other wells. Electrophoresis was run at 80V for 60 minutes and gel images taken and assessed for species by visually comparing the samples to reference DNA.

### 2.6.3 Identification of *C. hyperboreus*

*C. hyperboreus* is often identified from a spike on the $5^{th}$ thoracic segment from copepodite stage CIV. There is individual variation in how apparent this spike is. Under examination in the stereo microscope, the individuals were separated between a clear spike, a slight spike and no spike. The prosome length of every individual were measured to compare if the occurrence of a spike on the $5^{th}$ thoracic segment corresponded with certain size classes for *C. hyperboreus* described in table 3.

### 2.6.4 Species identification of *C. finmarchicus* and *C. glacialis* based on size

Prosome length was measured both on individuals separated by DNA analysis and for 100-150 *Calanus* spp. additional *Calanus* individuals from each station. Differences in the prosome length between the different species may be confirmed from correspondence with the prosome length in individuals identified to species with DNA analysis.

## 2.7 Photography and estimation of lipid content in live *Calanus* spp. spp.

Individuals of *Calanus* spp. were picked out of the zooplankton net sample before fixation. Each individual was placed inside a drop of water on a microscope slide and photographed with a calibrated Motic-camera connected to a Stereo microscope (Zeiss, Stemi 305 trino, Oberkochen - Germany) from a lateral position. For each magnification, the camera was calibrated with a calibration slide. Photographed individuals were preserved individually in cryogenic storage vials filled with 80% ethanol and stored at -80°C until DNA extraction.

Measurements were taken from the pictures of copepods with the program ImageJ (Schneider et al., 2012). Pixel-to-$\mu$m ratio was estimated using pictures of the calibration slide for each magnification. Several different measurements were taken; length and width of the prosome and lipid sac, length of the urosome and the area of the prosome and lipid sac (Fig. 6).

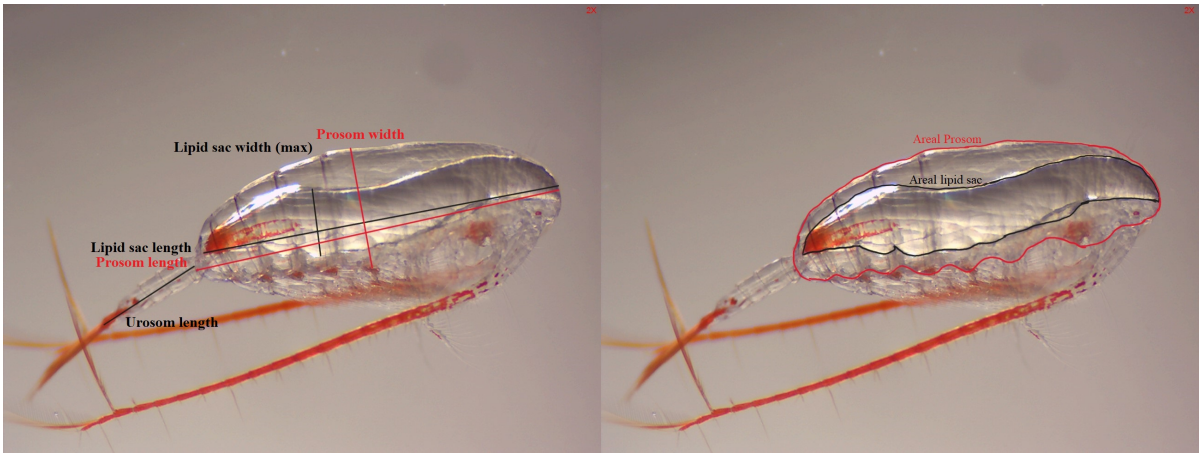


Figure 6: Measurements taken of *Calanus* spp. from a lateral position through a stereo microscope. A) Length and width of the lipid sac, prosome and length of the urosome. B) The lipid sac area and prosome area.

Lipid sac area is used as a proxy for individual lipid content, as it is the most direct measure of the lipid sac in a two-dimensional picture. Prosome area was used as a proxy for the individual size. Because the main incentive of this thesis is to explore if the relative amount of lipid per individual in overwintering stages, the adult females were excluded from further analysis. The adult females would already have started to utilize the lipid storage for reproduction and are expected to die before the winter.

A parametric model was chosen to estimate the function between the predictor (prosome area, PA) and response variable (lipid sac area, LA) as a fairly small number of data points were available. The logarithmic transformed variables appeared to have a linear relation, so a linear regression model was chosen to estimate the effect of prosome areal on lipid sac areal, Equation 4.

$$\ln(LA) = \beta_0 + \beta_1 \cdot \ln(PA) \tag{4}$$

The coefficients $\beta_0$ and $\beta_1$ are the intercept and slope of the linear regression between logarithmic transformed lipid areal (LA) and prosome areal (PA). If we solve Equation 4 for LA, there appears a exponential relationship between LA and PA (Equation 5).

$$LA = e^{\beta_0} \cdot PA^{\beta_1} \tag{5}$$

When the sample was separated into both species and copepodite stages, a small and uneven sample size was left for testing differences between lipid content at different location (Table 5).

Table 5: Number of individuals photographed and measured from the WP2 net sample.

| **Stations** | **Species** | | | | | | | | | | | **Sum** |
|---|---|---|---|---|---|---|---|---|---|---|---|---|
| | ***C. finnmarchicus*** | | | ***C.glacialis*** | | | | ***C.hyperboreus*** | | | | |
| | **CIV** | **CV** | **AF** | **CIII** | **CIV** | **CV** | **AF** | **CIII** | **CIV** | **CV** | **AF** | |
| Besselfjord A | - | 7 | 2 | - | - | 12 | 1 | 1 | 16 | 10 | 3 | 52 |
| Besselfjord C | - | 1 | - | - | 3 | 8 | 2 | 5 | 20 | 15 | 2 | 56 |
| Dove Bugt | - | 1 | - | - | 1 | 12 | 2 | 1 | 6 | 5 | - | 28 |
| Breddefjord | - | - | 1 | - | 6 | 8 | 1 | 2 | 12 | 4 | - | 34 |
| Ardencaple fjord | - | 6 | 1 | - | 5 | 8 | 1 | - | 8 | 3 | - | 32 |
| Eskimonæs | 1 | 2 | - | - | 5 | 4 | - | 1 | 12 | 4 | 1 | 30 |
| 76°North Bank | 1 | 3 | 1 | 3 | 6 | 25 | 6 | 2 | 13 | 9 | 5 | 74 |
| Davy Sund | - | 2 | - | 3 | 9 | 2 | - | - | 4 | - | - | 20 |
| **Sum** | 2 | 22 | 5 | 6 | 35 | 79 | 13 | 12 | 91 | 50 | 11 | 326 |

Since the regression on species-level showed an acceptable fit, it was adapted as an average growth curve, accounting for the size differences across various copepodite stages. With this model now capturing the variation in lipid sac area due to differences in prosome area, I proceeded to explore the potential impact of station by introducing it as an additional explanatory variable in the regression. A station's effect would be considered significant if there was no overlap between the 95% confidence interval between the station's intercept coefficient ($\beta_0$) (Equation 4). This approach allowed for larger sample size, as all copepodite would be considered. However, it also assumes that individuals at the different stations follows the same growth curve between lipid sac area and prosome area (similar $\beta_1$ ).

## 2.8 Vertical abundance and *in situ* lipid content measurement with Video Plankton Recorder (VPR)

The Video Plankton recorder (VPR, Seascan inc., USA) was used to detect the vertical distribution of *Calanus* spp. and visually determine lipid-content in the copepods. The VPR was equipped with a camera and strobe illumination, recording ca 20 images (frames) per s (Fig. 7). It was moved vertically up and down in the water column at a wire speed of 0,8-1,0 $ms^{-1}$, recording zooplankton *in situ*. An SBE49 CTD("Fastcat", Seabird Electronics inc., USA), and a fluorometer and turbidimeter (ECO Puck, WET Labs Inc., USA), attached to the VPR tow frame and recorded the environmental parameters for every image taken.

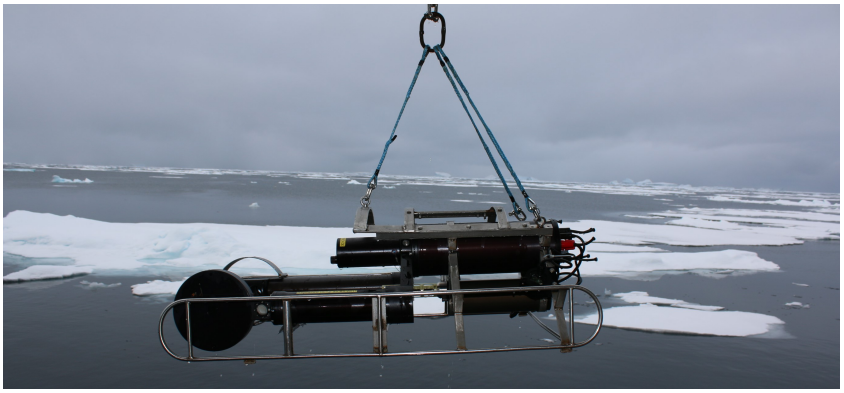

Figure 7: The video plankton recorder (VPR).

Regions of interest (ROIs) were extracted from the VPR data using the software Autodeck (Seascan Inc., USA). A ROI is a part of the frame where an object or organism are detected. The *Calanus* spp. could be photographed in any orientation, but only the individuals photographed in a lateral position were analysed further for lipid content. The vertical abundance of *Calanus* spp. was made from calculating the average number of individuals observed at a certain depth. The depth was then divided into depth-intervals, where the average number of individuals were calculated. The abundances are relative, where 1 is the highest density of *Calanus* observed in a depth interval at a station, so the different stations can be compared.

ImageJ (Schneider et al., 2012) was used to take measurements of the prosome length, width and area of the prosome and lipid sac, as well as the length of urosome when possible (Fig. 8). Difference in lipid content between stations was estimated, similarly to investigations of the individuals collected by WP-2 net in section 2.7. A multiple linear regression was fitted between the logarithmic transformed response variable lipid sac area ($mm^2$) and explanatory variable prosome area ($mm^2$) for different sampling locations.

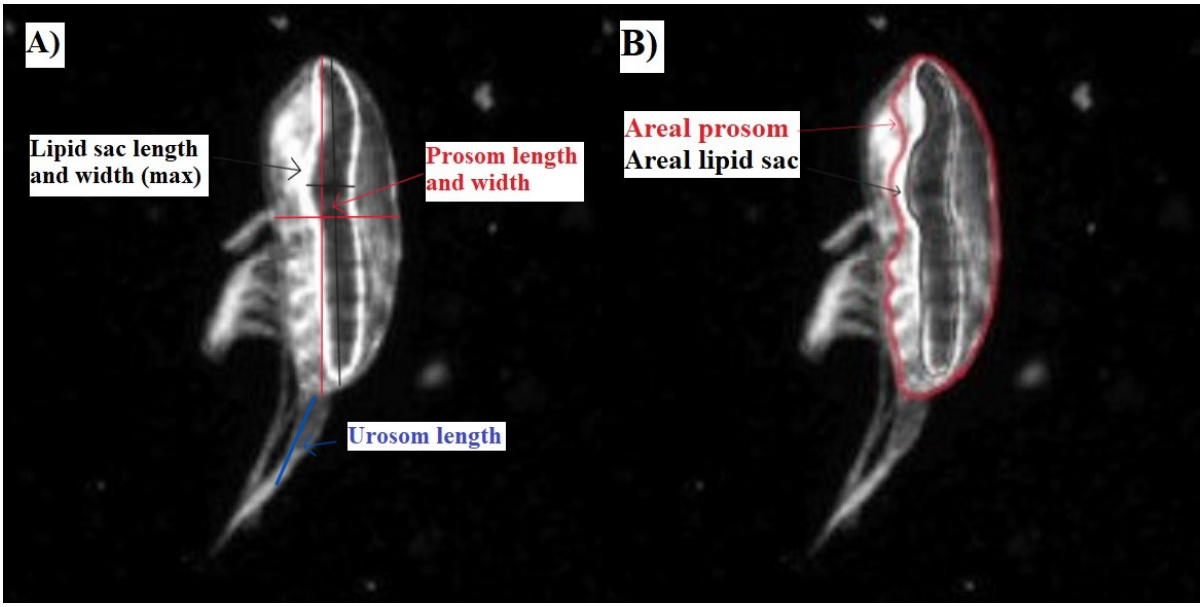


Figure 8: Measurements taken of *Calanus* spp. from a lateral position with the VPR. A) Length and width of the lipid sac, prosome and length of the urosome. B) The lipid sac area and prosome area.

### 2.8.1 Estimation of relative lipid fullness with depth

To assess the vertical distribution of individual lipid content independent of size, there was a need to make a proxy for individual lipid fullness. The chosen method is inspired by the methods used to account for *Calanus* size difference in Bailey (2010) and Baumgartner et al. (2011).

The coefficients ($\beta_0$ and $\beta_1$) fitted to the linear model between lipid sac areal and prosome areal (Equation 4) were used to estimate the expected lipid sac area ($\hat{LA}$) for the measured prosome area PA). The ratio between the measured lipid sac areal (LA) and expected lipid sac areal ($\hat{LA}$) was used as a proxy for relative lipid fullness (LF) (Equation 6). If the measured lipid sac area was larger than the expected lipid sac area, the relative lipid fullness (LF) would be above 1 ($LA > \hat{LA} \rightarrow LF > 1$), as well as the other way around ($LA < \hat{LA} \rightarrow LF < 1$).

$$LF = \frac{LA}{\hat{LA}} = \frac{LA}{e^{\beta_0} \cdot PA^{\beta_1}} \tag{6}$$

A two-sample independent t-test with significance level 0,05 was used to assess the difference in relative lipid fullness between individuals in the surface (upper 100 m) and deeper waters (below 100 m).

## 2.9 Estimation of Total lipid (TL) from lipid sac area

Total lipid (TL) in *Calanus* spp. can be estimated from lipid areal (LA) by Equation 7, (Vogedes et al., 2010).

$$\mathrm{TL} = 0,197\,\mathrm{A}^{1,38} \tag{7}$$

The Equation is derived from a linear regression of logarithmically transformed data on lipid sac area ($mm^2$) and total lipid ($mg$) obtained by gas chromatography. The estimation is based on 44 individuals of *C. finmarchicus*, *C. glacialis* and *C. hyperboreus*, stage CIV, CV and adult females(AF) collected around Svalbard. The model has a good fit with $r^2$=0,94. The values of lipid sac area used to estimate the model were in the same ranges as those measured in this study.

## 2.10 Other software used for statistics and data visualisation

All statistics and visualisation was done in RStudio (R Core Team, 2022). The dplyr package (Wickham et al., 2023) was used for data organisation. Data visualisation was done in the base packages in Rstuio and with the graphing package ggplot2 (Wickham, 2016). The figures were coloured with help from the packages colorspace (Zeileis et al., 2009) and RColourBrewer (Neuwirth, 2022).

# 3 Results

## 3.1 Hydrography and bottom topography

### 3.1.1 Water masses

There are two water masses advected into the Northeast Greenland shelf; Atlantic Water (AW) ($> 0°C$, $> 34,4$ PSU) and Polar Water (PW) ($< 0°C$, $< 34,4$ PSU) (Gjelstrup et al., 2022). A temperature-salinity diagram can be used to determine the presence of these water masses. PW was the main water mass at all sampling locations (Fig. 9). AW was recorded in Dove Bugt, Breddefjord, Ardencaple and Davy Sund. All stations, except Besselfjord C and 76°North Bank, had warm (>0°C) and fresh (PSU < 32) water, which is likely local surface water. The vertical profiles of salinity, temperature and fluorescence for all stations can be found in Appendix A (Fig. 33, 34, 35 and 36).

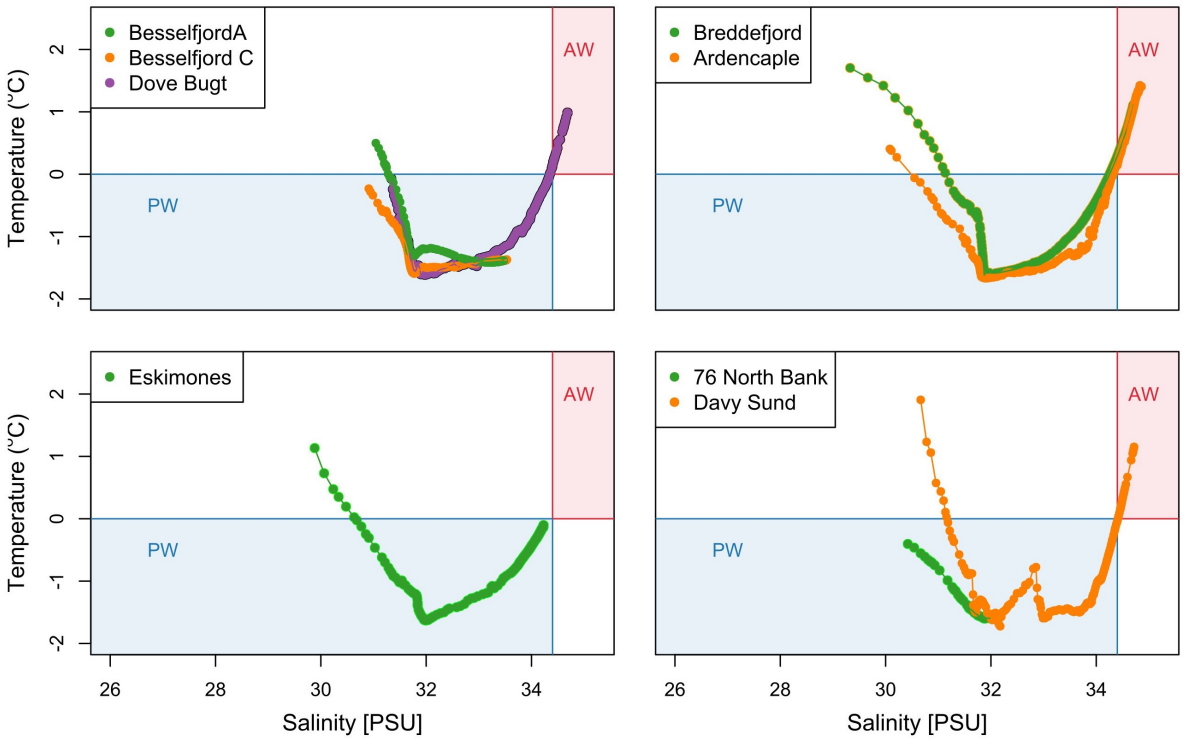


Figure 9: Temperature-Salinity diagram with boxes indicating Atlantic water (AW) and Polar water (PW). The water masses are defined in Gjelstrup et al. (2022).

### 3.1.2 Turbidity

A low turbidity, not exceeding 0,25 FTU for any station, was measured (Appendix B, Fig. 37). The highest turbidity was measured in the innermost station of Besselfjord and Breddefjord, as well as in Eskimones.

### 3.1.3 Bottom topography and fjord hydrography in Besselfjord and Breddefjord

Besselfjord has several shallow sills (-145 m at 12 km, -100 m at 33 km and -89 m at 52 km, 0 km is at the head of the fjord) separating three basins (Fig. 10). Besselfjord A is at the head of the fjord and Besselfjord C is sampled in the outermost, and deepest, basin. There was a body of AW (>34.4 PSU, > 0°C) in Dove Bugt (far right in Fig. 10), that was prevented from entering the fjord by the outermost sill. In addition to the shallow sill, there were islands between Besselfjorden C and Dove Bugt that limit the water flow (Fig. 2). A cold (-2°C) and a fresher (< 33 PSU) environment was observed inside Besselfjord. The water column was quite homogenous below a less saline layer (< 32 PSU) in the upper 100 m of the water column.

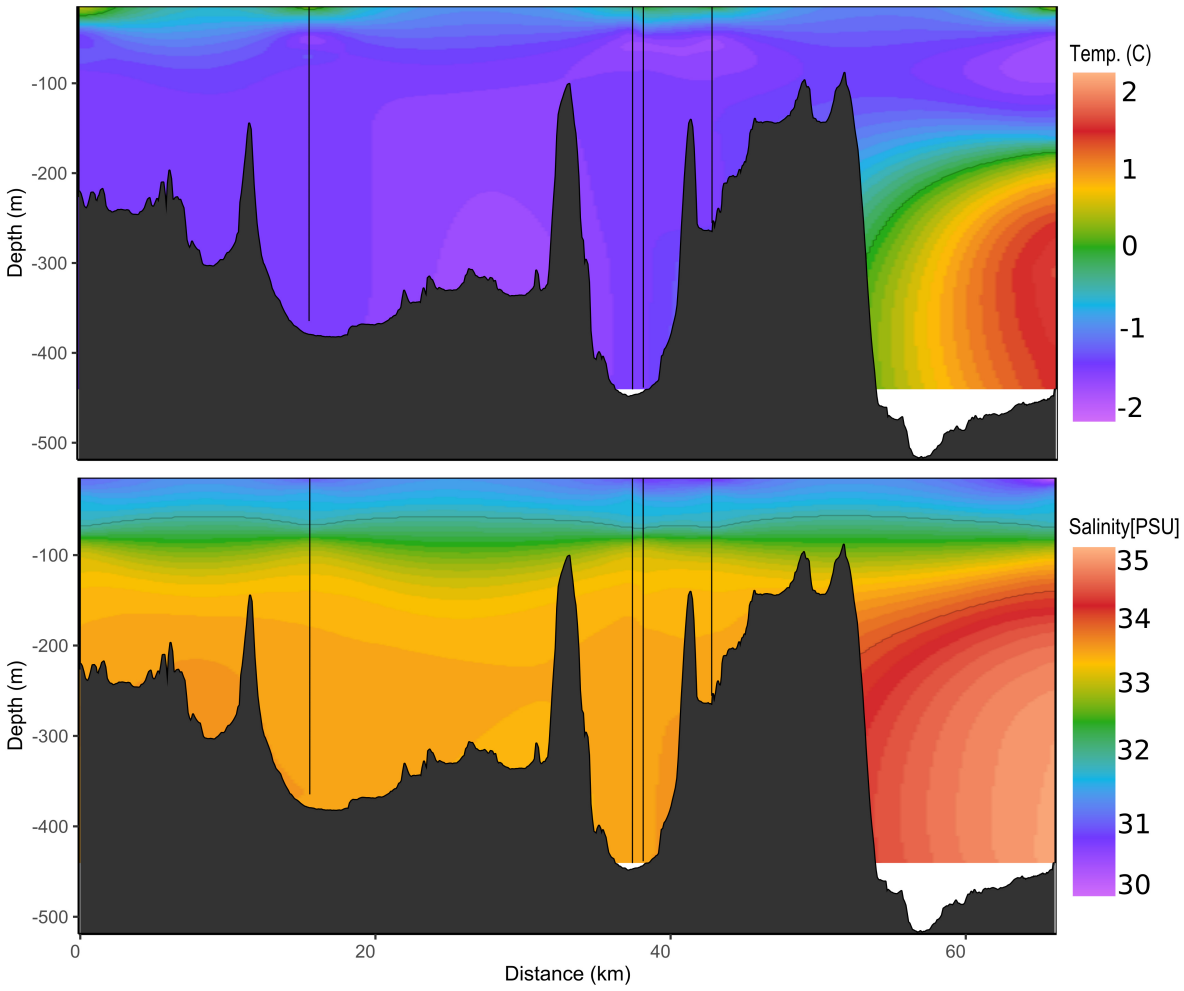


Figure 10: Contour plots of temperature (upper panel) and salinity (lower panel) for the section between the head of Besselfjord (Besselfjord A is at distance = 0 km, far left) to the fjord mouth that runs out in Dove Bugt. The black lines represent CTD casts.

Breddefjord is a fjord with a deep inner basin at -575 m depth, separated from a middle basin by a -180 m deep sill (at 44 km in Fig. 11, 0 km is at the head of the fjord) which again is separated from the outer area of Ardencaple by a -159 m deep sill (at 55 km in Fig. 11). Only one CTD was cast inside the fjord and one outside, at Ardencaple, which impacted the resolution of the transect. An inflow of AW (>34.4 PSU, > 0°C) was observed in the inner basin of Breddefjord (Fig.10). The 0°C isotherm (which indicates the upper AW boundary according to Gjelstrup et al. (2022)) was at -160 m depth. Above the AW there was a layer of cold and fresh PW (<34.4 PSU, < 0°C).

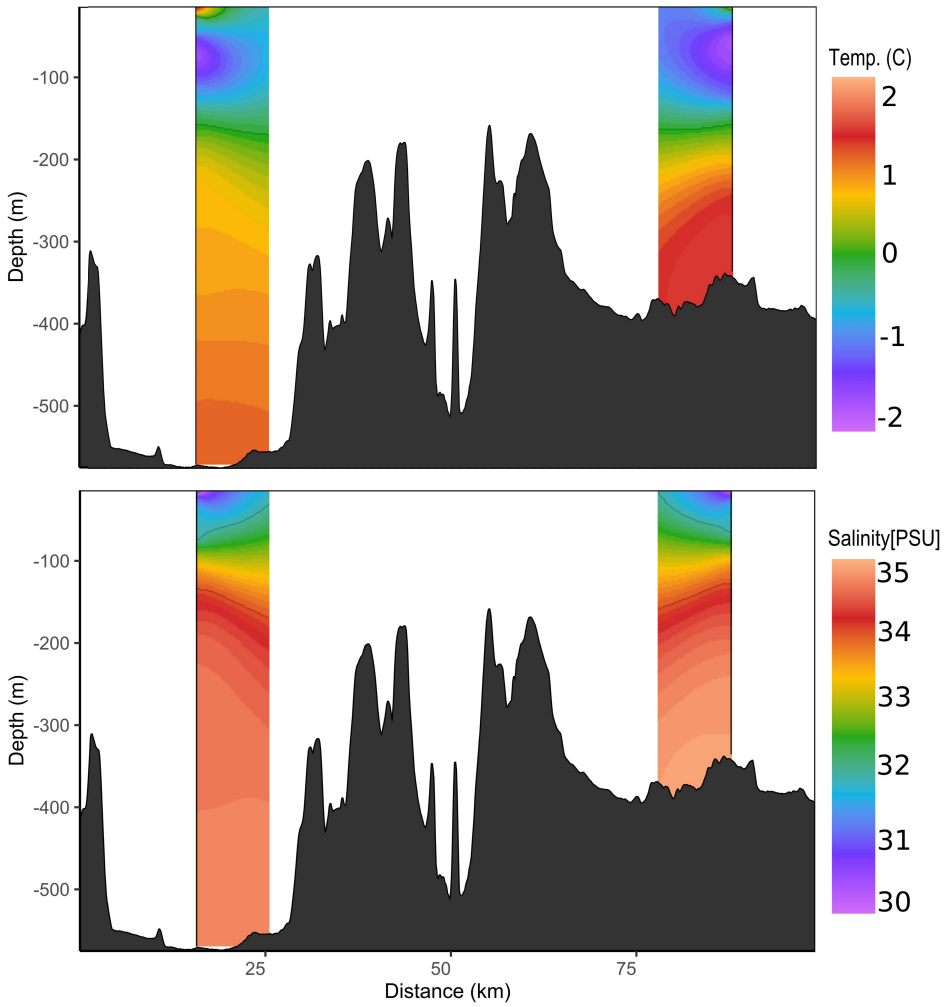


Figure 11: Contour plots of temperature (upper panel) and salinity (lower panel) for Breddefjord. Distance is from head of the fjord, far left in the transect. Low resolution of data is illustrated by a white area between the two stations; Breddefjord (station left in transect) and Ardencaple (station right in figure). The black lines represent the CTD casts.

## 3.2 Nutrient concentrations

### 3.2.1 Subarea 1: Dove Bugt and Besselfjord

The three stations, Dove Bugt, Besselfjord A and Besselfjord C had similar nutrient curves (Fig. 12). The surface water was depleted of nitrogen, and had lower concentrations of phosphate than the bottom water. Silicate levels rose at the surface, which was not expected. Less silicate was available in the deeper water at Dove Bugt compared to Besselfjord. The nutricline was measured to be at 100 m depth, and the bottom water had a concentration of nitrate and nitrogen around 10 $\mu$ mol $l^{-1}$.

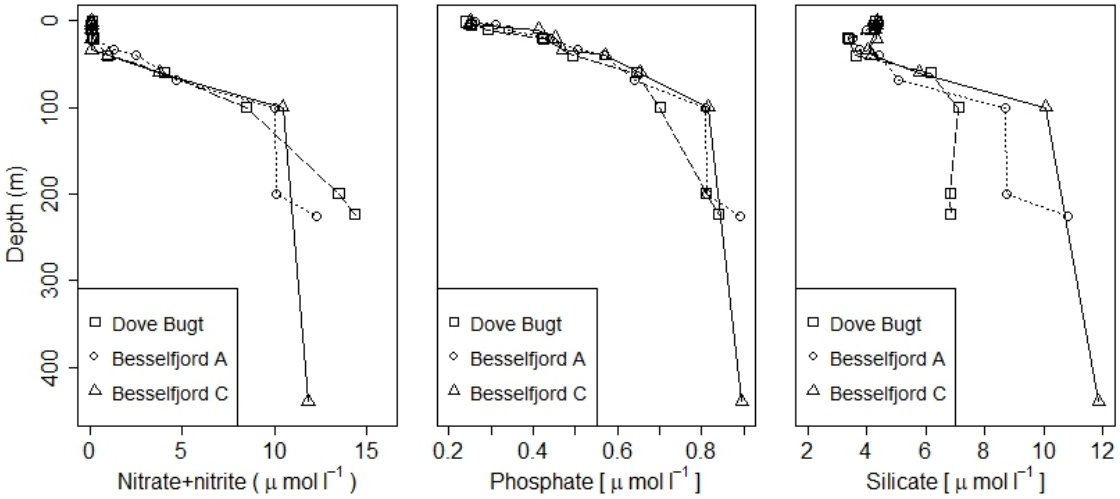


Figure 12: Vertical profiles of nutrients in subarea 1.

### 3.2.2 Subarea 2: Breddefjord and Ardencaple

Almost no nitrogen was left in the upper 40 m at both stations, but phosphate and silicate were present in the whole water column. A strong and short decline in silicate was observed around 40 m depth in Breddefjord. The nutricline was around 200 m, and the bottom waters had quite high concentration of nitrate and nitrite, with around 15 $\mu$ mol $l^{-1}$.

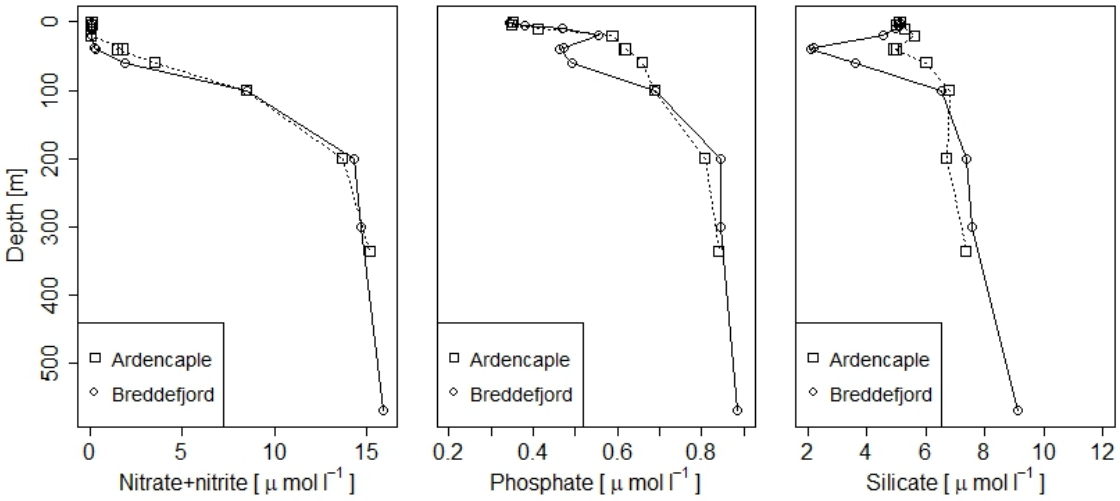


Figure 13: Vertical profiles of nutrients in subarea 2.

### 3.2.3 Subarea 3: Eskimones

The upper 40 m of Eskimones was depleted of nitrate and nitrite. There was still phosphate and silicate present in the surface. Silicate was high in the surface, but had a strong decline from around 7 $\mu$ mol $l^{-1}$ to 2 $\mu$ MOL $l^{-1}$ at 40 m depth. The nutricline appeared to be at 200 m depth, but might have been shallower, as there was a big gap between 100 and 200 m in the samples. The deeper water had a nitrogen concentration around 12 $\mu$ mol $l^{-1}$.

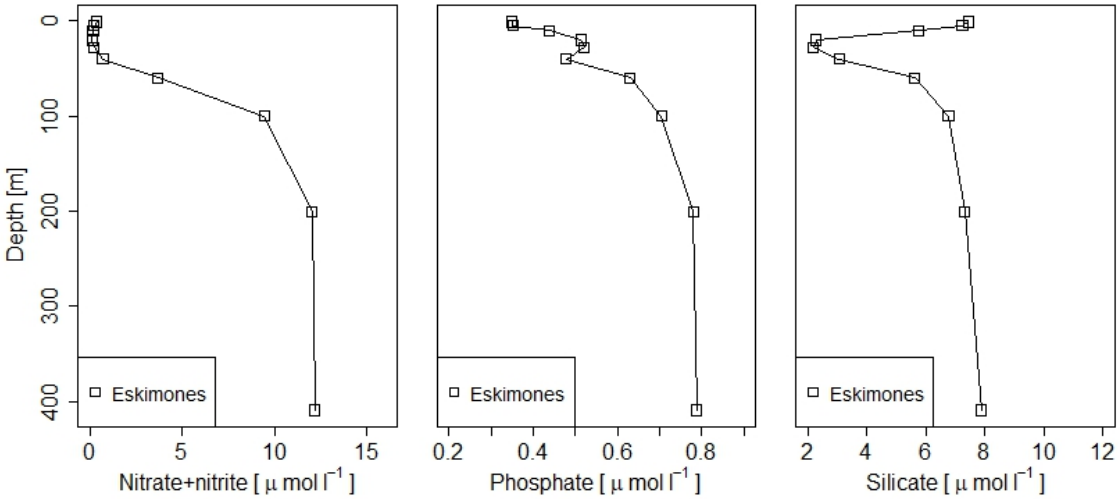


Figure 14: Vertical profiles of nutrients in subarea 3.

### 3.2.4 Subarea 4: On the shelf

Despite their large difference in latitude, the nutrient distribution had nearly the same shape for nitrogen and was similar for phosphate and silicate at 76° North Bank and Davy Sund. The phosphate and silicate profiles were nearly homogenous. This was not unexpected, as these shelf stations were strongly affected by the ocean currents and mixing. The upper 20 m were depleted of nitrogen, and there was no clear nutricline.

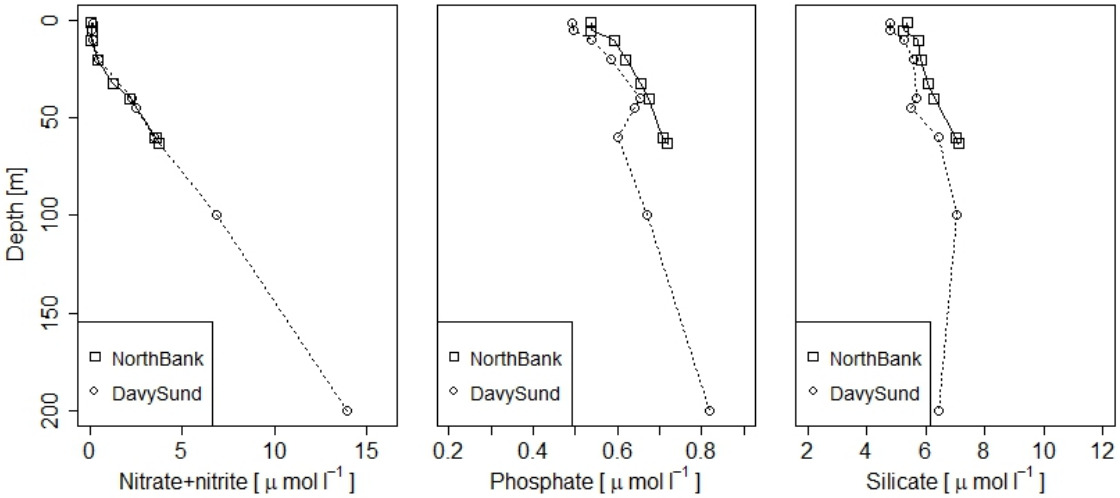


Figure 15: Vertical profiles of nutrients in subarea 4.

## 3.3 Chlorophyll *a*

The chlorophyll *a* maximum (Chl *a* max) was low at all stations ($< 1\ \mu\ g\ l^{-1}$) (Fig. 16). The Chl *a* max was lower at the inner fjord stations Besselfjord A ($0,30\ \mu\ g\ l^{-1}$) and Breddefjord ($0,24\ \mu\ g\ l^{-1}$). More open fjord locations such as Dove Bugt ($0,74\ \mu\ g\ l^{-1}$), Ardencaple ($0,68\ \mu\ g\ l^{-1}$) and Eskimones ($0,47\ \mu\ g\ l^{-1}$) had a higher Chl *a* max. Two samples were collected at Chl *a* max in Ardencaple (40 m). These samples displayed very different concentrations of Chl *a* ($0,36\ \mu\ g\ l^{-1}$ and $0,68\ \mu\ g\ l^{-1}$). The higher value is used as the Chl *a* max as it was collected from the first Niskin bottle, that likely closed closer to the actual depth. $0,68\ \mu\ g\ l^{-1}$ was also closer to the CTD fluorescence measurements of $0,7116\ mg \cdot m^{-3}$ (Appendix A, Fig. 34). In Eskimones the CTD downcast showed maximum of fluorescence at 28 m depth, but the Chl *a* concentrations determined by filtering the seawater indicated a Chl *a* max at the surface. The CTD do not log fluorescence above 15 m, which is the reason the surface bloom was not detected.

Dove Bugt had the highest concentration of Chl *a* and the shallowest Chl *a* max, after Eskimones, at 21 m depth. The other stations had a deep Chl *a* max. The southernmost station, Davy Sund, had the deepest Chl *a* max at 45 m depth. Chl *a* max at Breddefjorden and Ardencaple were a bit shallower

at 38 and 40 m. In Besselfjord and the shelf station outside, 76 °North Bank, Chl *a* max was at 32-34 m.

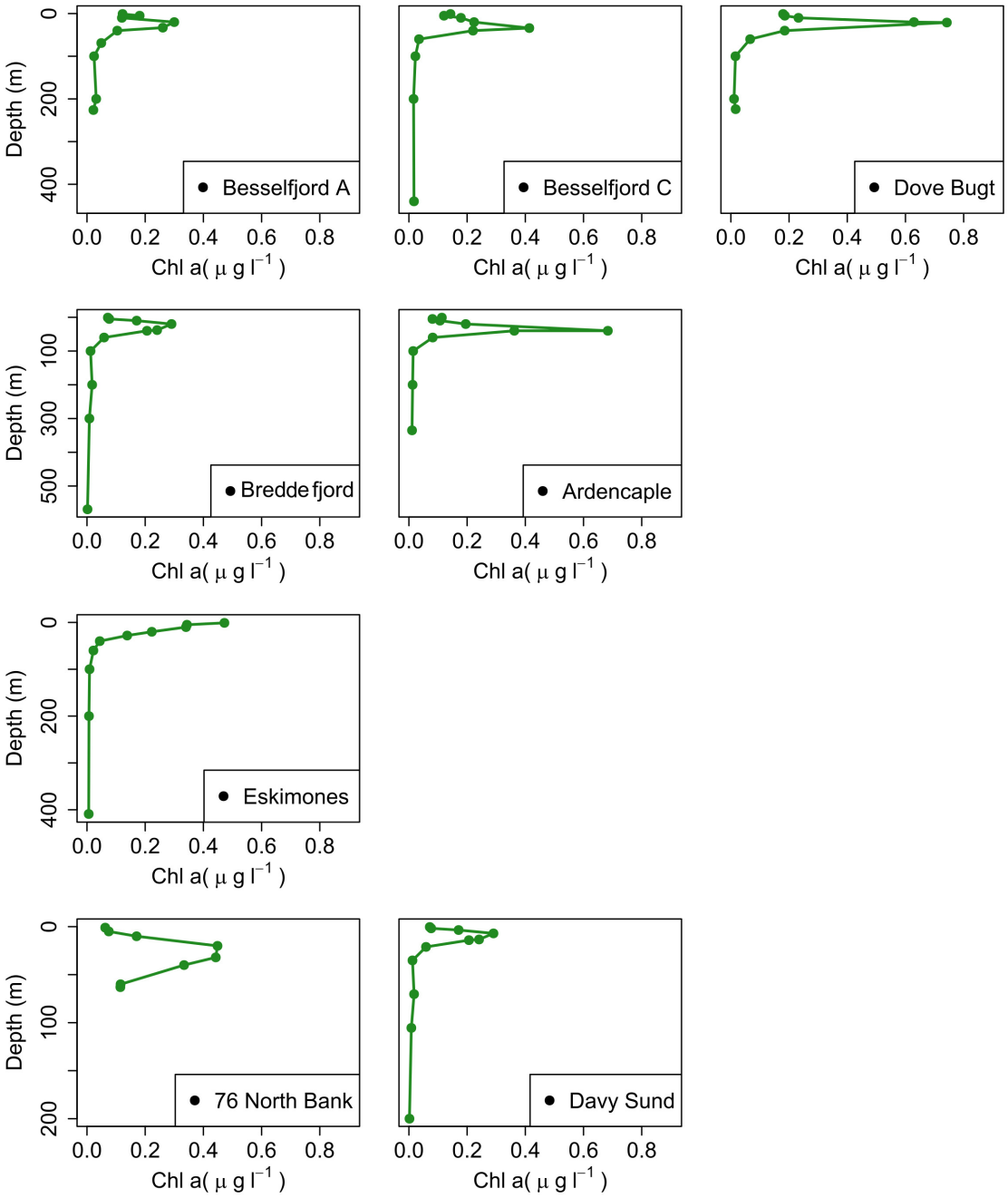


Figure 16: Vertical profiles of Chlorophyll *a* concentration.

## 3.4 Plankton community

### 3.4.1 Protist community

The protist community was dominated by flagellates at all stations (Fig. 17). The highest abundances were found in Ardencaple at Chl *a* max and in the surface of Besselfjord C and Dove Bugt. The abundance of protists was generally higher in the surface than at Chl *a* max, except in Ardencaple and Davy Sund. There was a higher proportion of diatoms at Eskimones, especially at Chl *a* max (28 m depth). Diatoms were also present in Besselfjord, Dove Bugt, Breddefjord and Ardencaple. No protist community sampling was conducted from the surface waters in the 76°North Bank staton, hence the blank bar (Fig. 17).

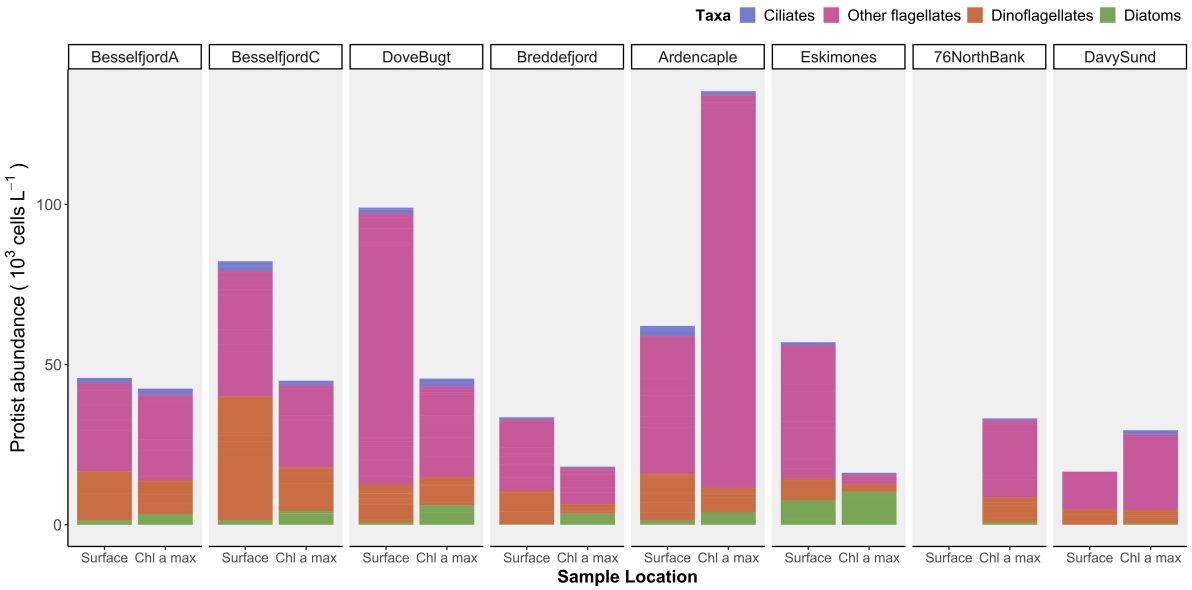


Figure 17: Absolute abundance ($10^3$ cells $L^-1$) of protists of different taxa at surface and Chl *a* max (Table 2).

### 3.4.2 Zooplankton community

*Calanus* spp. made up a fairly small percentage of the zooplankton community in the innermost fjord stations Besselfjord A (6 %) and Breddefjord (5%)(Table 6). *Calanus* spp. also made up a small part of the community at the northernmost shelf station, 76 North Bank (7%). Eskimones stood out for having a quite large (21%) part *Calanus* spp. In all other locations, *Calanus* spp. made up 11-14% of the zooplankton absolute abundance.

It must be noted that *Calanus* spp. is a big copepod and much larger than the smaller copepods like *Pseudocalanus* spp, *Microcalanus* spp., *Oithona similis* or *Triconia borealis*. *Calanus* spp. might have appeared more significant if the unit was changed to biomass instead of individuals per $m^2$. *Metridia*

Table 6: Absolute abundance of mesozooplankton [ind·$m^{-2}$], Absolute abundance of *Calanus* spp. and how much of the zooplankton absolute abundance consisted of *Calanus* spp. [%].

| **Station** | **Mesozooplankton abundance [ind·$m^{-2}$]** | **Calanus abundance [ind·$m^{-2}$]** | **Part Calanus [%]** |
|---|---|---|---|
| Besselfjord A | 41 136 | 2 442 | 6 |
| Besselfjord C | 60 895 | 8 768 | 14 |
| Dovebugt | 67 784 | 8 717 | 13 |
| Breddefjord | 148 589 | 6 873 | 5 |
| Ardencaple | 40 659 | 4 592 | 11 |
| Eskimones | 58 585 | 12 585 | 21 |
| 76°North Bank | 10 816 | 716 | 7 |
| Davy Sund | 80 715 | 8 828 | 11 |

*longa* is another big, common copepod species. In Besselfjord C, Breddefjord and Ardencaple *Metridia longa* was more abundant than *Calanus* spp.

*Pseudocalanus* spp. was the dominant taxon in Besselfjord, Dove Bugt and Breddefjord (Fig.18). In Ardencaple, Eskimones and on the shelf, *Oithona similis* was dominating. The small copepods *Microcalanus* spp. and *Tricona borealis* were quite abundant at all stations. An unusual copepod with a large, straight frontal spine was found in Breddefjorden (Appendix C, Table 11). It was classified as the abyssal, Atlantic species *Geatanus miles*.

Other interesting findings were nudibranches in Besselfjord A and the ice amphipod *Gammarus wilkitzkii* in Ardencaple (Table 11 in Appendix C). Breddefjord had a very high zooplankton abundance (Table 6), that included several species in the genus *Ostracoda* (Appendix C, Table 11). There was observed large *Appendicularia*, which was quite abundant in Besselfjorden, Dove Bugt and Davy Sund. Larvae from the benthos, meroplankton, were especially important in Dove Bugt, Breddefjord and Davy Sund. A high abundance of radiozoans was also observed in Dove Bugt (Appendix C, Table 11).

Invertebrate predators (*Paraeuchaeta* spp., Chaetognatha, Amphipoda, *Limacina helicina*, hydrozoans) were abundant in Besselfjord A, Dove Bugt, Breddefjord and Eskimones. Hydrozoans were present at all locations except Besselfjord C and Davy Sund (Table 11 in Appendix C). There is a possible underestimation of this taxaon due to its gelatinous structures getting destroyed by the plankton net or fixation.

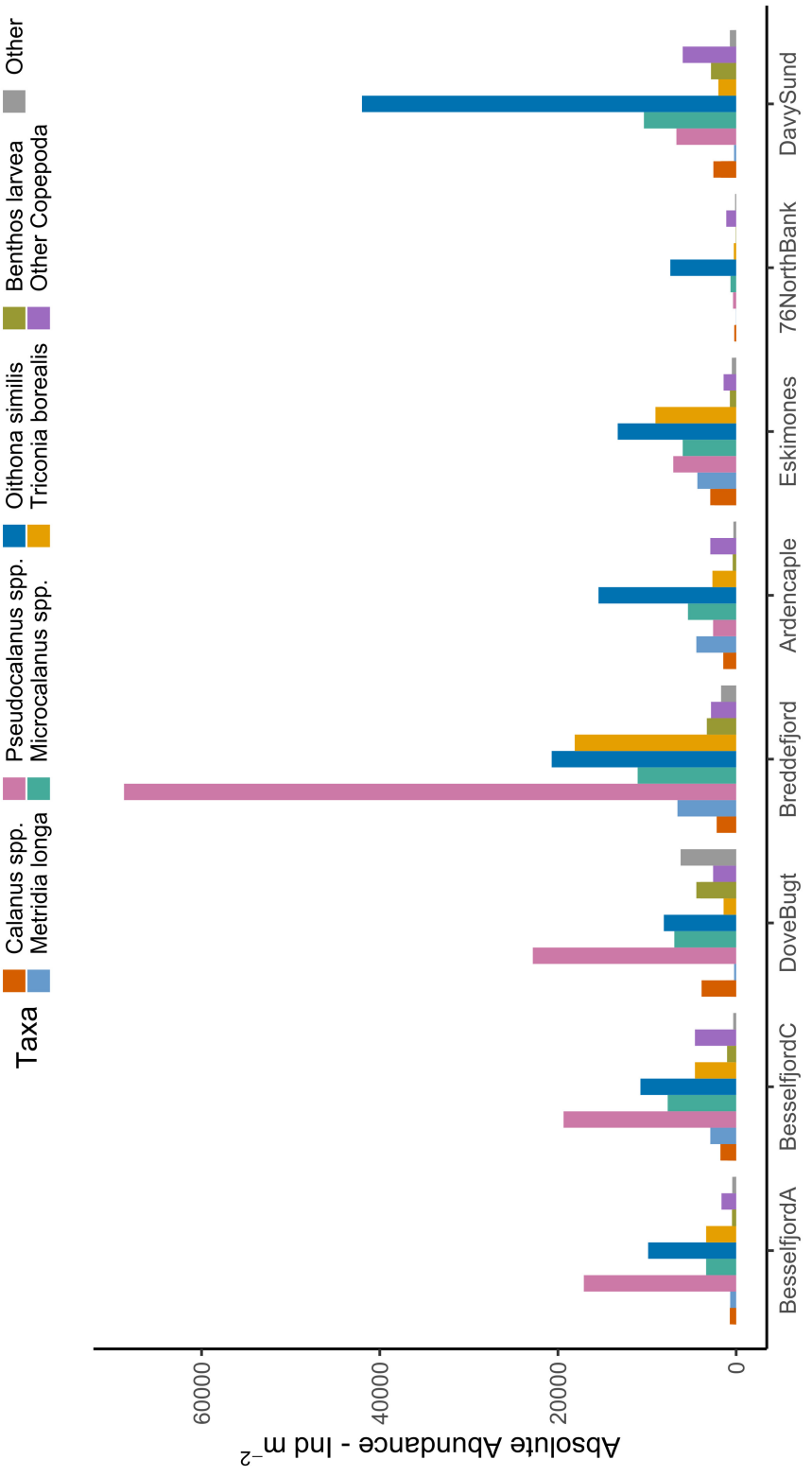


Figure 18: Zooplankton absolute abundance (ind $m^{-2}$) and community composition of different zooplankton groups. Abundances and more through taxa identification can be found in Table 11 Appendix C.

## 3.5 Species and stage composition of *Calanus* spp.

### 3.5.1 Identification of *C. hyperboreus*

The occurrence of a spike at the $5^{th}$ thoracic segment is partly inconsistent with larger sizes of *Calanus* (Table 7). Although there are larger individuals with a spike and smaller individuals with a rounded end of the prosome, a smaller size does not exclude the possibility of a spike at the prosome ending. In this thesis, *C. hyperboreus* is identified by prosome length (Table 3).

Table 7: Number of individuals of species identified as *C. hyperboreus* or *C. finmarchicus*/*C. glacialis* by size with clear, weak and no spike at the $5^{th}$ thoracic segment. The species determination is based on prosome length criteria described in table 3.

| **Stage** | **End of $5^{th}$ thoracic segment** | **Species determined by size** | |
|---|---|---|---|
| | | *C.finmarchicus* *C.glacialis* | *C.hyperboreus* |
| **CIV** | Clear spike | 3 | 119 |
| | Weak spike | 4 | 49 |
| | Round | 135 | 14 |
| **CV** | Clear spike | 6 | 89 |
| | Weak spike | 1 | 24 |
| | Round | 215 | 9 |
| **AF** | Clear spike | 4 | 29 |
| | Weak spike | 2 | 13 |
| | Round | 69 | 4 |

### 3.5.2 Identifying *C. finmarchicus* and *C. glacialis* to species based on size

Prosome length was measured on 1476 *Calanus* individuals. 706 individuals were in the size range of *C. finmarchicus* or *C. glacialis* (Table 3). 29 individuals of *C. finmarchicus* and 133 individuals of *C. glacialis* were determined from DNA analysis. The prosome length of *C. finmarchicus* and *C. glacialis* determined from DNA analysis did not correspond with two different peaks in the bimodal curve created by all individuals at stage CIV, CV and Adult females (Fig. 19). Based on these results, it is not possible to distinguish *C. finmarchicus* from *C. glacialis* by prosome length.

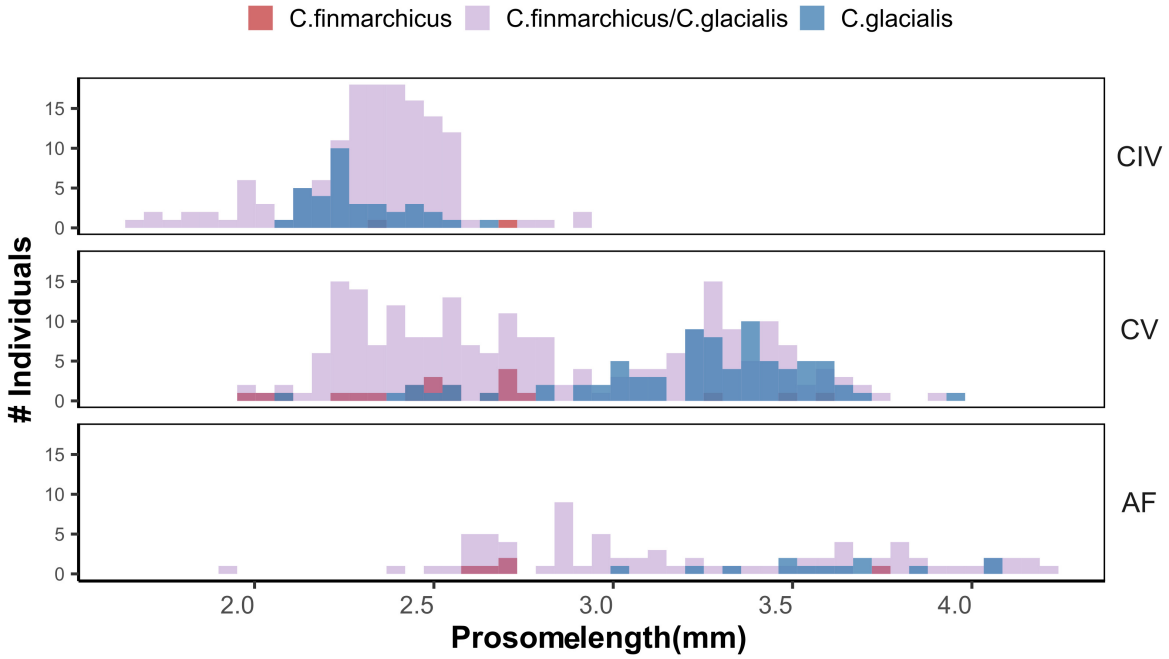


Figure 19: Prosome length distributions for *Calanus* stage CIV, CV and adult females (AF) determined to *C. finmarchicus* or *C. glacialis* from size by criteria described in table 3. Some individuals were assigned to *C. finmarchicus* (red) or *C. glacialis* (blue) based on DNA analysis.

### 3.5.3 Abundance of *Calanus* spp.

Dove Bugt, Breddefjord, Eskimones and Davy Sund had especially high abundances of *Calanus* (Fig. 20). *C. hyperboreus* dominated in Dove Bugt, Besselfjord C and Breddefjorden. Eskimones had the highest abundance, Davy Sund was the southern shelf station and had a clear dominance of *C. finmarchicus/C. glacialis*.

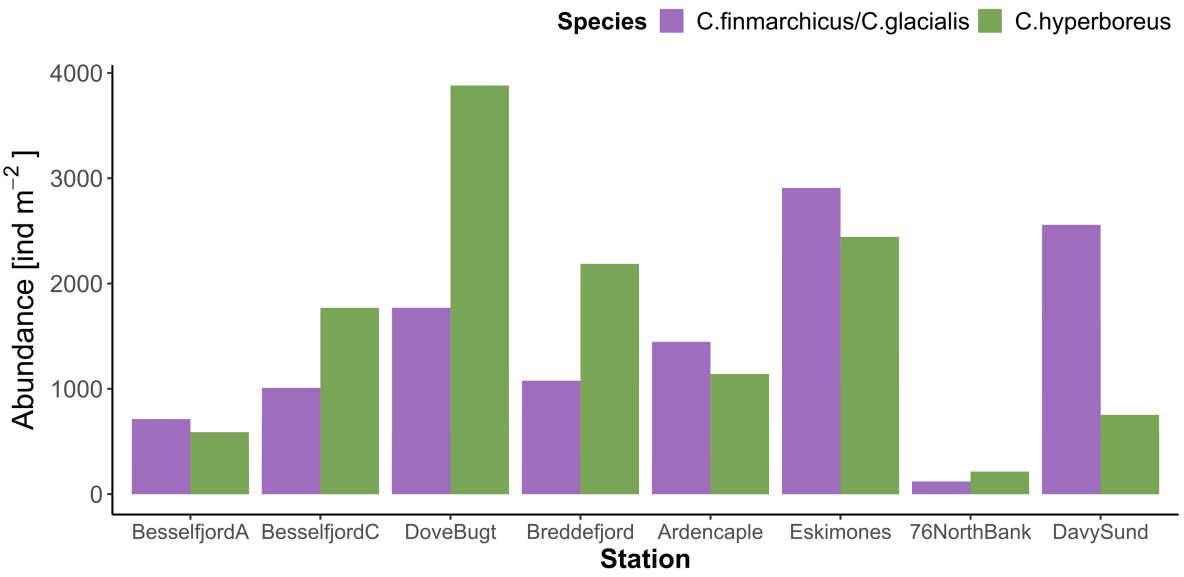


Figure 20: Absolute abundance [individuals per $m^{-2}$] of *C. hyperboreus* and *C. finmarchicus* / *C. glacialis* .

### 3.5.4 Stage distribution of *Calanus* spp.

*C. finmarchicus* and *C. glacialis* generally had a higher relative abundance of the oldest copepodite stage, CV, and adult females compared to *C. hyperboreus* (Fig. 21). Copepodite stage CIII and CIV dominated the relative abundance in *C. hyperboreus*, except in Besselfjord A, where the older CV were more abundant. Dove Bugt had an especially high abundance of *C. hyperboreus* stage CIII, and a surprisingly low abundance of adult *C. hyperboreus* females with only three individuals (Tab.11, Appendix C). Several young copepodites of stage CI, CII and CIII of *C. finmarchicus/C. glacialis* were present (Fig. 21).

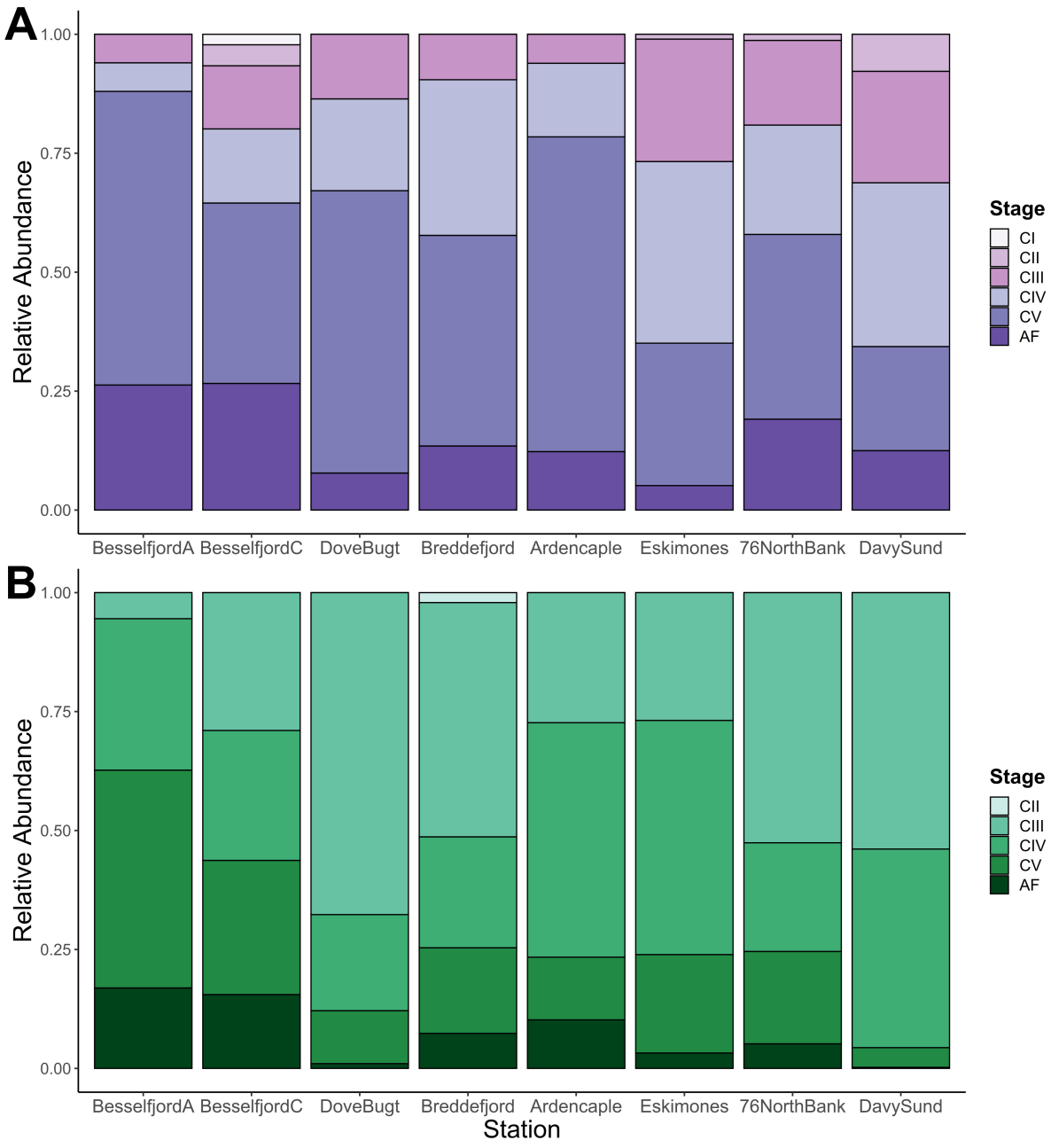


Figure 21: Copepodite stage distribution in A) *C.finmarchicus* or *C. glacialis* and B) *C. hyperboreus*.

## 3.6 Lipid content in *Calanus* spp. photographed with stereo microscope

### 3.6.1 Differences in lipid content between *Calanus* Species

A significant difference was observed between *C. glacialis* and *C. hyperboreus*, as indicated by non-overlapping confidence intervals (Fig.22). Despite both species having similar rates of increase ($\beta_1$ = 1.89 & 1.72, listed in table 8) *C. glaclialis* generally had a larger lipid area than *C. hyperboreus* for the same prosome area. It is however worth noting that *C. hyperboreus* have the potential to grow larger and therefore include individuals with the highest lipid area.

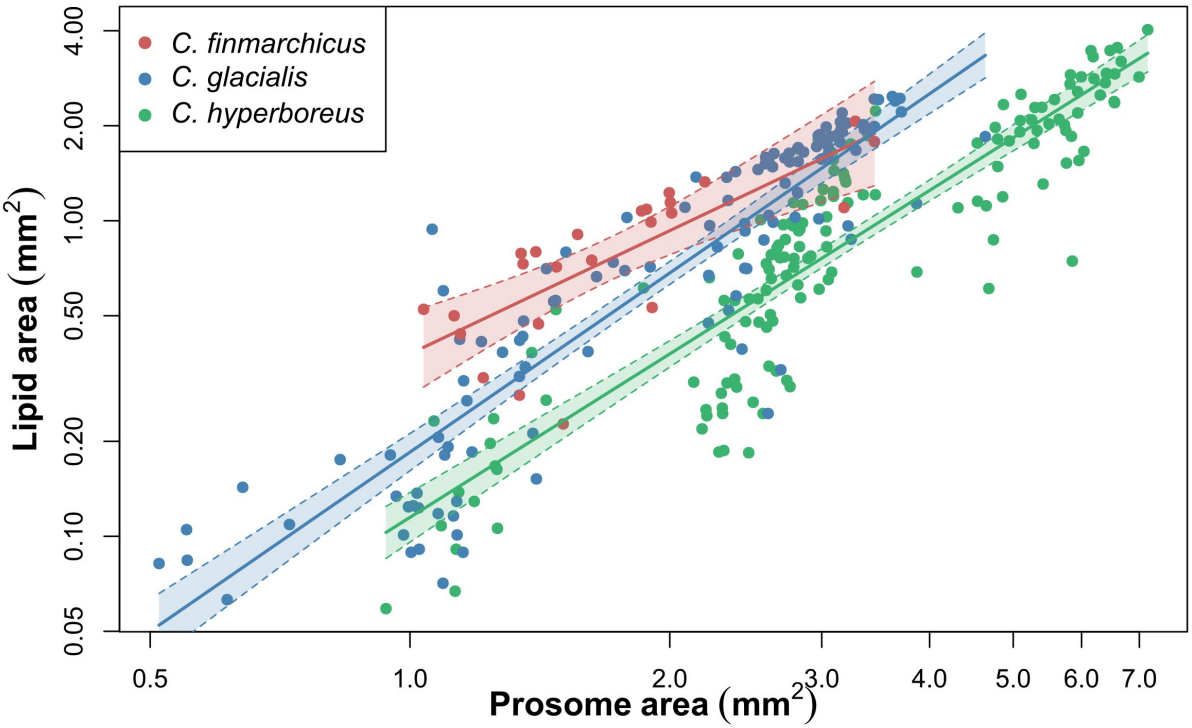


Figure 22: Lipid area over prosome area in *C. finmarchicus* (red), *C. glacialis* (blue) and *C.hyperboreus* (green) on a logarithmic scale. The lines are fitted by linear regression and displayed with 95 % confidence intervals. The fitted coefficients and $R^2$ are given in table 8.

Table 8: Coefficients, intercept [$\beta_0$] and slope [$\beta_1$] estimated by fitting lipid sac area (LA) as a function of prosome area (PA) in a parametric model, described in Equation 5. Models were fitted for each species, and the number of individuals [n] is also given.

| **Species** | **Stage** | **n** | $\beta_0$ | $\beta_1$ | $R^2$ |
|---|---|---|---|---|---|
| *C.finmarchicus* | CIV-CV | 24 | -0,97 $\pm$0, 15 | 1,30 $\pm$0, 24 | 0,58 |
| *C.glacialis* | CIII-CV | 120 | -1,69 $\pm$0, 07 | 1,89 $\pm$0, 08 | 0,82 |
| *C.hyperboreus* | CIII-CV | 153 | -2,16 $\pm$0, 09 | 1,72 $\pm$0, 07 | 0,79 |

The regression models explained a considerable part of the variation in the data (Table 8). While the assumptions of linear regression generally were met, they were not fulfilled perfectly (Appendix D).

Regarding *C. finmarchicus*, the sample size was relatively small, consisting of only 24 individuals, primarily in copepodite stage CV (Table 5). The regression from *C. finmarchicus* cannot be compared directly to *C. glacialis* and *C.hyperboreus* due to presence of three copepodite stages in the latter species as well as substantially a substentially larger dataset.

### 3.6.2 Differences in lipid content between copepodite stages

*Calanus* individuals in different stages allocate energy differently between growth and storage (Fig.23). These results are obtained by fitting a linear regression between the logarithmically transformed lipid sac area and prosome area for each copepodite stage (Equation 4 & Table 9). A higher rate of increase ($\beta_1$) indicate prioritisation of storing energy as lipid in the lipid sac. In the model for copepodite stage CIV in *C. hyperboreus*, certain individuals were excluded from the analysis. Specifically, three smaller individuals collected in Breddefjord were omitted from the regression because their prosome length fell far below the *C. hyperboreus* characteristics (Table 3). Additionally, an individual with a prosome length of 3,022 mm, collected in Dove Bugt, and a large individual of 4,415 mm, collected in Breddefjord C, were excluded from the regression due to their leverage on the model.

Table 9: Coefficients, intercept [$\beta_0$] and slope [$\beta_1$] estimated by fitting lipid sac area (LA) as a function of prosome area (PA) in a parametric model, described in Equation 5. Models were fitted for each stage within each species, and the number of individuals [n] is also given.

| **Species** | **Stage** | **n** | $\beta_0$ | $\beta_1$ | $R^2$ |
|---|---|---|---|---|---|
| *C.finmarchicus* | CV | 22 | -0,91 $\pm 0,15$ | 1,26 $\pm 0,23$ | 0,59 |
| *C.glacialis* | CIII | 6 | -1,92 $\pm 0,55$ | 0,85 $\pm 1,04$ | 0,14 |
| *C.glacialis* | CIV | 35 | -1,94 $\pm 0,13$ | 2,46 $\pm 0,64$ | 0,31 |
| *C.glacialis* | CV | 79 | -1,10 $\pm 0,18$ | 1,34 $\pm 0,18$ | 0,43 |
| *C.hyperboreus* | CIII | 12 | -2,95 $\pm 0,22$ | 5,34 $\pm 0,94$ | 0,77 |
| *C.hyperboreus* | CIV | 87 | -4,68 $\pm 0,34$ | 4,29 $\pm 0,34$ | 0,65 |
| *C.hyperboreus* | CV | 50 | -3,37 $\pm 0,54$ | 2,36 $\pm 0,31$ | 0,54 |

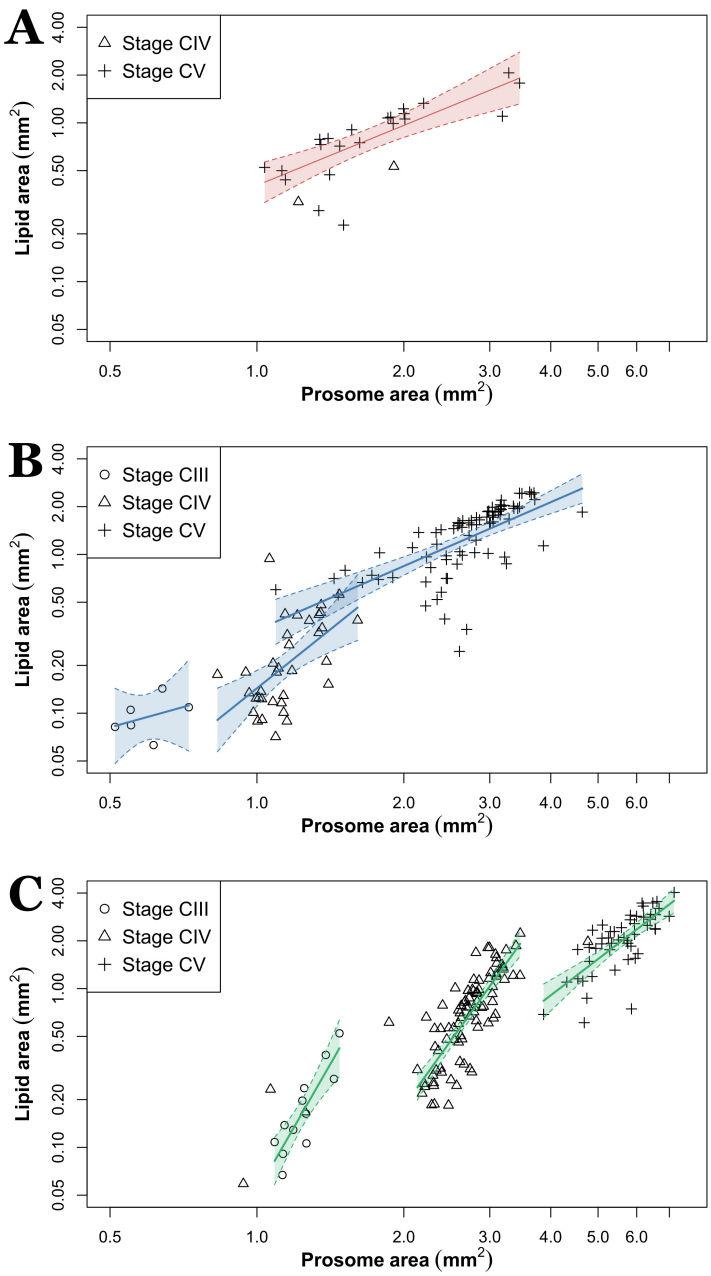


Figure 23: Lipid area $mm^2$ over prosome area $mm^2$ for different copepepodite stages of A) *C. finmarchicus*, B) *C. glacialis* and C) *C. hyperboreus* on logarithmic scales. The lines are fitted by linear regression and displayed with confidence intervals for each copepodite stage.

### 3.6.3 Difference in individual lipid content between stations - WP2

Difference between stations was assessed in *C. glacialis* and *C. hyperboreus* by multiple linear regression. It was assumed that the slope ($\beta_1$) between lipid sac area and prosome area remained constant. If the overlap between confidence intervals of the intercept coefficient ($\beta_0$) between stations is below 0.05, this would indicate location-specific differences in lipid content. *C. glacialis* was estimated to follow the model in Equation 8 and *C. hyperboreus* Equation 9. The intercept coefficient ($\beta_0$) mean and 95% confident interval for both models are displayed in Fig.24. There is no overlap between the confidence interval of $\beta_0$, and therefore no statistically significant difference in lipid sac between stations when size-induced differences were accounted for. The models are displayed graphically for all stations in Appendix E(Fig.41).

$$LA_{\,C.\ glacialis} = e^{\beta_0} \cdot PA^{1{,}898 \pm 0.091} \tag{8}$$

$$LA_{\,C.\ hyperboreus} = e^{\beta_0} \cdot PA^{1{,}716 \pm 0.075} \tag{9}$$

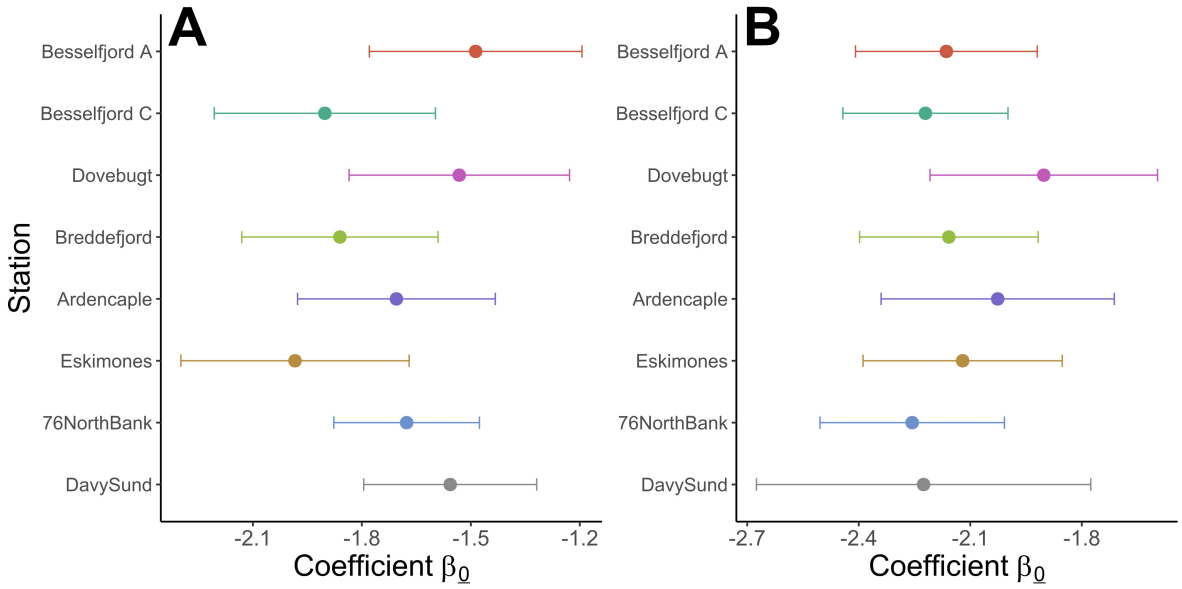


Figure 24: Mean and 95 % confidence intervals of the intercept coefficient ($\beta_0$) for A) *C. glacialis* and B) *C. hyperboreus* . The coefficients are estimated by multiple linear regression between the logarithmic transformed lipid sac area (response variable) and prosome area (explanatory variable) with station as an additional explanatory variable.

## 3.7 Relavtive vertical distribution and lipid content in *Calanus* - sampled with VPR

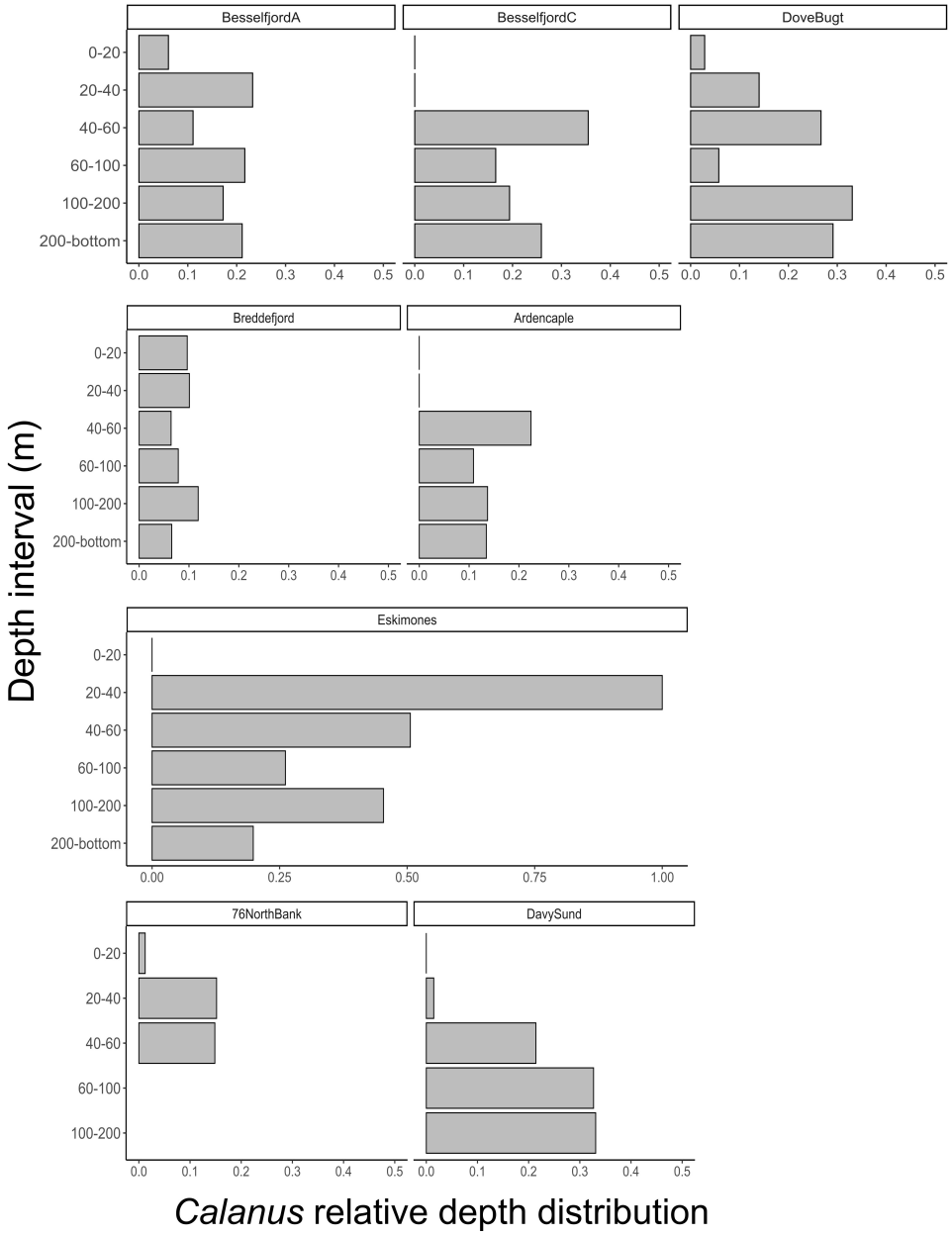


Figure 25: *Calanus* spp. relative depth distribution recorded with VPR.

### 3.7.1 Relative Vertical distribution

*Calanus* were present both in the surface and near the bottom at all stations (Fig. 25). A more or less clear bimodal distribution was observed, with some individuals at the surface and others deep in the water column. This trend was less evident in Breddefjord, where a relatively homogeneous *Calanus* depth distribution was observed. In Davy Sund, a larger proportion of *Calanus* was found in the water column's lower depths, unlike Eskimones where there was recorded a higher abundance between 20-40 mm depth. Also notice that the relative vertical abundance was twice as large at Eskimones than all the other stations (Fig. 25). No individuals of *Calanus* were recorded in the upper 40 m of the water column at Besselfjord C and Ardencaple. The time of sampling at these station (between 9 and 12 AM, Table. 1), did not differ from the sampling time of other stations where *Calanus* were present in the surface.

### 3.7.2 Difference in individual lipid content between stations - VPR

The same analysis as in section 3.6.3 was done to assess individual lipid content between stations. A parametric model, Equation 5, was fitted to the data to estimate the coefficients of the slope ($\beta_1$) and intercept ($\beta_0$). A constant slope was assumed for all stations, so the expected lipid sac area for a certain prosome length was given by Equation 10.

$$LA = e^{\beta_0} \cdot PA^{1.023 \pm 0.039} \tag{10}$$

No statistically significant difference was observed in the estimate of intercept ($\beta_0$) between stations, indicated by overlap in 95% confidence intervals (Fig. 26). Although there was no statistically significant difference between the stations, one can observe a higher coefficient at 76°North Bank and Dove Bugt, indicating a higher lipid sac area at a certain prosome length. In Besselfjorden A and Breddefjorden one can see the opposite, a lower $\beta_0$ which indicates a smaller lipid sac area at a certain prosome area.

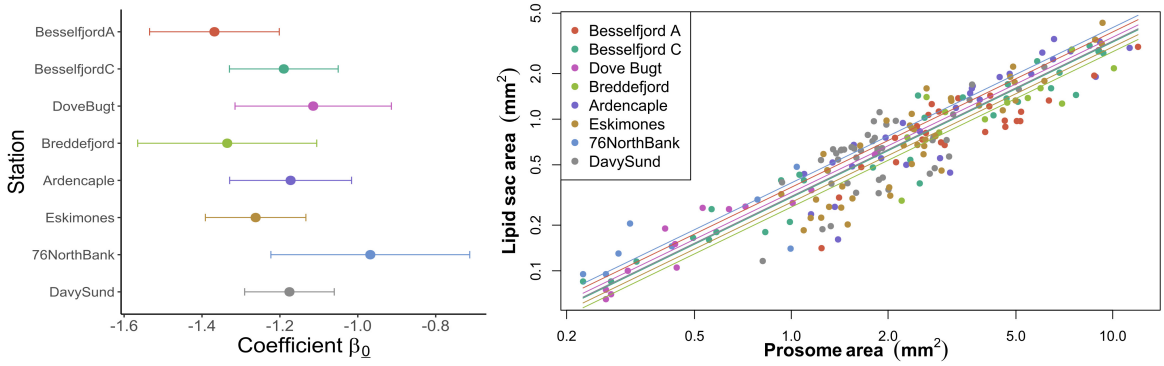


Figure 26: To the left: Mean and 95 % confidence intervals of the intercept coefficient ($\beta_0$) (Equation 10) when station is an additional explanatory variable for lipid sac area in *Calanus* spp. collected with VPR. To the right: Lipid sac area over prosome area on a logarithmic scale. The lines are visualizing how station affect the model of lipid sac area over prosome area through different intercept ($\beta_0$).

### 3.7.3 Difference in individual lipid content with depth - VPR

The VPR also recorded the depth at which each *Calanus* spp. picture was taken. This made it possible to look at the lipid content with depth. The total lipid and prosome length distribution with depth is found in Appendix F (Fig. 43, Fig. 42). To assess the relative lipid fullness of each individual, size-induced differences were accounted for by comparing the individual's lipid fullness to the lipid fullness estimated by the exponential model in Equation 4 with coefficients estimated to $\beta_0 = -1,18$ and $\beta_1 = 0,97$. The vertical distribution of relative lipid fullness is displayed for each station in (Fig27).

As there is no apparent significant difference between the stations, all individuals were included to assess if there was a difference in relative lipid fullness with depth. As there appeared to be little difference in relative lipid fullness between 100-200 and 200-bottom (Fig. 28), the individuals were only separated into two categories; surface waters (surface-100 m) and bottom waters (100 m-sea floor). 76 °North Bank was excluded from the analysis because of being shallower than 100 m.

An independent two-sample t-test was used to compare relative lipid fullness in the surface ($\leq 100m$, mean=0.861, SD=0.349, n=20) and deep waters ($\geq 100m$, mean=1.052, SD=0.385, n=301). There was a significant difference between the depths in relative lipid content (t(21.587)=-2.3665) with a p-value of 0.027.

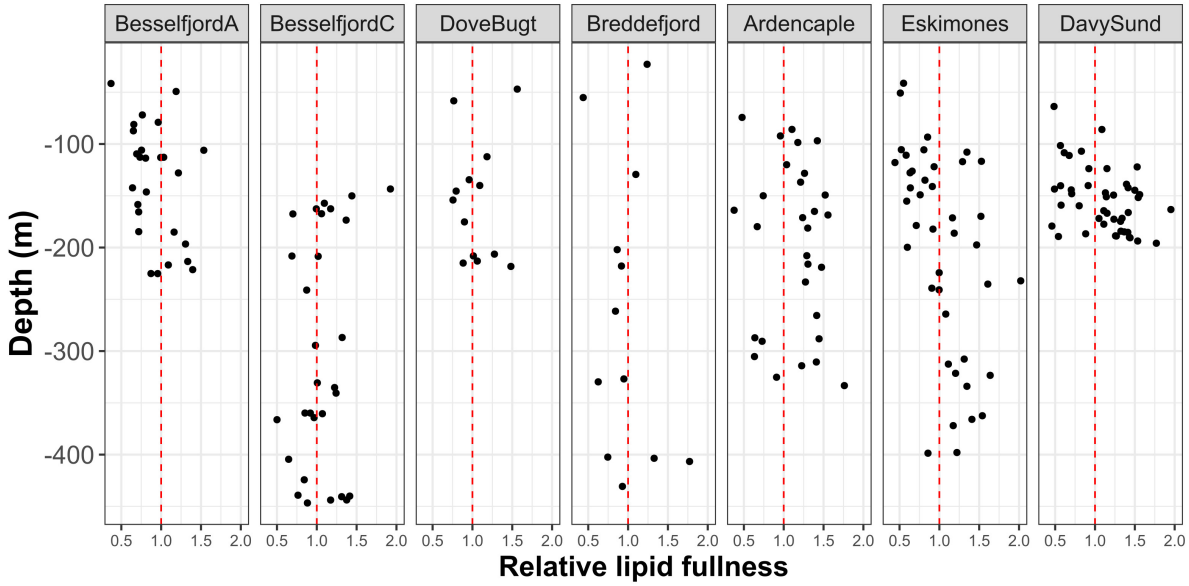


Figure 27: Relative lipid fullness with depth

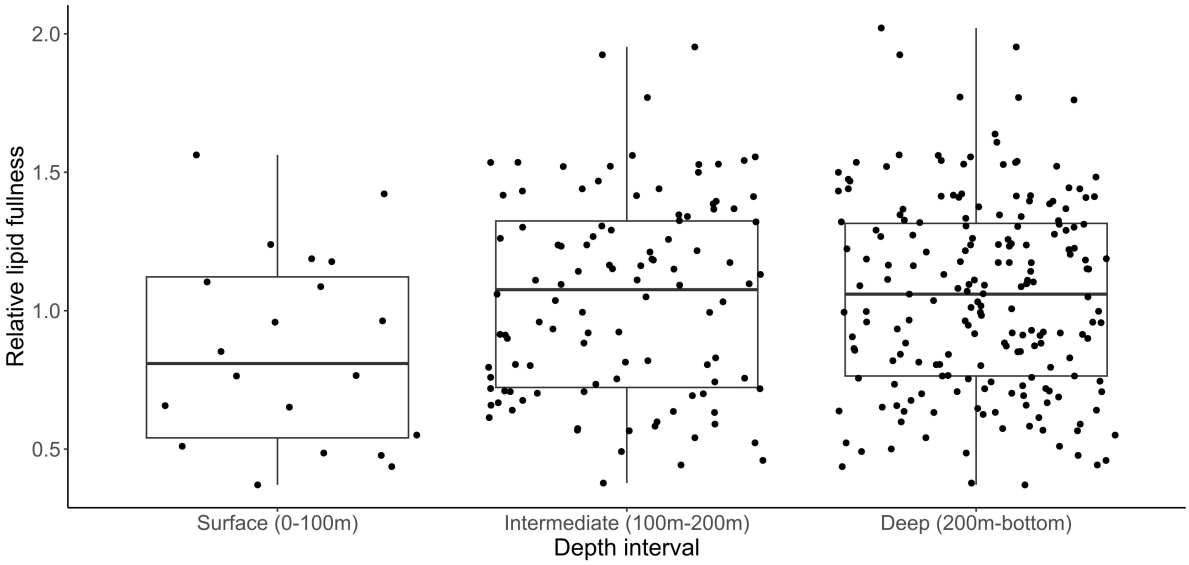


Figure 28: Relative lipid fullness in depth intervals.

# 4 Discussion

In this thesis, I have tried to determine how the lipid content in *Calanus* spp. depends on environmental factors in Northeast Greenland locations, an area that has been little studied compared to the Norwegian Arctic. The region west of the Fram Strait is known to be considerably more oligotrophic than the Svalbard coast, as it is the outflow shelf from the Arctic Ocean (Bluhm et al., 2015). This could lead to differences in the quality and quantity of available food for *Calanus* and thereby differences in copepod condition. In the first part of this discussion, I will assess if there is any difference in lipid accumulation between the *Calanus* species and compare the result to recent studies from the Svalbard area. Afterward I will discuss the difference in relative lipid fullness between surface and deep waters. In the third part of this discussion, I will assess if there are any differences between the stations in *Calanus* total lipid content. Lastly, I want to discuss how differences in the environment could be the reason for these possible differences in lipid content.

## 4.1 *Calanus* differences in individual lipid between *Calanus* species and copepodite stage

A significant difference in lipid accumulation was observed between *C. glacialis* and *C. hyperboreus* (Fig. 22). Total Lipid (mg) was calculated from lipid sac area ($mm^2$) and the proxy for size was changed to prosome length, to mirror this study to the study in Svalbard areas by Renaud et al. (2018). The adult females were also included (they were excluded from the thesis analysis, as they were expected to have utilized some of their lipid reserves for reproduction and would likely die before another overwintering). The difference prevailed after these modifications, implying a species-specific difference in total lipid content with size between *C. glacialis* and *C. hyperboreus* (Fig.29).

During this study in Northeast Greenland, the confidence intervals from the model estimated from the few recorded individuals of *C. finmarchicus* (n=24) had an overlap with the model of *C. glacialis* (Fig.29 Table 10). This indicates similarities between the species and is consistent with the findings in Renaud et al. (2018). However, contrary to the results in that study, the small stages of *C. hyperboreus* did not overlap with *C. glacialis* . When including all stages of *C. hyperboreus* (CIII-AF) in the model, the intercept ($\beta_0$) was similar to that of *C. glacialis* , but the slope ($\beta_1$) was lower (Table 10). According to these findings, *C. hyperboreus* in Northeast Greenland have a slower accumulation of total lipid with size than *C. glacialis* and all *Calanus* species in the Svalbard region (Renaud et al., 2018).

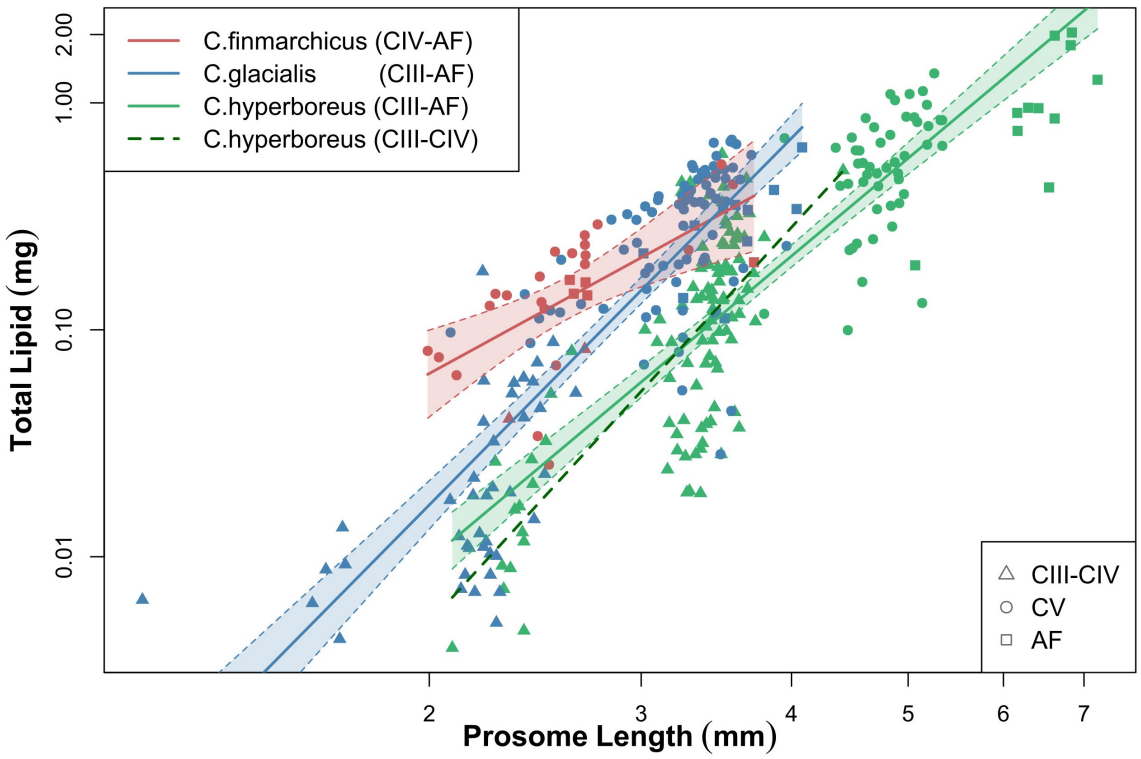


Figure 29: Total lipid *mg* over prosome length *mm* in *C. finmarchicus* (red), *C. glacialis* (blue) and *C. hyperboreus* (green) and smaller copepodite stages of *C. hyperboreus* (dotted, dark green) on a logarithmic scale. The different shaped points indicate different copepodite stages and the lines are fitted by linear regression and displayed with 95 % confidence intervals (The fitted coefficients and $r^2$ are given in Table 10).

Table 10: Coefficients fitted to the exponential relationship between total lipid (TL, in mg) and prosome length (PL, in mm) in different *Calanus* species. Models are from this study and that of Renaud et al. (2018). The relationship is modelled by the equation: TL= $e^{\beta_0} \cdot PL^{\beta_1}$. In addition, the table includes the number of sampled individuals (n) and how much of the variation in the data that is explained by this model ($R^2$).

| | **This study** | | | | **Renaud et al., 2018** | | |
|---|---|---|---|---|---|---|---|
| **Species, stage** | n | $\beta_0$ | $\beta_1$ | $R^2$ | n | $\beta_0$ | $\beta_1$ |
| *C. finmarchicus,* CIV-AF | 29 | $-4,76 \pm 0,69$ | $2,90 \pm 0,71$ | 0,38 | 373 | $-6,6 \pm 1,5$ | $4,9 \pm 0,5$ |
| *C. glacialis,* CIII-AF | 133 | $-7,80 \pm 0,31$ | $5,37 \pm 0.29$ | 0,77 | 290 | $-7,2 \pm 1,0$ | $5,1 \pm 0,3$ |
| *C. hyperboreus,* CIII-CIV | 103 | $-9,28 \pm 0,64$ | $5,79 \pm 0,54$ | 0,54 | 337 | $-7,9 \pm 1,1$ | $5,1 \pm 0,2$ |
| *C. hyperboreus,* CIII-AF | 164 | $-7,7 \pm 0,31$ | $4,45 \pm 0,22$ | 0,71 | 430 | $-6,0 \pm 1,2$ | $3,6 \pm 0,2$ |
| *Calanus* spp. | 326 | $-7,72 \pm 0,31$ | $4,45 \pm 0.22$ | 0,71 | 1430 | $-5,5 \pm 1,3$ | $3,4 \pm 0,1$ |

This difference could be a result of geographical differences, as Svalbard waters are dominated by the west Spitsbergen current bringing nutrient-rich water from the Atlantic, while the northeast Greenland shelf is dominated by the East Greenland current bringing nutrient-poor water from the Arctic basin.

The *C. hyperboreus* populations in Renaud et al. (2018) could have very different origins from those in this study. The *Calanus* species have high plasticity, and the significant difference in lipid fullness estimated for *C. hyperboreus* between Svalbard and Northeast Greenland (Table 10) could possibly be a result of the food availability between the populations.

Although *C. hyperboreus* have a lower average lipid content at similar prosome length than *C. glacialis* , a higher increase in lipid sac area with prosome area was found for all copepodite stages of *C. hyperboreus* (Fig. 23). The focus on accumulating lipids rather than body growth is an important adaptation to uncertain food supply, making it a good life strategy to survive winter (Falk-Petersen et al., 2007). The sudden drop in lipid content between the largest individuals of CIII and the smallest CIV could suggest a past diapause, where lipid storages were utilized (Fig. 23 B). If this is correct, *C. hyperboreus* undergo diapause already from stage CIII, supporting the theory of multi-year life cycles. *C. glacialis* only display this sudden drop in lipid sac area with prosome area from stage CIV (Fig. 23 C). There are also some individuals of CV that appears to have started lipid accumulation at a higher intercept. This could be individuals that finish their life cycle in one year, evolving from egg to copepodite stage CV in one season and moulting to reproductive females during the winter. Most individuals underwent a drop in lipid sac area, suggesting diapause between stage CIV and CV and therefore a two-year life cycle in *C. glacialis*.

Another possibility is difference in sampling time and sample size between Renaud et al. (2018) and this study. This study had its sampling period in the end of August/start of September 2022. This is earlier than the sampling of *C. finmarchicus/C. glacialis* conducted in mid-September/early October (2012 & 2014) in Renaud et al. (2018). This study's sampling period overlaps with the sampling of *C. hyperboreus* in (Renaud et al., 2018), which was conducted between August and October in 2010, 2012 and 2014. The sampling size of this study is also smaller (Table 10).

## 4.2 Difference in *Calanus* lipid content with depth

There was found a statistically significant difference in relative lipid fullness between the surface layer (upper 100 m) and deeper waters (below 100 m) (Fig. 28). This supports hypothesis 2, that *Calanus* located in deeper waters have a lipid sac that fills up more of the body cavity. It must be taken into account that only 20 individuals were recorded from the surface (upper 100 m), against 282 in the deeper waters (below 100 m), which might influence the statistical robustness of these findings.

The mean in individual lipid fullness was similar for intermediate (100-200 m) and deep (200 m-bottom) waters (Fig. 28). However, there might be some difference between the stations, demonstrated by different numbers of individuals with a relative lipid fullness above or below one at 100-200 m (Fig. 27). In Besselfjord A and Eskimones, there were more individuals with a relative lipid fullness below 1 at 100-200 m. In Besselfjord C and Ardencaple, there were instead more individuals with a relative lipid fullness above 1 in this depth interval. There were individuals with relative lipid fullness $> 1$ at the bottom at all stations. As different species and copepodite stages is not taken into account, or how

much lipid the different species and copepodite stages needs to accumulate to survive diapause, it is therefore not possible to conclude if the descended *Calanus* is well or badly prepared for overwintering.

The proxy "relative lipid fullness" was used to account for the effect of size on lipid content. It is important to look at the relative lipid fullness as a measure of whether the individuals' lipid content is below or above the expected lipid content, not as a condition factor, where above 1 is good condition and below 1 is bad condition. Relative lipid fullness is not a condition factor in this study, but mere a measure if the individual is below or above average lipid fullness in this sample. It is not certain that the sample is representative for the true population. The population sampled is probably skewed towards higher lipid fullness as there were more individuals sampled for lipid content below 100 m (Fig. 28), while the density of *Calanus* was as high, and often even higher, above 100 m (Fig.25). If there were more samples, and more equal division between depths, the proxy "relative lipid fullness" could be used as a condition factor, as done in Bailey (2010).

## 4.3 Difference in *Calanus* lipid content between sampling locations

### 4.3.1 Difference between individuals of *C. glacialis* and *Calanus*

No statistically significant differences were observed in lipid content between the different stations when accounting for size-dependent differences in individuals collected with the WP2-net (Fig.24) or VPR (Fig.26). It is possible that this result does not reflect the true situation, as it does not take into account the different allocation between lipid sac area and prosome area within copepodite stage but uses size to account for the prosome growth. Unfortunately, the number of individuals collected is not sufficient to assess lipid sac area differences within each species and copepodite stage at all stations.

Although there is no apparent difference in lipid content between stations when size- and species-specific differences were accounted for, there was a difference in absolute abundance, and species and copepodite stage composition between the different stations.

### 4.3.2 Difference in Total Lipid in the *Calanus* population

Total lipid (TL) was estimated for all individuals, and the bootstrap method was applied to resample the mean within species and stage (See distribution of TL within species and stage in Appendix G, Fig. 44). According to the central limit theorem, the distribution of sample means had a normal distribution. The mean and standard error of the sample means was used as the estimated lipid content per individual within that stage and species. The estimated lipid content per individual was multiplied with the estimate of absolute abundance per station (Table 11 in Appendix C) to calculate the total lipid content in the *Calanus* population per $m^2$ (Fig. 30). The foundation of this method is the assumption that the combined sample from all stations is a representative selection of *C. finmarchicus/C. glacialis* and *C. hyperboreus* in Northeast Greenland coastal locations. Another assumption is that the *Calanus* populations had the same size and lipid content ranges for a copepodite stage within a species,

independent of location. This thesis does not investigate whether the latter assumption is met.

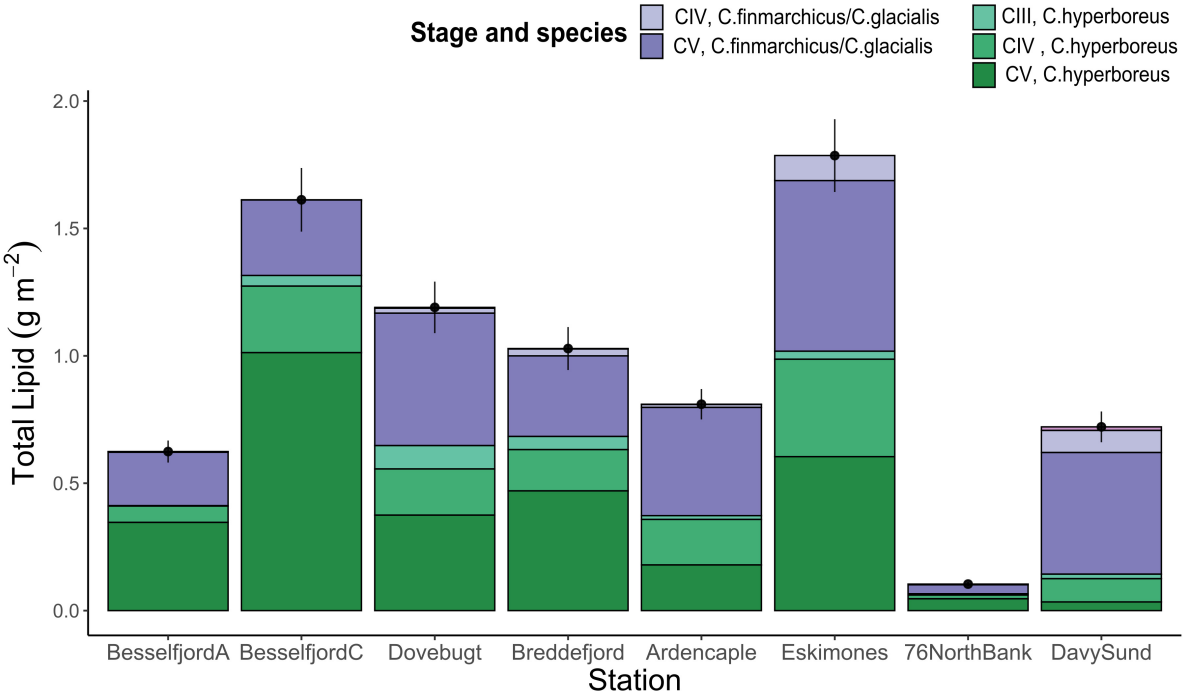


Figure 30: Total lipid $g\ m^{-2}$ in the lipid sac of overwinteringstages of *Calanus* spp.

When shifting the view from absolute abundance of *Calanus* (Fig. 20) to total lipid in *Calanus* (Fig. 30), a different pattern emerges between the different stations. The older stages (CV in *C. glacialis* , CIV and CV in *C. hyperboreus* ) contribute most to the total lipid per $m^2$ in location, although these are not the dominant stages in abundance. For example, Dove Bugt clearly had the highest abundance of *Calanus* in subarea 1 (Fig.20), but a higher relative abundance of smaller copepodite stages than in Besselfjord C (Fig. 21). This caused a higher total lipid in Besselfjord C compared to Dove Bugt, even if the *Calanus* abundance was modest. Eskimones had the highest total lipid (Fig. 30), which is a combination of high relative abundance and older copepodite stages.

## 4.4 Differences in lipid content as an effect of abiotic and biotic environmental factors

*Calanus* is a part of a complex food web within a habitat that undergo extreme seasonal variations. The population is being regulated top-down by planktonic predators, as well as fish, birds and other animals like whales. The quantity and quality of food for *Calanus* is also likely to regulate the population bottom-up. Sea ice is covering these fjords long after the sun has returned, so sea ice algae could be an important part of *Calanus* annual diet. As *Calanus* only makes up a very small percent of the

zooplankton community (Table 6) it could be competition for food between *Calanus* and the other mesozooplankton taxa as the larger *Metridia longa* or smaller copepods as *Pseudocalanus* or *Triconia borealis*.These biotic factors are shaping the community within the framework of abiotic factors. There are many unknown variables to take into account, and one have to bear this in mind when trying to simplify nature and uncover patterns in the chaos. Below, I will discuss some of the factors that were possible to evaluate and which I believe to be important.

### 4.4.1 Stage of seasonal cycle

Low Chl *a* concentrations (Fig. 16), a protist community dominated by flagellates (Fig. 17) and nutrient depletion of the surface (Fig. 12, 13, 14, 15) are properties of an autumn situation (Daase et al., 2021). The peak in primary production following ice break up has passed, and it appears as *Calanus* at all locations have started seasonal vertical migration to spend the winter in the depth of the fjord (Fig. 25).

In all stations, except the southernmost Davy Sund (which also has the deepest Chl *a* max at 45 m), there are still *Calanus* in the surface 100 m. Several stations have individuals of *C. glacialis* stage CI-CIII and *C. hyperboreus* stage CII (Fig. 21). These smaller copepodite stages are not overwintering stages, according to Daase et al. (2021). We will never know if they managed to accumulate enough energy for moulting into an overwintering stage and join the other, fat *Calanus* in the deep darkness of the fjord. In Eskimones it was an estimated 2039 individuals of stage CII and CIII of *C. finmarchicus*/ *C. glacialis* (Table 11 in Appendix C). The highest relative abundance of *Calanus* in the depth interval 20-40 m (Fig. 25) corresponded with high abundance of big diatoms at 28 m (Fig. 17). This indicates active feeding and might imply that even more lipid will be stored in *Calanus* before winter is coming. Eskimones was also the first station where the ice broke up. This does support hypothesis 3A as the longer ice free season correspond with a higher amount of *Calanus* lipid.

### 4.4.2 Inflow of Atlantic Water

One of the initial hypotheses in this thesis was that Atlantic Water would shift the *Calanus* complex towards the smaller *C. finmarchicus*. Atlantic water was present at the southernmost shelf station Davy Sund, as well as in Dove Bugt, Breddefjord and Ardencaple (Fig. 9). Besselfjorden has no inflow of Atlantic Water due to the shallow sill at the entrance of the fjord (Fig. 10). Hypothesis 3B. appears to be falsified in this study, as the presence of Atlantic water in Breddefjord does not increase the amount of *C. finmarchicus* , according to DNA analyses. Only one specimen of *C. finmarchicus* was found in Breddefjord, compared to nine individuals in the innermost station of the Besselfjord, where the main water mass was Polar water (Table 5).

Few recorded individuals of *C. finmarchicus* in Breddefjord could be a result of picking individuals for DNA analysis, instead of systematically analysing all individuals in a subsample. The larger *Calanus* individuals are then more likely to be selected, while smaller *C. finmarchicus*, would get underrepresented.

However, the absolute abundance of *C. hyperboreus* was higher than *C. finmarchicus*/*C. glacialis* inside Breddefjord (Fig. 20). The Atlantic Water was covered by a 160m thick layer of colder, fresher Polar water, which might not make the conditions favourable for *C. finmarchicus* (Aarflot et al., 2018). However, it has also been recorded large plasticity and niche overlap between species (Weydmann-Zwolicka et al., 2022). In fjords at the Svalbard Archipelago it was observed that temperature preferences were more different between the *Calanus* in different fjords than between different species.

Several specimens of *C. finmarchicus* were found in Besselfjord, where there was no Atlantic Water. This could be *C. finmarchicus* , highly adapted to a cold and fresh environment, or it could be a result of misclassification. The primer used, G-150, only separates between *C. finmarchicus* and *C. glacialis* (Smolina et al., 2014). *C. hyperboreus* was determined by size as it can appear as both *C. finmarchicus* and *C. glacialis* in the DNA analysis. These individuals appearing as *C. finmarchicus* could possibly be a population of small *C. hyperboreus* . Smaller individuals with a spike at the $5^{th}$ thoracic segment were also detected (Table 7), which is a caracteristic of *C. hyperboreus* . In Billefjord, a high-Arctic sill fjord in the Svalbard archipelago, there have been observations indicating a population of *C. hyperboreus* with a 1-year life cycle (Arnkværn et al., 2005). Smaller-sized *C. hyperboreus* has also been recorded in Scoresby Sound, which is located further south on the east Greenland coast (Digby, 1954). It was suggested by (Ussing, 1938), that these individuals indicated a population *C. hyperboreus* with a 1-year life cycle (Digby, 1954).

### 4.4.3 Turbidity

The water was clear at all stations, with turbidity less than 0,25 FTU. This is far below the measured turbidity in Young Sound, which was linked to an increase in heterotrophic production at the expense of primary production (Sejr et al., 2022). It must be noted that the timing of sampling in Sejr et al. (2022) was end of July to middle of August, to be timed with the peak of freshwater discharge. That is one month before this study was conducted. However, from the result in this study there were not high enough turbidity values for light to be a limiting factor on photosynthesis. As there was found no gradient in turbidity, it is not possible to assess hypothesis 3C.

### 4.4.4 Nutrients and strength of the nutrient-diatom link

The surface at all stations were depleted of nutrient at the time of sampling (Fig. 12, 13, 14 & 15). Because the seasonality in Arctic fjords with sea ice formation that creates a homogeneous water column during winter, one can estimate the net community uptake of nitrogen by trapezoid integration from surface to intrusion depth (Def. in (Laanemets et al., 2004)) (Fig.31). The intrusion depth appears to be at 250 m for all stations, except Besselfjord A and C where it is at 100 m depth. In addition to a homogeneous water column at time onset of the pelagic bloom, it is assumed no supply of terrestrial nitrogen or atmospheric fixation of nitrogen.

Stations with the presence of Atlantic Water (Dove Bugt, Breddefjord and Ardencaple) have had

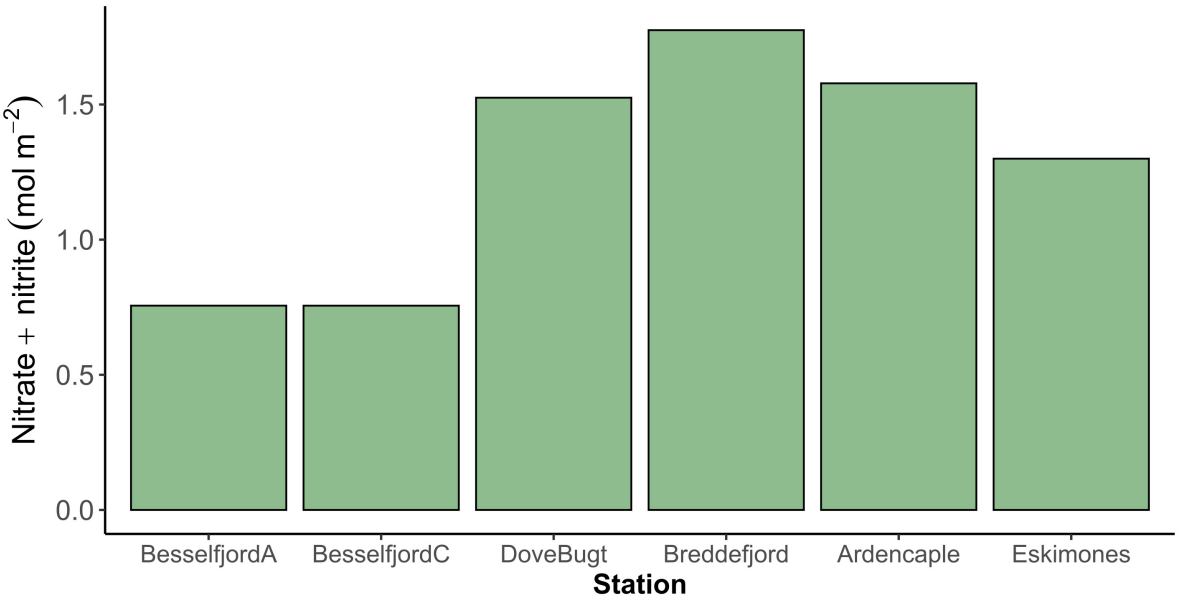


Figure 31: Net community nitrogen uptake from intrusion depth to surface.

higher nitrogen concentrations than stations dominated by Polar Water (Besselfjord and Eskimones) (Fig. 31). However, the difference between Eskimones and the three Atlantic-influenced locations is not large. It can be speculated whether the high nutrients in Eskimones could arise from the glacier, Wordies Gletcher, further into Godthaabs Golf (Fig.5). It is not known if this glacier is still marine-terminating as it is many years since 1952, and a more recent sattelite photo has not been obtained. Breddefjord have had the highest nutrient concentration at the onset of spring, perhaps because of the combination of Atlantic Water and a marine terminating glacier.

*Calanus* feed most efficiently on larger cells (Levinsen et al., 2000), and diatoms have been linked to high nutrient environments with a pycnocline that prevents the heavy, silicate-armored cells from sinking. As the time of sampling was in post-bloom conditions, the protist community was largely dominated by flagellates (Fig. 17). However, the same method used previously, on net community nitrogen uptake, can be applied to estimate the uptake of silicate. By using an empirically estimated ratio between silicate and nitrogen uptake in diatoms (Brzezinski, 1985), the amount of nitrogen taken up in diatoms during the spring can be estimated. It was assumed that silicate was exclusively utilized by diatoms. As the intrusion depth of silicate was 100 m at all locations, the integration was done from the surface to this depth. The pattern of the total amount of nitrogen estimated to have been used in the upper 100 meters (Fig. 32) is the same between the stations as the net estimated nitrogen uptake (Fig. 31). The nitrogen estimated to be used by diatoms is not (Fig.32) following this trend. Actually, the stations with most nutrients have the weakest nutrient-diatom link.

The nutrient-diatom link was very strong in Besselfjord, as most of the nitrogen in the surface was

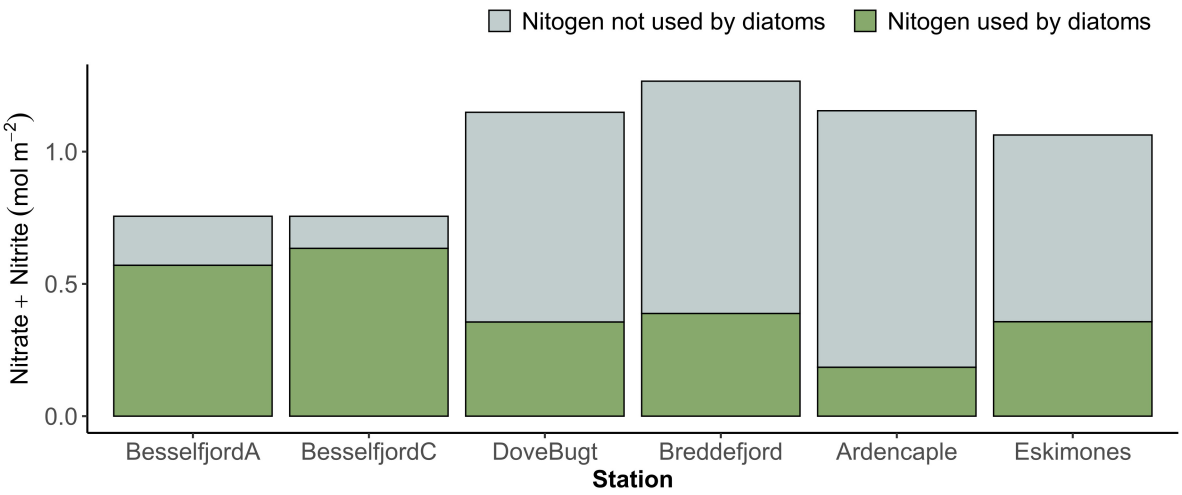


Figure 32: Amount of nitrogen estimated to be utilized by diatoms in the upper 100 m of the water column.

estimated to have been utilized by diatoms (Fig. 32). At all other locations, diatoms were estimated to have taken up much less of the nitrogen. It is important to bear in mind the assumptions of this method. Vertical mixing, that would homogenize the nutrient concentrations, is assumed in the time frame between the ice algae bloom and pelagic bloom. This would homogenize the nutrient concentrations in the water column. It is likely that more open areas would have more mixing compared to the narrow Besselfjord. A possible sea ice algae bloom in the land fast ice would likely be dominated by pennate diatoms (**?**). Differences in the degree of vertical mixing between the locations in the time frame between the sea ice bloom and pelagic phytoplankton bloom would violate the assumption of a homogenous water column. If it had been less mixing between the possible ice algae bloom and phytoplankton bloom in Besselfjord, so it already was a gradient of declining silicate towards the surface, this would have increased the estimated nitrogen-diatom link.

Although there seems to be different strengths of the nutrient-diatom link at different locations, the question remains whether this amplifies further up in the food chain by influencing the *Calanus* lipid content. Besselfjord C displays a strong nutrient-diatom link and a high total lipid content in *Calanus* (Fig. 32 & Fig. 30). This is consistent with the model of energy flow in the Arctic pelagic food web (Daase et al., 2021). However, this does not appear to be the case in Besselfjord A. The nutrient-diatom link is similar to Besselfjord C, but the total abundance is much lower, especially for *C. hyperboreus* , causing a smaller amount of lipid stored in *Calanus*. Eskimones has a weak nutrient-diatom link, and still has the highest amount of lipid stored in *Calanus* (Fig. 30).

The estimate of the nutrient-diatom link is built on strict assumptions. Because of the uncertainty whether these assumptions are met, it is not possible to draw any conclusions about the difference in lipid content in *Calanus*.The only way to truly know which organisms have been in the water column

and sea ice during the spring is by sampling frequently during the season.

### 4.4.5 Total *Calanus* lipid induced by differences in plankton ecology

If the estimated differences in the nutrient-diatom links are close to reality, there must also be other variables affecting the *Calanus* lipid. In the following section, I will briefly discuss differences in the plankton community that could possibly alter the total *Calanus* lipid content. I will compare the fjords Besselfjord A with Besselfjord C and Breddefjord to Eskimones. The fjords which are being compared have a similar strength of the estimated nutrient-diatom link (Fig. 32).

The inner basin of Besselfjord has considerably less estimated total lipid stored in *Calanus* than the outer Besselfjord C (Fig. 30). This difference could arise from differences in zooplankton ecology. There were more plankton (60 895 ind $m^2$) in the middle basin, where 14% consisted of *Calanus* , while the inner Besselfjord A had a lower abundance of zooplankton (31 136 ind $m^{-2}$) and only 6% *Calanus*. We observed three times more planktonic predators of *Calanus* in the inner basin. We also noted gelatinous substances in the plankton net when sampling at Besselfjord A, likely to be the remains of jellyfish such as large ctenophores or hydromedusae. Thus, one possible explanation for this difference in abundance between the stations could be the higher predator density in the inner basin, causing both reduction in the total abundance of *Calanus* , as well as a shift in the *Calanus* complex towards the smaller *C. finmarcicus/C. glacialis*. The shift towards smaller sizes could be driven by predators targeting larger individuals of *Calanus*. However, this needs to be looked into further, and the total predator pressure from both invertebrate and vertebrate predators should be taken into account before drawing any conclusions. These findings are not completely consistent with the findings of Beroujon (2019) from middle/late September 2019 who found a much larger abundance of the hydromedusa *Aglantha digitale* and Cnidaria further towards the mouth of the fjord. There was still a higher abundance of Chaetognatha in the inner fjord, consistent with the results of this study.

Eskimones had the highest estimated amount of *Calanus* lipid per $m^2$ (Fig. 30). Eskimones was also the station that had the biggest fraction of the total abundance, consisting of *Calanus* (21%, Table 6). Breddefjord was estimated to have a similar amount of nitrogen taken up by diatoms (Fig. 32), and slightly higher nitrogen uptake over the season (Fig.31) than Eskimones. Although Breddefjord clearly had the highest abundance of zooplankton with 148 659 ind $m^{-2}$, only 5% was *Calanus* (Table 6). A clear difference between the two stations was the abundance of *Pseudocalanus* spp. (Fig. 3.4). *Pseudocalanus* has a much smaller weight, and therefore biomass, than *Calanus*. It does have an important role in the Bering Sea as a link between primary producers and higher trophic levels (Cleary et al., 2016). Also in the sub-arctic systems in northern Norway, small copepods have been found to have an important role in the lipid storage (Barth-Jensen, 2023). *Pseudocalanus* has a flexible diet, and heterotrophic flagellates have been recorded as a common prey, making it less dependent on diatoms than *Calanus* (Lischka and Hagen, 2007). It would be interesting to have a closer look into the role of *Pseudocalanus* in Besselfjord and whether the abundance of this taxon is the reason for

the low *Calanus* abundance by competing for resources. It would also be interesting to know if this high abundance of *Pseudocalanus* and low abundance of *Calanus* is a typical or abnormal situation for Breddefjorden. It has been observed that a shift in the zooplankton community from larger to smaller copepods can cause a dramatic shift in energy flow and ecosystem structure (Coyle et al., 2011).

The abundant *Calanus* in Eskimones could be relying on larger heterotrophic protists, which make up a significant part of the copepod diet in Young Sound (Levinsen et al., 2000). Size ranges of the sampled protist taxa should be investigated further to investigate if there are larger celled protists in Eskimones, which might support the high amount of accumulated lipid in *Calanus*.High abundances of *Calanus* in Eskimones were recorded with both the VPR and WP2 net, indicating that the abundances were not a result of the patchy distribution of *Calanus*.

# 5 Conclusion and future outlook

*Calanus* spp. have a key role in the highly seasonal Arctic pelagic food web because of their ability to efficiently harvest and store energy from the spring bloom through the dark winter. This thesis has estimated the lipid content of *Calanus* spp. in Northeast Greenland fjords at an autumn situation to investigate how different environmental factors may influence the accumulation of lipid in preparation for overwintering.

In addition to size-induced differences, there were significant differences in lipid content between *C. glacialis* and *C. hyperboreus*, which contradicts findings from the Svalbard region. *C. hyperboreus* had lower lipid content than same-sized *C. glacialis*, but since *C. hyperboreus* can grow larger, they can also hold a larger amount of lipid. Although there was no difference in individual lipid content between locations when species and size-induced differences were accounted for, total *Calanus* lipid per $m^2$ was estimated to differ between the fjords, due to differences in abundance and composition of the *Calanus* community.

The environmental factors indicated a post-bloom situation at all locations, and *Calanus* spp. had started the transition from actively feeding to seasonal migration. The exception was the southernmost fjord, Eskimones (in Godthaab Golf), where a large part of the *Calanus* population was still feeding on diatoms in the upper part of the water column. Deep dwelling *Calanus* had higher lipid content relative to size, supporting the hypothesis that individuals with high lipid fullness are the first to migrate.

We observed inflow of warm, saline Atlantic water into Breddefjord, despite a sill at 160 m depth. However, there was no higher abundance of the Atlantic *C. finmarchicus* in this fjord. A weak nutrient-diatom link in Breddefjord may have shifted the community towards smaller copepods, such as *Pseudocalanus* spp. This was in strong contrast to Besselfjorden, where a shallow sill prevented inflow of Atlantic Water. Here a strong nutrient-diatom link and high total amount of lipid in *Calanus* was observed, in accordance with the conceptual model of energy flow in Arctic pelagic ecosystem. The station with the most total lipid stored in *Calanus*, Eskimones, had no inflow of Atlantic Water and high estimated net community nitrogen uptake, but a weak nitrogen-diatom link. This suggests other important sources for food for these *Calanus*.

The Greenland Ice sheet is melting, introducing more terrestrial matter and freshwater into the Greenlandic fjords. However, at all locations sampled in this study the water was clear, which was different from the trend in Young Sound, where reports indicate that coastal darkening has shifted primary production from autotrophy to heterotrophy. These results show that there is a need to record more environmental variables throughout several seasons to draw better conclusions about what influences the important lipid accumulation in *Calanus*.

Sea ice algae is an important source of carbon for *Calanus* around the Svalbard archipelago. The presence, timing or magnitude of sea ice algal blooms have not been studied at the locations which are included in this thesis. Satellite pictures give the time of ice break up, but the amount of snow on the

ice, quality of ice, and sea ice algae composition can not be obtained by remote sensing. With a warming climate, the environmental parameters connected to sea ice might change. *Calanus* has been observed to rely on sea ice algae for reproduction in the Svalbard area and is therefore affected by earlier or later onset of spring and ice break up. There is a need to examine the importance of sea ice algae for *Calanus* in Northeast Greenland, preferably through regular sampling during the whole productive season.

Another source of carbon that has not been thoroughly investigated in this thesis is the role of microbial pathways through bacterial degradation of terrestrial carbon, as well as primary production by small autotrophic picoplankton that have been found to excel under increased freshwater conditions. There is a need to study the importance of the microbial food chain in relation to *Calanus* lipid accumulation to assess how an increased reliance on this pathway will influence the Arctic pelagic energy flow in Northeast Greenland in a future predicted to be influenced by increased freshwater and allochthonous carbon.

This thesis has also assumed no difference in size ranges of copepodite stages between populations in different locations. This assumption should be investigated further, as differences have been found in *Calanus* size-ranges because of environmental variables on the Svalbard side of Fram Strait. There is also a need to study the ecology of the entire zooplankton communities in the Northeast Greenland fjords, as this could affect both the structure of the *Calanus* spp complex and suggest other paths for lipid storage within the system, for example in smaller copepods.

Northeast Greenland is an area of the Arctic that has not been studied much. This is mainly because it is the main outflow from the Arctic Ocean, and large multiyear ice floes and gigantic ice bergs have made the task of navigating in these waters extremely difficult and dangerous. This is about to change. Less sea ice and highly advanced icebreakers are now making these regions accessible not only to science, but also to tourism, fisheries, and maritime shipping -These represent new stressors in a region that is already challenged with a warming climate. This study contributes to baseline knowledge, which can be used to assess the effect of changes in the environment.

Besselfjorden is an especially interesting fjord, as the shallow sills at the entrance prevent inflow of Atlantic water, which could make it a cold, fresh oasis for Arctic species seeking refuge in a warming future. This could maybe also pose as a sister-fjord to the much-studied Billefjord in Svalbard. As the TUNU project is the only one to sample zooplankton in Besselfjord, there is a need for more thorough examination of the zooplankton ecology within this fjord. To conclude, it is important to gather more knowledge about this little-studied, unique region to understand the dynamics of the Arctic pelagic ecosystem before additional human stressors are introduced. Through knowledge-based management, we should try to step into the era of climate change with precaution. In this way we must try our utmost to protect the pathways of energy which all life in the Arctic pelagic ecosystems rely on.

# References


Aarflot, J. M., H. R. Skjoldal, P. Dalpadado, and M. Skern-Mauritzen (2018). Contribution of *Calanus* species to the mesozooplankton biomass in the barents sea. *ICES journal of marine science 75*(7), 2342–2354.

Army Map Service (AMSC), Corps of Engineers, U.S. Army (1952). Eskimonæs. Map. Scale 1:250,000.

Arndt, J. E., W. Jokat, B. Dorschel, R. Myklebust, J. A. Dowdeswell, and J. Evans (2015). A new bathymetry of the Northeast Greenland continental shelf: Constraints on glacial and other processes. *Geochemistry, Geophysics, Geosystems 16*(10), 3733–3753.

Arnkværn, G., M. Daase, and K. Eiane (2005). Dynamics of coexisting *Calanus finmarchicus*, *Calanus glacialis* and *Calanus hyperboreus* populations in a high-arctic fjord. *Polar biology 28*(7), 528–538.

Bailey, A. M. (2010). Lipids and diapause in *Calanus* spp. in a high-arctic fjord: state-dependent strategies? tracking lipids through the polar night.

Barth-Jensen, C. (2023). Population dynamics and production of small, marine copepods in highly seasonal arctic and sub-arctic environments.

Baumgartner, M., N. Lysiak, C. Schuman, J. Urban-Rich, and F. Wenzel (2011). Diel vertical migration behavior of *Calanus finmarchicus* and its influence on right and sei whale occurrence. *Marine ecology. Progress series (Halstenbek) 423*, 167–184.

Beroujon, T. (2019). Zooplankton communities on the Northeast coast of Greenland. how can we explain vertical and regional distribution?

Beroujon, T., J. S. Christiansen, and F. Norrbin (2022). Spatial occurrence and abundance of marine zooplankton in Northeast Greenland. *Marine Biodiversity 52*(5), 1–19.

Bluhm, B., K. Kosobokova, and E. Carmack (2015). A tale of two basins: An integrated physical and biological perspective of the deep arctic ocean. *Progress in Oceanography 139*, 89–121. Overarching perspectives of contemporary and future ecosystems in the Arctic Ocean.

Brzezinski, M. A. (1985). The si:c:n ratio of marine diatoms: Interspecific variability and the effect of some environmental variables1. *Journal of Phycology 21*(3), 347–357.

Choquet, M., M. Hatlebakk, A. K. S. Dhanasiri, K. Kosobokova, I. Smolina, J. E. Søreide, C. Svensen, W. Melle, S. Kwaśniewski, K. Eiane, M. Daase, V. Tverberg, S. Skreslet, A. Bucklin, and G. Hoarau (2017). Genetics redraws pelagic biogeography of *Calanus*. *Biology Letters 13*(12), 20170588.

Choquet, M., K. Kosobokova, S. Kwaśniewski, M. Hatlebakk, A. K. S. Dhanasiri, W. Melle, M. Daase, C. Svensen, J. E. Søreide, and G. Hoarau (2018). Can morphology reliably distinguish between the copepods *Calanus finmarchicus* and *C. glacialis*, or is dna the only way? *Limnology and Oceanography: Methods 16*(4), 237–252.

Cleary, A. C., E. G. Durbin, T. A. Rynearson, and J. Bailey (2016). Feeding by *Pseudocalanus* copepods in the bering sea: Trophic linkages and a potential mechanism of niche partitioning. *Deep-sea research. Part II, Topical studies in oceanography 134*, 181–189.

Cottier, F., F. Nilsen, R. Skogseth, V. Tverberg, J. Skardhamar, and H. Svendsen (2010, 11). Arctic fjords: A review of the oceanographic environment and dominant physical processes. *Geological Society of London Special Publications 344*, 35–50.

Coyle, K. O., L. B. Eisner, F. J. Mueter, A. I. Pinchuk, M. A. Janout, K. D. Cieciel, E. V. Farley, and A. G. Andrews (2011). Climate change in the southeastern bering sea: impacts on pollock stocks and implications for the oscillating control hypothesis. *Fisheries Oceanography 20*(2), 139–156.

Cushing, D. (1973). The natural regulation of fish populations. *Sea fisheries research*, 399–411.

Daase, M., J. Berge, J. Søreide, and S. Falk-Petersen (2021, 02). *Ecology of Arctic Pelagic Communities*, pp. 219–259.

Daase, M. and K. Eiane (2007, 06). Mesozooplankton distribution in northern svalbard waters in relation to hydrography. *Polar Biology 30*, 969–981.

Danish Meteorological Institute (2022). Arctic ice charts from danish meteorological institute. Available online at `https://ocean.dmi.dk/arctic/icecharts_gl_northcentraleast.uk.php`. Accessed: August 11, 2023.

Digby, P. S. B. (1954). The biology of the marine planktonic copepods of scoresby sound, east Greenland. *Journal of Animal Ecology 23*(2), 298–338.

Falk-Petersen, S., C. Hopkins, and J. Sargent (1990, 01). Trophic relationships in the pelagic, arctic food web. *Trophic Relationships in the Marine Environment*, 315–333.

Falk-Petersen, S., V. Pavlov, S. Timofeev, and J. R. Sargent (2007). *Climate variability and possible effects on arctic food chains: The role of Calanus*, pp. 147–166. Berlin, Heidelberg: Springer Berlin Heidelberg.

Farmer, D. M. and H. J. Freeland (1983). The physical oceanography of fjords. *Progress in Oceanography 12*(2), 147–219.

Finley, A., S. Banerjee, and øyvind Hjelle (2022). *MBA: Multilevel B-Spline Approximation*. R package version 0.1-0.

Gjelstrup, C. V. B., M. K. Sejr, L. de Steur, J. S. Christiansen, M. A. Granskog, B. P. Koch, E. F. Møller, M. H. S. Winding, and C. A. Stedmon (2022). Vertical redistribution of principle water masses on the Northeast Greenland shelf. *Nature communications 13*(1), 7660–7660.

Grolemund, G. and H. Wickham (2011). Dates and times made easy with lubridate. *Journal of Statistical Software 40*(3), 1–25.

Hatlebakk, M., K. Kosobokova, M. Daase, and J. E. Søreide (2022). Contrasting life traits of sympatric *Calanus glacialis* and *C. finmarchicus* in a warming arctic revealed by a year-round study in isfjorden, svalbard. *Frontiers in Marine Science 9*.

Hjelle, Ø. (2001). Approximation of scattered data with multilevel b-splines. *SINTEF report, Tech. Rep.*.

Hop, H. and H. Gjøsæter (2013). Polar cod (Boreogadus saida) and capelin (Mallotus villosus) as key species in marine food webs of the arctic and the barents sea. *Marine biology research 9*(9), 878–894.

IPCC (2023). *Climate Change 2021 – The Physical Science Basis: Working Group I Contribution to the Sixth Assessment Report of the Intergovernmental Panel on Climate Change*. Cambridge University Press.

Karlson, B., C. Cusack, and E. Bresnan (2010). Microscopic and molecular methods for quantitative phytoplankton analysis.

Karnovsky, N., A. Harding, W. Walkusz, S. Kwasniewski, I. Goszczko, J. Wiktor, H. Routti, A. Bailey, L. McFadden, Z. Brown, G. Beaugrand, and D. Gremillet (2010). Foraging distributions of little auks alle alle across the Greenland sea: implications of present and future arctic climate change. *Marine ecology. Progress series (Halstenbek) 415*, 283–293.

Kunisch, E. H., M. Graeve, R. Gradinger, H. Flores, ø. Varpe, and B. A. Bluhm (2023). What we do in the dark: Prevalence of omnivorous feeding activity in arctic zooplankton during polar night. *Limnology and oceanography*.

Laanemets, J., K. Kononen, J. Pavelson, and E.-L. Poutanen (2004). Vertical location of seasonal nutriclines in the western gulf of finland. *Journal of Marine Systems 52*(1), 1–13.

Lee, R. F., W. Hagen, and G. Kattner (2006). Lipid storage in marine zooplankton. *Marine ecology. Progress series (Halstenbek) 307*, 273–306.

Lee, S., G. Wolberg, and S. Shin (1997). Scattered data interpolation with multilevel b-splines. *IEEE transactions on visualization and computer graphics 3*(3), 228–244.

Levinsen, H., J. T. Turner, T. G. Nielsen, and B. W. Hansen (2000). On the trophic coupling between protists and copepods in arctic marine ecosystems. *Marine ecology. Progress series (Halstenbek) 204*, 65–77.

Li, W. K. W., F. A. McLaughlin, C. Lovejoy, and E. C. Carmack (2009). Smallest algae thrive as the arctic ocean freshens. *Science 326*(5952), 539–539.

Lischka, S. and W. Hagen (2007). Seasonal lipid dynamics of the copepods pseudocalanus minutus (calanoida) and oithona similis (cyclopoida) in the arctic kongsfjorden (svalbard). *Marine biology 150*(3), 443–454.

Mattingly, K., J. Turton, J. Wille, B. Noël, X. Fettweis, A. Rennermalm, and T. Mote (2023, 03). Increasing extreme melt in Northeast Greenland linked to foehn winds and atmospheric rivers. *Nature Communications 14*, 1743.

Meire, L., J. Mortensen, P. Meire, T. Juul-Pedersen, M. K. Sejr, S. Rysgaard, R. Nygaard, P. Huybrechts, and F. J. R. Meysman (2017). Marine-terminating glaciers sustain high productivity in Greenland fjords. *Global Change Biology 23*(12), 5344–5357.

Middelbo, A. B., M. K. Sejr, K. E. Arendt, and E. F. Møller (2018). Impact of glacial meltwater on spatiotemporal distribution of copepods and their grazing impact in young sound ne, Greenland. *Limnology and Oceanography 63*(1), 322–336.

Møller, E. F., P. THOR, and T. G. NIELSEN (2003). Production of doc by *Calanus finmarchicus*, textitC. glacialis and textitC. hyperboreus through sloppy feeding and leakage from fecal pellets. *Marine ecology. Progress series (Halstenbek) 262*, 185–191.

Montero-Pau, J., A. Gómez, and J. Muñoz (2008). Application of an inexpensive and high-throughput genomic dna extraction method for the molecular ecology of zooplanktonic diapausing eggs. *Limnology and Oceanography: Methods 6*(6), 218–222.

Mundy, C., D. Barber, and C. Michel (2005). Variability of snow and ice thermal, physical and optical properties pertinent to sea ice algae biomass during spring. *Journal of Marine Systems 58*(3), 107–120.

Neuwirth, E. (2022). *RColorBrewer: ColorBrewer Palettes*. R package version 1.1-3.

Norrbin, M. F. (1996). Timing of diapause in relation to the onset of winter in the high-latitude copepods *Pseudocalanus* acuspes and acartia longiremis. *Marine ecology. Progress series (Halstenbek) 142*(1/3), 99–109.

Parsons, T. R. (2013). *A manual of chemical & biological methods for seawater analysis*. Elsevier.

R Core Team (2022). *R: A Language and Environment for Statistical Computing*. Vienna, Austria: R Foundation for Statistical Computing.

Renaud, P. E., M. Daase, N. S. Banas, T. M. Gabrielsen, J. E. Søreide, Ø. Varpe, F. Cottier, S. Falk-Petersen, C. Halsband, D. Vogedes, K. Heggland, and J. Berge (2018, 06). Pelagic food-webs in a changing Arctic: a trait-based perspective suggests a mode of resilience. *ICES Journal of Marine Science 75*(6), 1871–1881.

Rignot, E., A. Bjork, N. Chauche, and I. Klaucke (2022). Storstrømmen and l. bistrup bræ, north Greenland, protected from warm atlantic ocean waters. *Geophysical Research Letters 49*(5), e2021GL097320.

Sakshaug, E., G. Johnsen, S. Kristiansen, C. Von Quillfeldt, F. Rey, D. Slagstad, F. Thingstad, et al. (2009). Phytoplankton and primary production. *Ecosystem Barents Sea*, 167–208.

Schneider, C., W. Rasband, and K. Eliceiri (2012, 07). Nih image to imagej: 25 years of image analysis. *Nature Methods 9*.

Sejr, M. K., A. Bruhn, T. Dalsgaard, T. Juul-Pedersen, C. A. Stedmon, M. Blicher, L. Meire, K. D. Mankoff, and J. Thyrring (2022). Glacial meltwater determines the balance between autotrophic and heterotrophic processes in a Greenland fjord. *Proceedings of the National Academy of Sciences 119*(52), e2207024119.

Slagstad, D., P. F. J. Wassmann, and I. Ellingsen (2015). Physical constrains and productivity in the future arctic ocean. *Frontiers in Marine Science 2*, 1–23.

Smolina, I., S. Kollias, M. Poortvliet, T. G. Nielsen, P. Lindeque, C. Castellani, E. F. Møller, L. Blanco-Bercial, and G. Hoarau (2014). Genome- and transcriptome-assisted development of nuclear insertion/deletion markers for *Calanus* species (copepoda: Calanoida) identification. *Molecular Ecology Resources 14*(5), 1072–1079.

Søreide, J. E., E. Leu, J. Berge, M. Graeve, and S. Falk-Petersen (2010). Timing of blooms, algal food quality and *Calanus glacialis* reproduction and growth in a changing arctic. *Global Change Biology 16*(11), 3154–3163.

Tarling, G. A., J. J. Freer, N. S. Banas, A. Belcher, M. Blackwell, C. Castellani, K. B. Cook, F. R. Cottier, M. Daase, M. L. Johnson, K. S. Last, P. K. Lindeque, D. J. Mayor, E. Mitchell, H. E. Parry, D. C. Speirs, G. Stowasser, and M. Wootton (2022). Can a key boreal *Calanus* copepod species now complete its life-cycle in the arctic? evidence and implications for arctic food-webs. *Ambio 51*(2), 333–344.

Thingstad, T. F., R. G. J. Bellerby, R.-A. Sandaa, E. F. Skjoldal, T. Tanaka, R. Thyrhaug, B. Topper, G. Bratbak, K. Y. Børsheim, J. K. Egge, M. Heldal, A. Larsen, C. Neill, J. Nejstgaard, and S. Norland (2008). Counterintuitive carbon-to-nutrient coupling in an arctic pelagic ecosystem. *Nature 455*(7211), 387–390.

Ussing, H. H. (1938). *The biology of some important plankton animals in the fjords of East Greenland.* CA Reitzel.

Varpe, Ø., M. Daase, and T. Kristiansen (2015). A fish-eye view on the new arctic lightscape. *ICES journal of marine science 72*(9), 2532–2538.

Varpe, Ø. and M. Ejsmond (2018, 12). Trade-offs between storage and survival affect diapause timing in capital breeders. *Evolutionary Ecology 32*.

Vogedes, D., Ø. Varpe, J. E. Søreide, M. Graeve, J. Berge, and S. Falk-Petersen (2010, 06). Lipid sac area as a proxy for individual lipid content of arctic calanoid copepods. *Journal of Plankton Research 32*(10), 1471–1477.

Weydmann-Zwolicka, A., F. Cottier, J. Berge, S. Majaneva, P. Kukliński, and A. Zwolicki (2022). Environmental niche overlap in sibling planktonic species *Calanus finmarchicus* and textitC. glacialis in arctic fjords. *Ecology and Evolution 12*(12), e9569. e9569 ECE-2022-05-00783.R1.

Wickham, H. (2007). Reshaping data with the reshape package. *Journal of Statistical Software 21*(12), 1–20.

Wickham, H. (2016). *ggplot2: Elegant Graphics for Data Analysis*. Springer-Verlag New York.

Wickham, H., M. Averick, J. Bryan, W. Chang, L. D. McGowan, R. François, G. Grolemund, A. Hayes, L. Henry, J. Hester, M. Kuhn, T. L. Pedersen, E. Miller, S. M. Bache, K. Müller, J. Ooms, D. Robinson, D. P. Seidel, V. Spinu, K. Takahashi, D. Vaughan, C. Wilke, K. Woo, and H. Yutani (2019). Welcome to the tidyverse. *Journal of Open Source Software 4*(43), 1686.

Wickham, H., R. Francois, L. Henry, K. Muller, and D. Vaughan (2023). *dplyr: A Grammar of Data Manipulation*. R package version 1.1.2.

Wood, S. (2017). *Generalized Additive Models: An Introduction with R* (2 ed.). Chapman and Hall/CRC.

Wood, S., N., Pya, and B. S"afken (2016). Smoothing parameter and model selection for general smooth models (with discussion). *Journal of the American Statistical Association 111*, 1548–1575.

Wood, S. N. (2003). Thin-plate regression splines. *Journal of the Royal Statistical Society (B) 65*(1), 95–114.

Wood, S. N. (2004). Stable and efficient multiple smoothing parameter estimation for generalized additive models. *Journal of the American Statistical Association 99*(467), 673–686.

Wood, S. N. (2011). Fast stable restricted maximum likelihood and marginal likelihood estimation of semiparametric generalized linear models. *Journal of the Royal Statistical Society (B) 73*(1), 3–36.

Wordie, J. M., R. C. Wakefield, W. F. Whittard, and G. Manley (1930). Cambridge east Greenland expedition, 1929: Ascent of petermann peak. *The Geographical Journal 75*(6), 481–502.

WoRMS Editorial Board. World register of marine species. Available from `https://www.marinespecies.org` at VLIZ. Accessed 2023-08-11. doi:10.14284/170.

Zeileis, A., K. Hornik, and P. Murrell (2009). Escaping RGBland: Selecting colors for statistical graphics. *Computational Statistics & Data Analysis 53*(9), 3259–3270.

Zoller, K., J. S. Laberg, T. A. Rydningen, K. Husum, and M. Forwick (2023). A high arctic inner shelf–fjord system from the last glacial maximum to the present: Bessel fjord and southwest dove bugt, Northeastern Greenland. *Climate of the past 19*(7), 1321–1343.

Zoller, K. M. (2020). Last glacial maximum – holocene palaeoenvironment in bessel fjord and southwestern dove bugt, Northeast Greenland.

# A CTD profiles

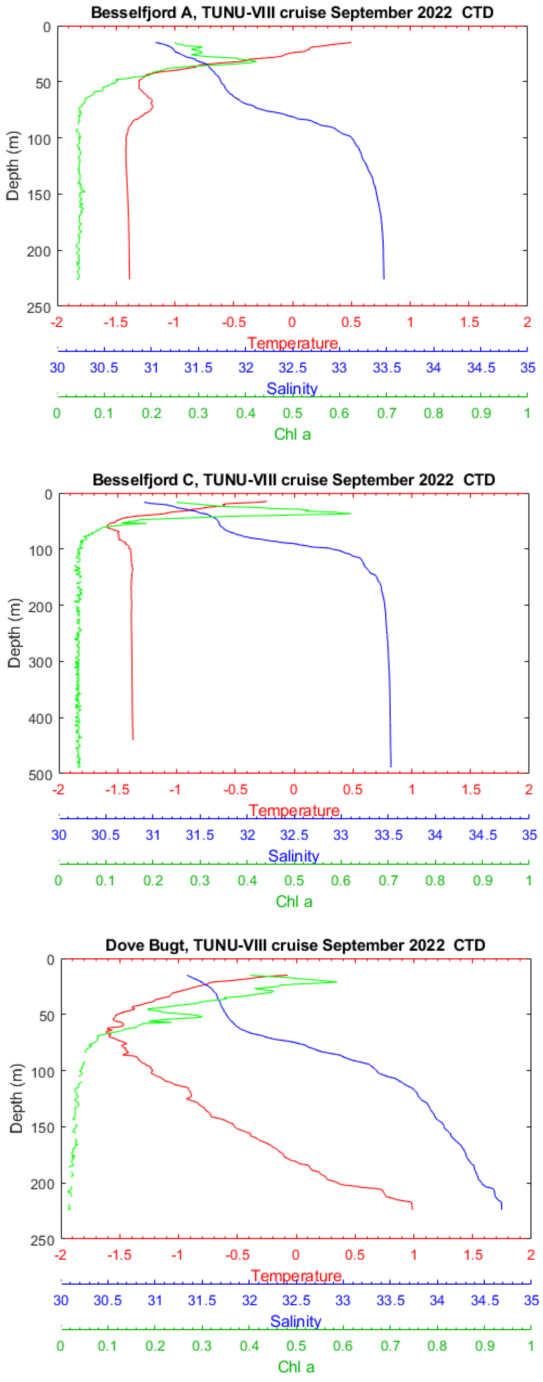


Figure 33: Temperature, salinity and Chl *a* with depth in subarea 1.

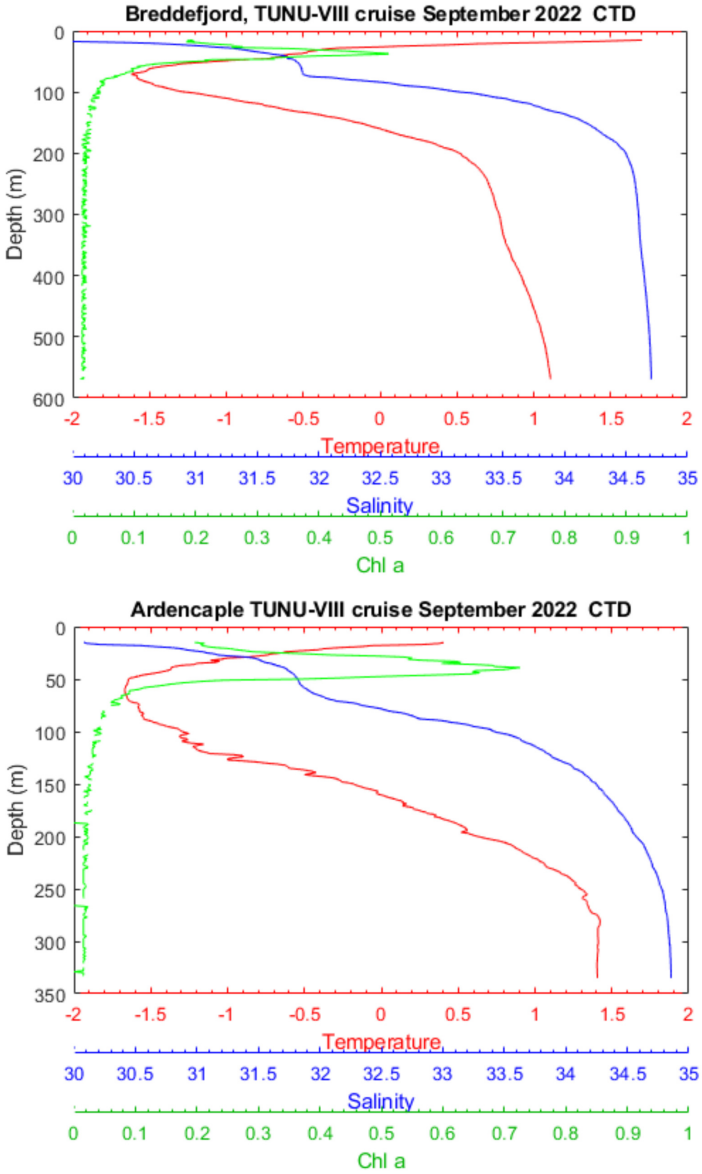


Figure 34: Temperature, salinity and Chl *a* with depth in subarea 2.

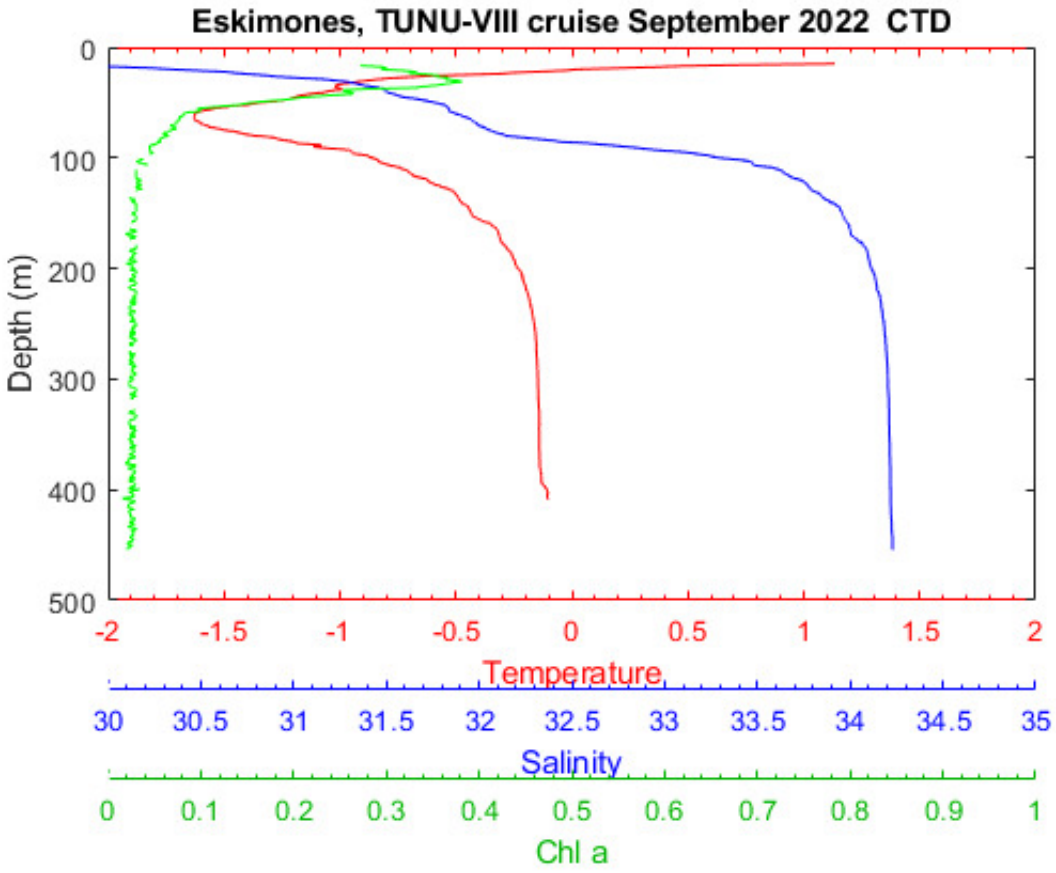


Figure 35: Temperature, salinity and Chl *a* with depth in subarea 3.

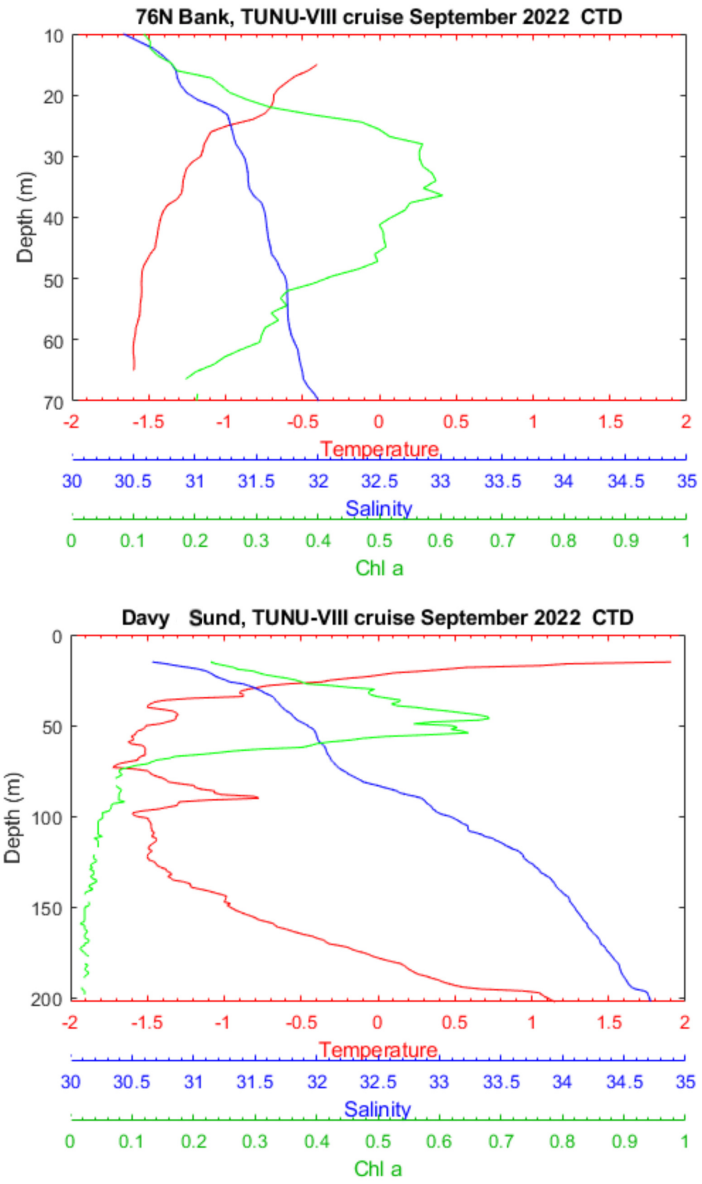


Figure 36: Temperature, salinity and Chl *a* with depth in subarea 4.

# B Appendix B: Turbidity

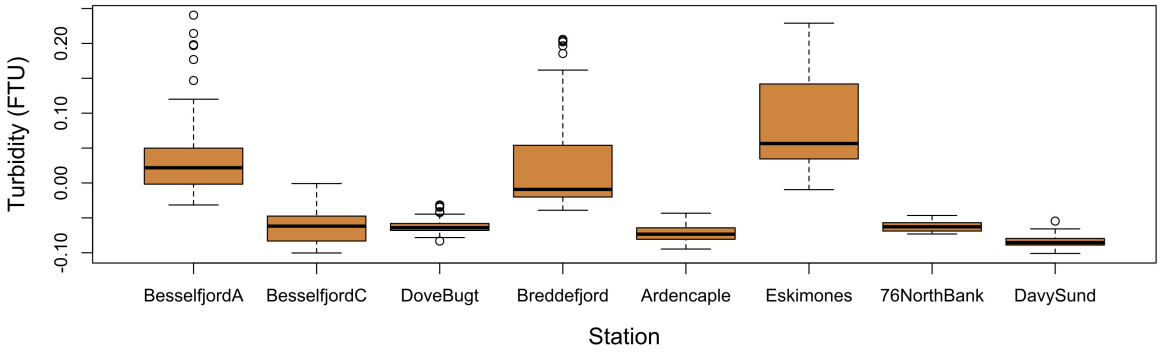


Figure 37: Turbidity in the upper 200m (whole water column for shallower stations).

# C Zooplankton community

Table 11: Mesozooplankton absolute abundance [Ind $\cdot m^{-2}$].

| Taxa in figure | Genus | Species | Stage | BesselfjordA | BesselfjordC | Dovebugt | Breddefjord | Ardencaple | Eskimonæs | 76°North Bank | DavySund |
|---|---|---|---|---|---|---|---|---|---|---|---|
| Calanus spp. | **Copepoda** | *C.finmarchicus/C.glacialis* | CI | - | 59 | - | - | - | - | - | - |
| *Calanus spp.* | **Copepoda** | *C.finmarchicus/C.glacialis* | CII | - | 118 | - | - | - | 78 | 4 | 579 |
| *Calanus spp.* | **Copepoda** | *C.finmarchicus/C.glacialis* | CIII | 69 | 353 | 406 | 232 | 133 | 1961 | 55 | 1741 |
| *Calanus spp.* | **Copepoda** | *C.finmarchicus/C.glacialis* | CIV | 69 | 415 | 575 | 796 | 338 | 2908 | 71 | 2558 |
| *Calanus spp.* | **Copepoda** | *C.finmarchicus/C.glacialis* | CV | 713 | 1009 | 1770 | 1077 | 1447 | 2281 | 120 | 1626 |
| *Calanus spp.* | **Copepoda** | *C.finmarchicus/C.glacialis* | AF | 304 | 708 | 232 | 327 | 269 | 392 | 59 | 927 |
| *Calanus spp.* | **Copepoda** | *C.hyperboreus* | CII | - | - | - | 93 | - | - | - | - |
| *Calanus spp.* | **Copepoda** | *C.hyperboreus* | CIII | 70 | 1770 | 3881 | 2187 | 633 | 1334 | 214 | 753 |
| *Calanus spp.* | **Copepoda** | *C.hyperboreus* | CIV | 410 | 1668 | 1159 | 1035 | 1141 | 2443 | 93 | 583 |
| *Calanus spp.* | **Copepoda** | *C.hyperboreus* | CV | 589 | 1722 | 637 | 799 | 305 | 1028 | 79 | 58 |
| *Calanus spp.* | **Copepoda** | *C.hyperboreus* | AF | 217 | 947 | 58 | 326 | 236 | 160 | 21 | 3 |
| *Metridia longa* | **Copepoda** | *Metridia longa* | | 671 | 2902 | 232 | 6588 | 4471 | 4353 | 18 | 235 |
| *Pseudocalanus spp.* | **Copepoda** | *Pseudocalanus spp.* | | 17098 | 19373 | 22824 | 68706 | 2588 | 7059 | 353 | 6706 |
| *Microcalanus spp.* | **Copepoda** | *Microcalanus spp.* | | 3373 | 7686 | 6941 | 11059 | 5412 | 6000 | 635 | 10353 |
| *Oithona similis* | **Copepoda** | *Oithona similis* | | 9882 | 10745 | 8118 | 20706 | 15451 | 13294 | 7394 | 42000 |
| *Triconia borealis* | **Copepoda** | *Triconia borealis* | | 3373 | 4627 | 1412 | 18118 | 2667 | 9059 | 265 | 2000 |
| Benthos larvea | **Polychaeta** | Polychaeta | | - | - | - | 84 | - | 118 | - | - |
| Benthos larvea | **Polychaeta** | trochophore larvae | | 157 | - | 118 | - | - | - | - | - |
| Benthos larvea | **Bivalvia** | veliger larvae | | 471 | - | 4000 | 3059 | - | 471 | 18 | - |
| Benthos larvea | **Gastropoda** | veliger larvae | | 392 | 157 | 824 | 3294 | 235 | 353 | 35 | - |
| Benthos larvea | **Echinodermata** | Pluteus larvae | | 314 | 1020 | 4471 | - | 392 | 706 | 35 | 2824 |
| Other Copepoda | **Copepoda** | Nauplii | | 1647 | 4627 | 2588 | 1412 | 2902 | 1412 | 1112 | 6000 |
| Other Copepoda | **Copepoda** | *Paraeuchaeta spp.* | | 78 | - | - | 16 | 78 | 824 | - | - |
| Other Copepoda | **Copepoda** | *Chiridius obtusifrons* | | - | - | - | 471 | 157 | - | - | - |
| Other Copepoda | **Copepoda** | *Scolecithricella* sp. | | 78 | - | - | 2824 | 549 | - | - | 235 |
| Other Copepoda | **Copepoda** | *Gaetanus miles* | | - | - | - | 235 | - | - | - | - |
| Other Copepoda | Copepoda | *Microcetella norwegica* | | - | - | - | - | - | - | 18 | - |
| Other Copepoda | Harpacticid copepode | | | - | - | - | - | - | - | - | 78 |
| Other Copepoda | **Copepoda** | *Centropages typicus* | | - | - | - | - | - | 353 | - | - |
| Other | **Amphipoda** | *Gammarus wikitscki* | | - | - | - | - | - | - | 2 | |
| Other | **Amphipoda** | *Themisto libellula* | | - | 118 | - | - | - | - | - | |
| Other | **Amphipoda** | amfipode sp. | | - | 78 | 235 | 56 | - | 471 | - | - |
| Other | **Appendicularia** | *Fritillaria borealis* | | 157 | 314 | 154 | - | - | - | - | 588 |
| Other | **Appendicularia** | *Oikopleura* spp. | | 235 | 327 | 38 | 8 | - | - | 124 | 235 |
| Other | **Chaetognatha** | *Eukrohnia hamata* | | 78 | 154 | 145 | 471 | 78 | - | - | 706 |
| Other | **Chaetognatha** | *Sagitta elegans* | | 440 | 38 | 145 | 235 | - | 118 | - | - |
| Other | **Cirriped** | nauplii | | - | - | - | - | 78 | - | - | - |
| Other | **Diplostraca** | *Evadne* sp. | | - | 78 | - | - | - | - | 53 | - |
| Other | **Gastropoda** | Nudibranch | | 23 | - | - | - | - | - | - | - |
| Other | **Hydrozoa** | *Aglantha digitale* | | 46 | - | 118 | 64 | 78 | - | 18 | - |
| Other | **Hydrozoa** | Hydrozoa indet. | | 157 | - | 235 | 1695 | 235 | 471 | - | - |
| Other | Mysida | Mysida | | - | - | - | 24 | 78 | 118 | - | - |
| Other | **Ostracoda** | *Discoconchoecia sp.* | | 23 | - | - | 1412 | 157 | 471 | - | - |
| Other | **Ostracoda** | *Obtusoesia obtusata* | | - | - | - | 706 | 314 | 118 | - | - |
| Other | **Ostracoda** | *Boroecia maxima* | | - | - | - | 235 | - | - | - | - |
| Other | **Ostracoda** | *Boroecia borealis* | | - | - | - | 235 | - | - | - | - |
| Other | **Platyhelminthes** | Platyhelminthes | | - | - | 118 | - | - | - | - | - |
| Other | **Pteropoda** | *Limacina helicina* | | - | - | - | 4 | 78 | - | 24 | - |
| Other | **Radiozoa** | Radiozoa | | - | - | 6235 | - | - | 235 | - | - |
| Other | **Hydroid** | | | - | - | - | 78 | - | - | - | - |

# D Model checking

In 3.6 there were made several linear regressions. In the following section, the goodness-of-fit of these linear regressions will be evaluated by diagnostic plots. The coefficients, standard deviation and $R^2$ can be found in table 8 and 9.

There are four assumptions of linear regression:

1 **Linearity** A linear relationship exists between the explanatory and response variable.

2 **Independence of residuals** The residuals (difference between observed and predicted value) should be independent. This means there is no systematic pattern in the residuals.

3 **Homoscedasticity** Constant variation in the residuals over different values of the explanatory variable.

4 **Normal distribution of residuals** The residuals should be normally distributed with a mean of 0.

These assumptions can be addressed through four diagnostic plots, which can be used to assess the model and how well the model fit the data.

1 **Residuals vs fitted** This plot assesses assumption 2 and 4 in a linear regression. In a perfect linear regression, the plot should show random scatter around 0, indicating independence and homoscedasicity and independence in residuals.

2 **Normal Q-Q** This plot check the assumption of normal distribution in residuals. A straight line indicate normally distributed residuals.

3 **Scale-location** Assess the spread of residuals across predicted values. If there is constant variance, homoscedasicity, there should be a random distribution of points around a horizontal line.

4 **Residuals Vs Leverage** This plot, also called Cook's distance plot, identify points that have a strong impact on the regression model's coefficients. The plot show standardized residuals against leverage values to identify influential points.

## D.1 *C. finmarchicus* - WP2

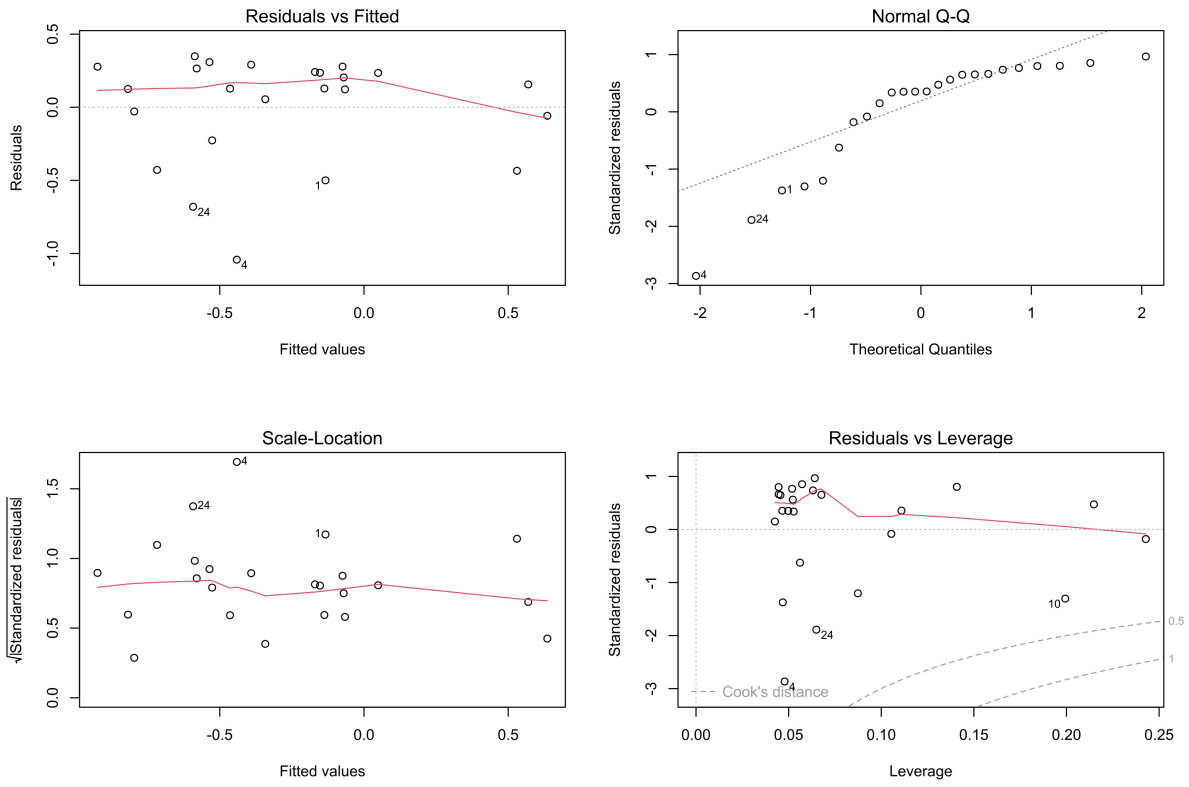


Figure 38: Diagnostic plots for the linear regression of lipid areal over prosome areal in *C. finmarchicus*. Coefficients, number of samples and $R^2$ is in table 8.

The assumptions of linear regression are not fully met in the case of *C.finmarchicus*, perhaps due to the limited number of samples available for the regression analysis (n=24). Despite this limitation, there is a random distribution of residuals over fitted values, centred around 0, indicating independence of residuals, see figure 38. This also indicate homoscedasicity, further supported by the horizontal line in the scale-location plot. Anyway, the assumption of normality in residuals is not completely met, evidenced by the S-shape pattern observed in the normal Q-Q plot.

## D.2 *C. glacialis* - WP2

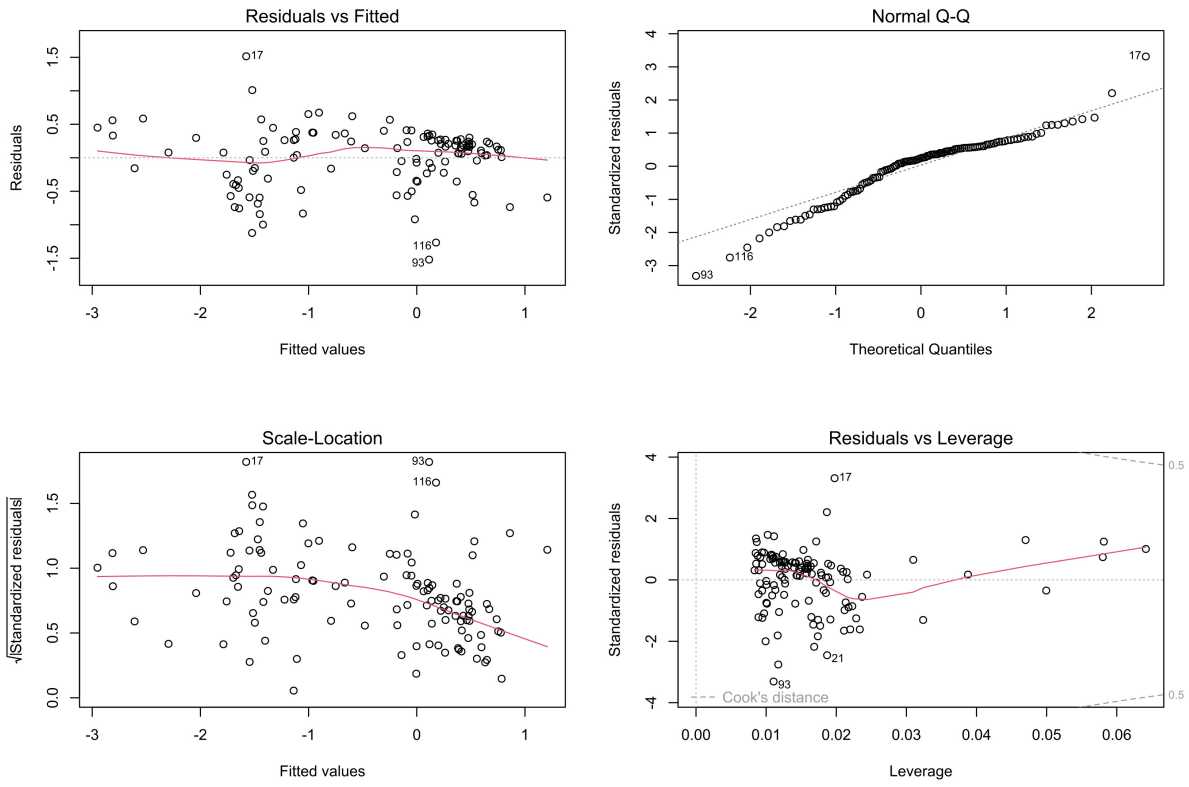


Figure 39: Diagnostic plots for the linear regression of lipid areal over prosome areal in *C. glacialis*. Coefficients, number of samples and $R^2$ is in table 8.

In *C. glacialis* the assumptions of linear regression are neither fully met, see figure 39. The residuals vs fitted plot shows a relatively random distribution of residuals, except toward the of the scale in fitted values, where the residuals seem to be clumped together. This might indicate heteroscedasticity, which is further supported by a downward trend towards the end of the scale-location plot. These findings suggest a violation of assumption 3 of linear regression, the assumption of constant variance in residuals. Additionally, the normal Q-Q plot shows a slight S-shape, indicating a potential violating of the assumption of normal distribution of residuals.

## D.3 *C. hyperboreus* - WP2

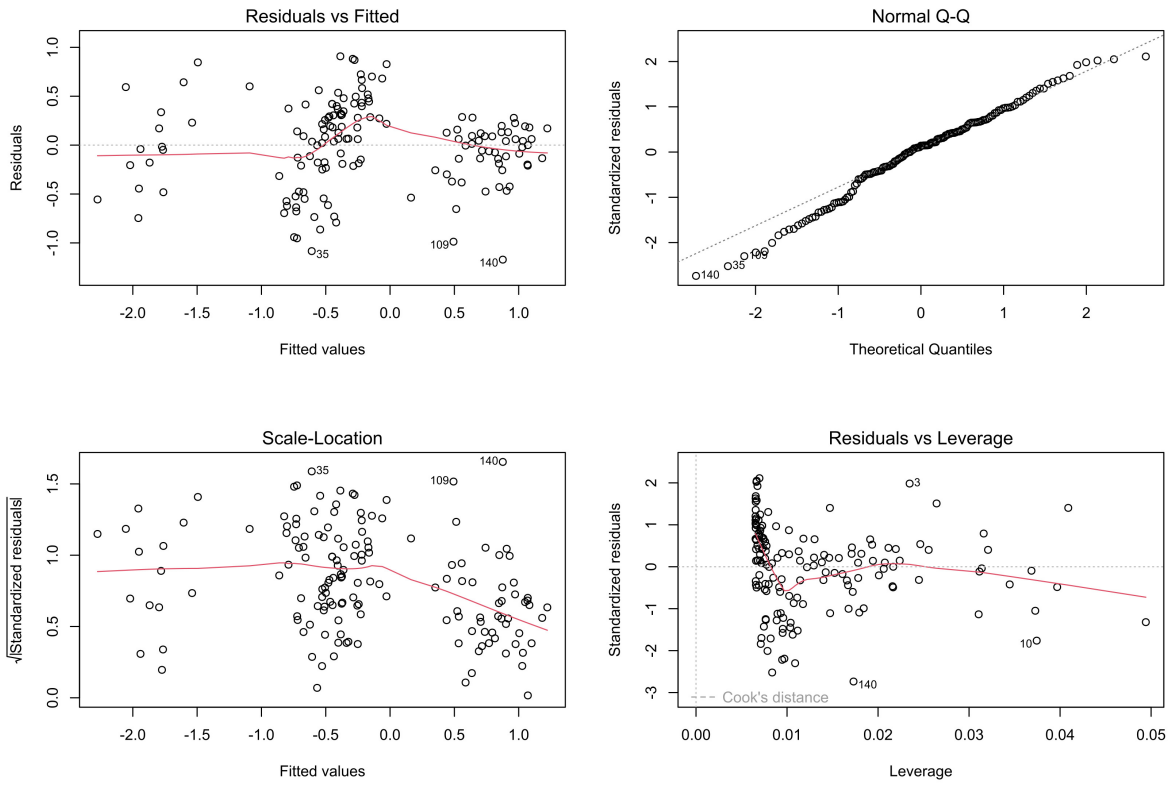


Figure 40: Diagnostic plots for the linear regression of lipid areal over prosome areal in *C. hyperboreus*. Coefficients, number of samples and $R^2$ is in table 8.

*C. hyperboreus* appears to meet most of the assumptions of linear regression, see figure 40. The residuals are distributed quite randomly around a predominantly horizontal line in the residuals vs. fitted values plot. However, there are observable clusters of data points at certain intervals of fitted values, especially at the higher end of the fitted values scale. This, together with the downward trend in the scale-location plot, are suggesting possible heteroscedasticity in the data. Nevertheless, the assumption of normal distribution in residuals appears to be met, and there are no significant outliers or overly influential data points.

# E Individual lipid content between stations

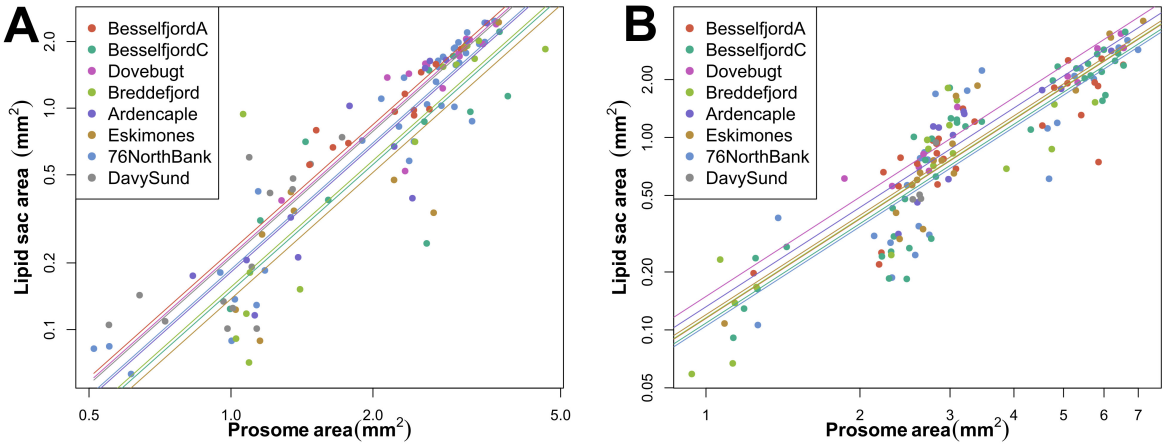


Figure 41: Lipid sac area over prosome areal in A) *C. glacialis* and B) *C. hyperboreus* on a logarithmic scale. The lines are fitted by multiple linear regression with station as an additional explanatory variable.

# F Total lipid and prosome length with depth - VPR

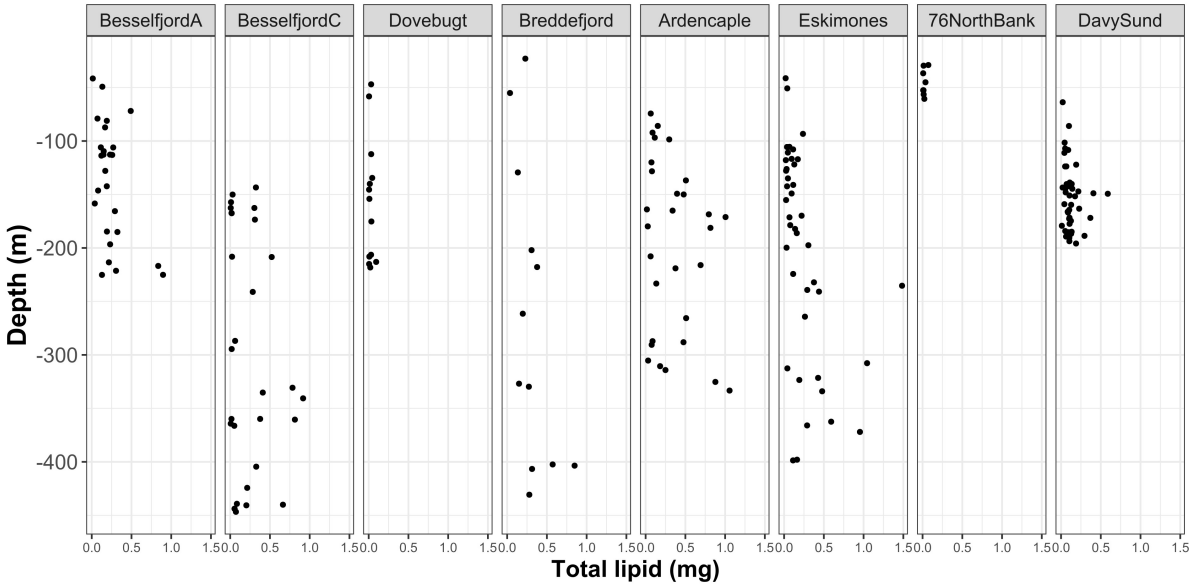


Figure 42: Total lipid with depth

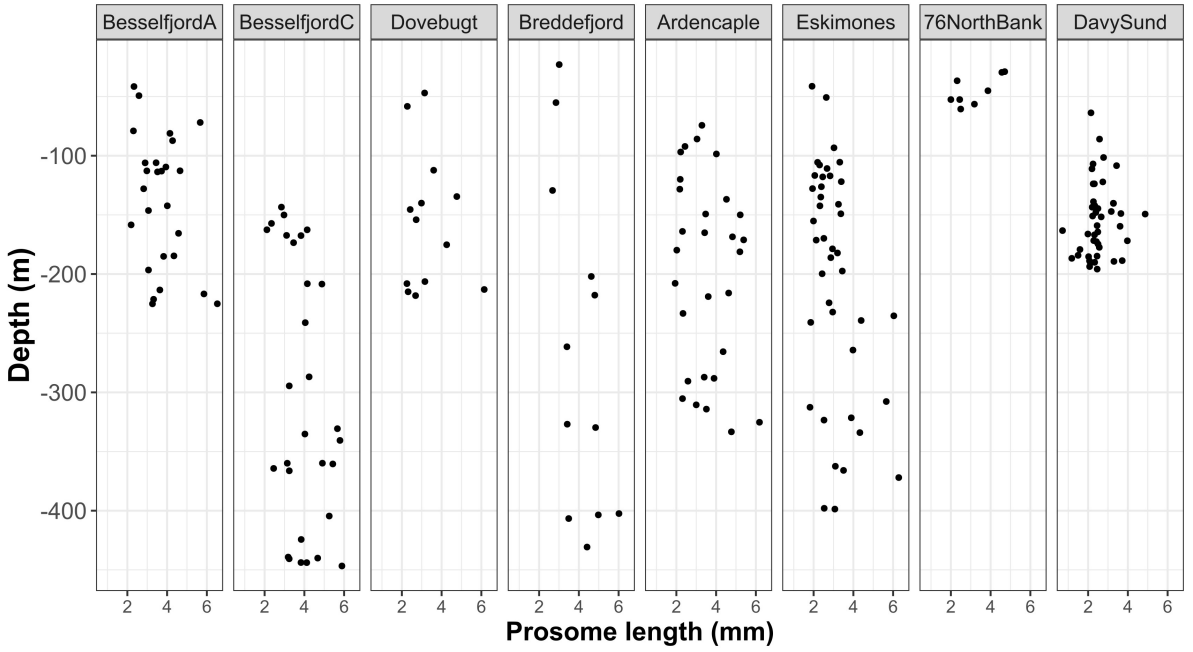


Figure 43: Prosome length with depth

# G Total lipid per individual in *Calanus*

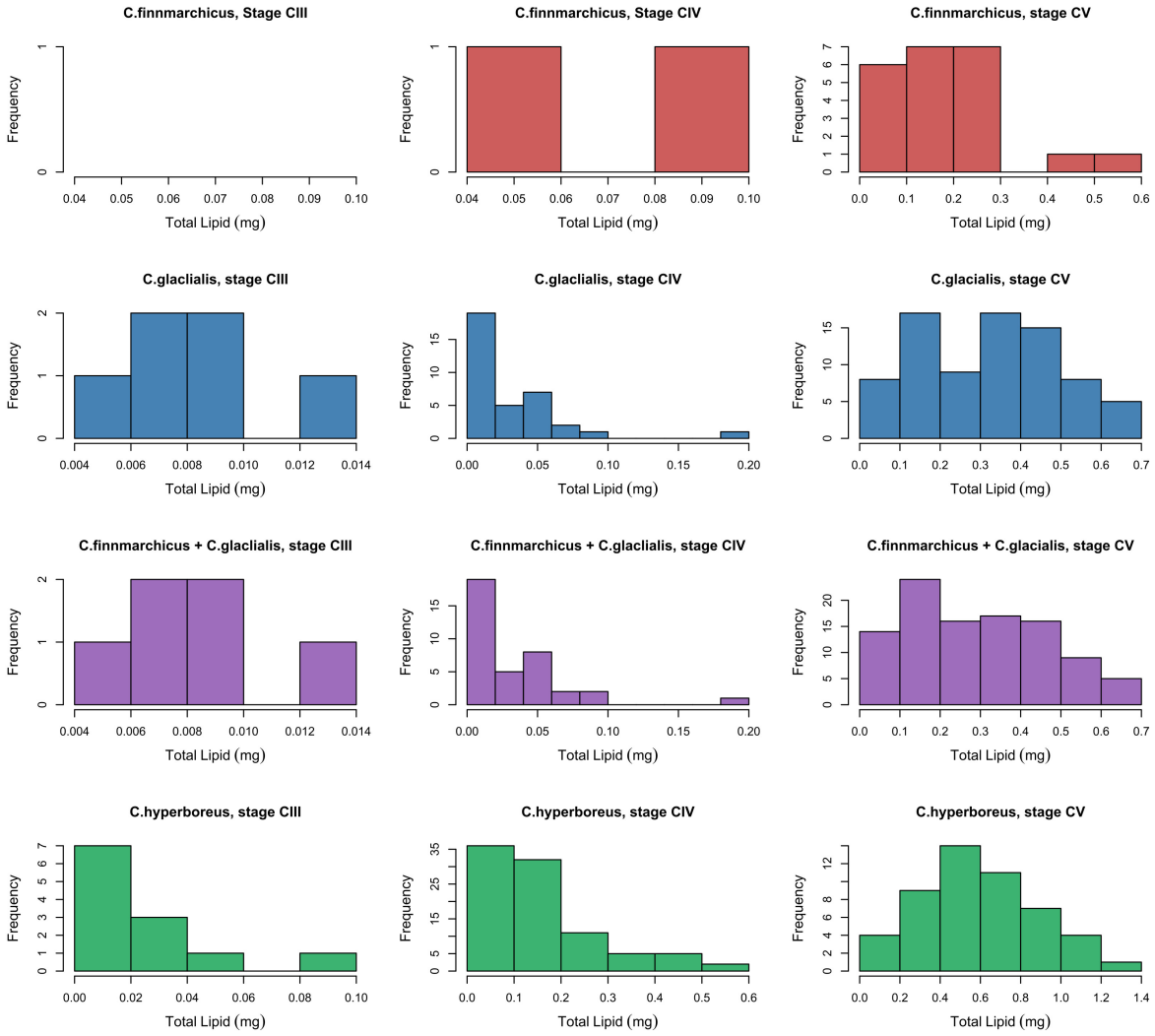


Figure 44: Distribution of total lipid content for the different copepodite stages in A) *C. finmarchicus*, B) *C. glacialis*, C) *C. finmarchicus* and *C. glacialis* and D) *C. hyperboreus*.